

ISTANBUL TECHNICAL UNIVERSITY ★ INSTITUTE OF SCIENCE AND TECHNOLOGY

**DETERMINATION OF SPATIAL DISTRIBUTION OF
PRECIPITATION ON POORLY GAUGED COASTAL REGIONS**

**Ph.D. Thesis by
Ebru ERİŞ**

Department: Civil Engineering

Programme: Hydraulics and Water Resources Engineering

FEBRUARY 2011

**DETERMINATION OF SPATIAL DISTRIBUTION OF
PRECIPITATION ON POORLY GAUGED COASTAL REGIONS**

**Ph.D. Thesis by
Ebru ERİŞ
(501062503)**

**Date of submission : 9 December 2010
Date of defence examination: 23 February 2011**

**Supervisor (Chairman) : Prof. Dr. Necati AĞIRALIOĞLU (ITU)
Members of the Examining Committee : Prof. Dr. H. Kerem CİĞİZOĞLU (ITU)
Assoc. Prof. Dr. Ömer L. ŞEN (ITU)
Prof. Dr. H. Gonca COŞKUN (ITU)
Prof. Dr. M. Emin BİRPINAR (YTU)**

FEBRUARY 2011

İSTANBUL TEKNİK ÜNİVERSİTESİ ★ FEN BİLİMLERİ ENSTİTÜSÜ

**GÖZLEM VERİLERİ AZ OLAN KIYI BÖLGELERİNDE YAĞIŞ
DAĞILIMININ BELİRLENMESİ**

DOKTORA TEZİ

Ebru ERİŞ

(501062503)

Tezin Enstitüye Verildiği Tarih : 9 Aralık 2010

Tezin Savunulduğu Tarih: 23 Şubat 2011

Tez Danışmanı : Prof. Dr. Necati AĞIRALIOĞLU (İTÜ)
Diğer Jüri Üyeleri : Prof. Dr. H. Kerem CİĞİZOĞLU (İTÜ)
Doç. Dr. Ömer L. ŞEN (İTÜ)
Prof. Dr. H. Gonca COŞKUN (İTÜ)
Prof. Dr. M. Emin BİRPINAR (YTÜ)

ŞUBAT 2011

Science is nothing more than a courage of looking at the facts from different aspects.

FOREWORD

First of all I would like to thank my supervisor Prof. Dr. Necati Ađıraliođlu for the opportunity he gave me, for his precious guidance, patience and understanding whilst supervising my studies. His enthusiasm, insight, and precision have enormously influenced my development.

I would like to thank Prof. Dr. H. Kerem Cıđızođlu for his advices, interesting discussions and thorough comments. Assoc. Prof. Dr. mer Ltfi Ően is also acknowledged for valuable advices and inspiration that provide me to see big picture of hydrologic processes. I am very thankful to Prof. Dr. Hafzullah Aksoy for his motivation to my scientific curiosity and for the short period role he had in this PhD as a committee member.

This study was undertaken as a part of a research project funded by Scientific and Technical Research Council of Turkey (TUBITAK) under the project number 106M043. I would like to thank the many people I have collaborated with during this project. Thanks also to TUBITAK for the financial support on this project and doctorate scholarship.

I also wish to express my sincere gratitude to all my friends and department members in both Ege University and Istanbul Technical University.

Finally, I would like to thank my family for their love, for always believing in me and for their unconditional support.

December 2010

Ebru ERİŐ
Civil Engineer

TABLE OF CONTENTS

	<u>Page</u>
FOREWORD	vii
TABLE OF CONTENTS	ix
ABBREVIATIONS	xi
LIST OF TABLES	xiii
LIST OF FIGURES	xv
LIST OF SYMBOLS	xix
SUMMARY	xxi
ÖZET	xxiii
1. INTRODUCTION	1
1.1 Importance of the Topic	1
1.2 Outline of the Study	1
2. LITERATURE REVIEW	3
2.1 Literature Review for Precipitation	3
2.2 Literature Review for Runoff Coefficient	5
2.3 Literature Review for Flow Depth Mapping	6
2.4 Literature Review for Evapotranspiration	8
2.5 Motivation of Study.....	9
3. STUDY AREA AND DATA USED	11
3.1 Study Area	11
3.2 Meteorological Data	11
3.2.1 Precipitation data	11
3.2.2 Temperature and evaporation data.....	14
3.2.3 Wind and Relative Humidity Data	18
3.3 Streamflow Data.....	20
3.4 Digital Elevation Model Data.....	23
4. EFFECTS OF GEOGRAPHICAL/TOPOGRAPHICAL PARAMETERS ON PRECIPITATION DISTRIBUTION	27
4.1 Effects of Geographical/Topographical Parameters.....	27
4.1.1 Effects of longitude.....	27
4.1.2 Effects of latitude.....	28
4.1.3 Effects of distance from sea.....	29
4.1.4 Effects of elevation	29
4.2 Effects of Coastline Angle	31
5. DERIVATION OF ISOHYETAL MAPS	35
5.1 Methods	35
5.1.1 Inverse distance weighted (IDW)	35
5.1.2 Radial basis function (RBF)	36
5.1.3 Kriging	38
5.1.4 Multiple linear regression (MLR).....	43
5.2 Application	46
5.2.1 Isohyetal map using IDW	46
5.2.2 Isohyetal map using RBF.....	47

5.2.3 Isohyetal map using Kriging.....	48
5.2.4 Isohyetal map using MLR.....	50
5.3 Evaluation.....	56
6. VALIDATION OF ISOHYETAL MAPS	61
7. DERIVATION OF FLOW DEPTH MAP	65
7.1 Introduction	65
7.2 Method.....	66
7.3 Application and Evaluation	67
8. DERIVATION OF EVAPOTRANSPIRATION MAP.....	71
8.1 Introduction	71
8.2 Estimation of Potential Evapotranspiration.....	72
8.2.1 Method.....	72
8.2.2 Estimation of Evaporation and Potential Evapotranspiration for Coastal Zone.....	73
8.2.3 Estimation of Evaporation and Potential Evapotranspiration for Inland Zone.....	77
8.3 Estimation of Actual Evapotranspiration	80
8.3.1 Method.....	80
8.3.2 Estimation of Actual Evapotranspiration for Coastal and Inland Gauges	81
8.4 Application and Evaluation	81
9. DETERMINATION OF PRECIPITATION FROM STREAMFLOW AND EVAPOTRANSPIRATION DATA	85
9.1 Introduction	85
9.2 Method.....	85
9.3 Application and Evaluation	86
10. CONCLUSIONS.....	95
REFERENCES	99
APPENDIX	109
CURRICULUM VITAE.....	113

ABBREVIATIONS

AET	: Actual Evapotranspiration
DEM	: Digital Elevation Model
DMI	: State Meteorological Service (with Turkish acronym as Devlet Meteoroloji İşleri)
DSI	: State Hydraulics Works (with Turkish acronym as Devlet Su İşleri)
EIE	: Electrical Power Resources Survey and Development Administration (with Turkish acronym as Elektrik İşleri Etüt İdaresi)
EMAP	: Estimated Mean Annual Precipitation
ET	: Evapotranspiration
GIS	: Geographical Information System
IDW	: Inverse Distance Weighted
MAE	: Mean Absolute Error
MLR	: Multiple Linear Regression
MSL	: Mean Sea Level
OMAP	: Observed Mean Annual Precipitation
PET	: Potential Evapotranspiration
RE	: Relative Error
RBF	: Radial Basis Function
RMSE	: Root Mean Square Error
SEBAL	: Surface Energy Balance Algorithm for Land
SE	: Standard Error
SLR	: Simple Linear Regression
SRTM	: Shuttle Radar Topographic Mission
TIN	: Triangulated Irregular Network
UTM	: Universal Transverse Mercator
VIF	: Variance Inflation Factor

LIST OF TABLES

	<u>Page</u>
Table 3.1 : Characteristics of rain gauges.	12
Table 3.2 : Temperature and evaporation data availability and data range.....	15
Table 3.3 : Number of directions in which maximum wind speed occurs.....	18
Table 3.4 : Mean wind speed and mean relative humidity data and data range.....	20
Table 3.5 : Characteristics of flow gauges.	21
Table 4.1 : Coastline angles of rain gauges.....	33
Table 5.1 : Frequently used variogram models.	42
Table 5.2 : Parameters of theoretical variogram for precipitation data.....	49
Table 5.3 : Correlation coefficients of precipitation and independent variables.	51
Table 5.4 : Coefficients and regression statistics of calibration stage of the MLR models*	52
Table 5.5 : Validation results based on the MLR models.	56
Table 5.6 : Comparison of models.	57
Table 7.1 : Parameters of theoretical variogram for flow data.....	69
Table 7.2 : Validation results based on flow depth map.	70
Table 8.1 : Daylight coefficient (<i>C</i>) for Thornthwaite formula.	73
Table 8.2 : Regression coefficients and statistics.....	74
Table 8.3 : Parameters of theoretical variogram for actual evapotranspiration data.	83
Table 9.1 : Statistics of prediction errors.	87
Table 9.2 : Comparison of the runoff coefficients.	91
Table A.1 : Availability of precipitation data.	110
Table A.2 : Availability of streamflow data.....	111

LIST OF FIGURES

	<u>Page</u>
Figure 3.1 : Study area and locations of the rain and flow gauges.	13
Figure 3.2 : Difference between observed and adjusted precipitation data.	14
Figure 3.3 : Monthly average temperature data for (a) coastal, (b) inland region. ...	16
Figure 3.4 : Monthly average evaporation data for inland gauges.....	16
Figure 3.5 : Monthly average temperature and evaporation data for coastal gauges.	17
Figure 3.6 : Gauges which have relative humidity and wind speed data (Giresun, Akcaabat, Trabzon and Rize gauges have also evaporation data).	19
Figure 3.7 : Difference between observed and adjusted flow data.	22
Figure 3.8 : Extracting flow direction and accumulation, stream network and basins (Chinnayakanahalli et al., 2006).....	23
Figure 3.9 : Cross section of DEM surface.	24
Figure 3.10 : Physical representation of flow direction grids (a) directional arrows, (b) flow network and (c) flow direction grid (modified from Maidment, 2002 and Url-2, 2010).	24
Figure 3.11 : (a, b) Number of cells draining into a given cell along the flow network and (c) flow accumulation grid (modified from Maidment, 2002 and Url-2, 2010).	25
Figure 3.12 : Grids; (a) flow direction and (b) flow accumulation.	26
Figure 3.13 : Drainage basins of the flow gauges.	26
Figure 4.1 : Distribution of mean annual precipitation versus longitude.....	28
Figure 4.2 : Distribution of mean annual precipitation versus latitude.....	28
Figure 4.3 : Distribution of mean annual precipitation versus distance from sea....	29
Figure 4.4 : Distribution of mean annual precipitation versus elevation.	30
Figure 4.5 : Mean annual precipitation in a schematic transect from the two different valleys (a) valley C1; (b) valley C2 (for position of the cross-section see Figure 3.1).	31
Figure 4.6 : Angle between the coast gauge and topographic obstacle (A; coastline angle, EP; effect point, D; effective distance from a gauge).....	32
Figure 4.7 : Determination coefficients (R^2) for various distances (D).	33
Figure 5.1 : Schematic presentation and notation of theoretical semivariogram.....	40
Figure 5.2 : An example of empirical (experimental) and theoretical semivariogram models.	42
Figure 5.3 : RMSE and power values for different number of neighbors for IDW method.	46
Figure 5.4 : Cross validation results of observed and estimated precipitation values for IDW method.	47
Figure 5.5 : RMSE values for different basis functions.....	47
Figure 5.6 : Cross validation results of observed and estimated precipitation values for RBF method.....	48
Figure 5.7 : Experimental variogram of the annual precipitation with spherical model fitted.	48

Figure 5.8 : Spatial autocorrelation (Moran's I) of mean annual precipitation by sampling distance (h).....	50
Figure 5.9 : Cross validation results of observed and estimated precipitation values for Kriging method.	50
Figure 5.10 : Scatter diagrams of observed and estimated mean annual precipitation for the (a) all gauges (Model 1), (b) coastal gauges (Model 2), (c) inland gauges (Model 3), (d) all gauges (Model 4).	54
Figure 5.11 : Scatter diagrams of residuals for the (a) all gauges (Model 1), (b) coastal gauges (Model 2), (c) inland gauges (Model 3), (d) all gauges (Model 4).	55
Figure 5.12 : Isohyetal maps generated from (a) IDW, (b) RBF, (c) Kriging and (d) MLR.	58
Figure 5.13 : Smoothed isohyetal map generated from Kriging.	59
Figure 5.14 : Validation results of models.	60
Figure 5.15 : Grid system used for MLR.	60
Figure 6.1 : Runoff coefficients for flow gauges.	62
Figure 6.2 : Precipitation and flow data of Uzungol rain gauge and Serah flow gauge.....	62
Figure 7.1 : Mean annual flow-area relationship.	67
Figure 7.2 : Histogram of residuals and normal plot.	68
Figure 7.3 : Experimental variogram of the flow depth with Gaussian model fitted.	69
Figure 7.4 : Cross validation results of observed and estimated flow depth values.	69
Figure 7.5 : Flow depth map for the study area.	70
Figure 8.1 : Scatter diagram of observed and estimated E_{pan} values.	74
Figure 8.2 : E_{pan} values estimated from MLR equation and PET values for coastal gauges (6, 9, 10, 12, 15, 16, and 17).....	75
Figure 8.3 : E_{pan} values, observations and estimations from simple linear regression equation using PET values for gauges (2, 7, 8, 13 with Ordu and Unye).	76
Figure 8.4 : Flow chart of estimation of evaporation for inland zone.....	78
Figure 8.5 : E_{pan} values, observations and estimation by the method shown in Figure 8.4 for gauges (20, 21, 22, 25, 27, 34, 37 and 38).....	79
Figure 8.6 : Plot of Turc-Pike model.	80
Figure 8.7 : AET values estimated using Turc-Pike method.	81
Figure 8.8 : Annual values of precipitation (P), evaporation (E_{pan}), potential evapotranspiration (PET) and actual evapotranspiration (AET).....	82
Figure 8.9 : Relative humidity of the gauges (2, 9, 13, 16 and 17) and average relative humidity of coastline.	82
Figure 8.10 : Experimental variogram of AET with Spherical model fitted.	83
Figure 8.11 : Cross validation results of observed-estimated AET values.....	84
Figure 8.12 : Evapotranspiration map for the study area.	84
Figure 9.1 : Illustration of combining two different raster data.	85
Figure 9.2 : Isohyetal map from water balance.	86
Figure 9.3 : Scatter diagrams of observed and estimated mean annual precipitations from water balance method for (a) coastal, (b) inland and (c) whole gauges.	87
Figure 9.4 : An example of points using in combination raster data and MLR analysis equations.	89
Figure 9.5 : Adjusted isohyetal map for the coastal part of the Eastern Black Sea Region.....	89

Figure 9.6 : Scatter diagram of observed and estimated precipitations from adjusted isohyetal map for (a) coastal, (b) inland and (c) whole gauges.....	90
Figure 9.7 : Annual runoff coefficients determined from adjusted isohetal map for flow gauges.	90
Figure 9.8 : Spatial distribution of runoff coefficients.....	91
Figure 9.9 : Areas used in the runoff coefficient determination studies.	92
Figure 9.10 : Correction ratio for the study area.....	92
Figure 9.11 : Correction ratio for the mountainous river basins worldwide (Adam et. al., 2006).....	93
Figure 9.12 : Location of the Kalkandere gauge and it surrounding rain gauges with precipitation values.	93

LIST OF SYMBOLS

R^2	:	Determination coefficient
$Z^*(x_o)$:	Estimation value
$Z(x_i)$:	Observed value
λ	:	Weights
d	:	Distance
$\phi()$:	Radial basis function
$\gamma(h)$:	Semivariogram function
h	:	Lag distance
$C(x_i, x_j)$:	Covariance function
μ	:	Lagrange multiplier
a	:	Range, Thornthwaite formula exponent
c	:	Sill
β_i	:	Regression coefficient
p	:	Power value
P_{est}, P_{obs}	:	Estimated, observed precipitation
X	:	Longitude
Y	:	Latitude
H	:	Elevation
L	:	Distance from sea
A	:	Coastline angle, basin area
α	:	Critical value
C	:	Runoff coefficient, daylight coefficient
Q	:	Flow depth
G	:	Net discharge of groundwater
dS	:	Net change in storage
dt	:	Time increment
K_p	:	Pan coefficient
T_m	:	Monthly mean temperature
I	:	Heat index

DETERMINATION OF SPATIAL DISTRIBUTION OF PRECIPITATION ON POORLY GAUGED COASTAL REGIONS

SUMMARY

Precipitation is the main driver of hydrologic system. Determination of its spatial distribution has an importance in terms of hydrological applications and water resources assessment. Particularly, the effects of orography and coastline on precipitation distribution should be taken into account in mountainous and/or coastal regions. This necessity is forced by the limited number of rain gauges which have also a nonhomogenous distribution. The rain gauges are mostly established in the valley floors and near the settlement areas, therefore they cannot represent the precipitation distribution on the slopes. In this study, it is aimed to determine the spatial distribution of precipitation for the coastal part of Eastern Black Sea Region. The region is poorly gauged and is assumed to show orographic effects. It is tried to generate the most accurate isohyetal map using annual total precipitation data recorded in rain gauges of the region. For this purpose, the relationships between precipitation and geographical/topographical variables as well as configuration of coastline are investigated. It is found that the coastline configuration has a considerable effect on precipitation distribution. These effects are converted to equations with the help of regression analysis; different isohyetal maps are derived using both regression equations and conventional methods. Results are compared to each other. Isohyetal maps are validated with annual runoff coefficients; as a result underestimation of precipitation on higher elevations and slopes is comprehended. Water balance approach is applied for more accurate precipitation estimation. Thus, flow depth and evapotranspiration maps are delineated and combined to create a new precipitation map. Regression equations which are developed before and represent better precipitation distribution on the coastline and valleys are embedded into new precipitation map. This precipitation map is called as adjusted isohyetal map.

It can be said that this study is the first in terms of combination of precipitation distribution which is represented by water balance on slopes and by regression on coastline and valleys, separately, for the coastal part of the Eastern Black Sea Region. Additionally, a new variable, coastline angle, is introduced in the regression equations to represent the coastline configuration. Coastline angle is found to be a weighty variable that affects precipitation characteristics not only of coastal gauges but also inland gauges.

GÖZLEM VERİLERİ AZ OLAN KIYI BÖLGELERİNDE YAĞIŞ DAĞILIMININ BELİRLENMESİ

ÖZET

Yağış hidrolojik sistemin en önemli girdisidir. Yağışın alandaki dağılımının belirlenmesi hidrolojik uygulamaların ve su kaynaklarının doğru değerlendirilmesi açısından büyük önem taşır. Özellikle dağlık ve/veya kıyı bölgelerde hem orografiyi hem de kıyı etkilerini yağışın dağılımını belirlemede hesaba katmak gerekebilir. Bu gerekliliği, dağlık bölgelerde yağış gözlem istasyonlarının az ve düzensiz olması zorlaştırır. Genelde vadi içlerine ve yerleşim bölgeleri yakınına kurulan bu tür istasyonlar yamaç kısımlardaki yağış dağılımını temsil edemez. Bu çalışmada da, orografik yağış özelliği gösterdiği bilinen ve sınırlı sayıda yağış gözlem istasyonuna sahip Doğu Karadeniz Bölgesinin kıyı kesimi için yağış dağılımının belirlenmesi amaçlanmıştır. Bölgedeki mevcut yağış istasyonlarına ait yıllık toplam yağış verileri kullanılarak en doğru eşyağış haritası çıkarılmaya çalışılmıştır. Bu amaçla öncelikle yağışın coğrafik/topoğrafik değişkenler ve kıyı şekli ile olan ilişkisi araştırılmış ve kıyı şeklinin yağış dağılımında hatırı sayılan bir etkisi olduğu görülmüştür. Bu etkiler regresyon analizi yardımıyla denklemlere dönüştürülmüş, bu denklemler ve geleneksel yöntemler yardımıyla farklı eşyağış haritaları elde edilerek birbirleriyle karşılaştırılmıştır. Eşyağış haritalarının doğruluğu yıllık akış katsayıları ile kontrol edilmiş ve bu kontrol sonucu yağış istasyonlarının yüksek kotlarda ve yamaçlardaki yağışı temsil etmediği belirlenmiştir. Daha doğru bir yağış dağılımı tahmini için su dengesi yaklaşımına başvurulmuştur. Böylece bölgenin akım derinliği ve evapotranspirasyon haritaları çizilip, birleştirilerek yeni bir eşyağış haritası elde edilmiştir. Elde edilen harita, kıyıyı ve vadileri daha iyi temsil ettiği düşünülen ve önceden çıkarılmış regresyon denklemleri ile birleştirilerek en son halini almıştır.

Çalışma, Doğu Karadeniz Bölgesinin kıyı kesimine ait yamaçlardaki yağış dağılımının temsilinde su dengesinin, kıyı ve vadilerdeki yağış dağılımının temsilinde ise regresyon denklemlerinin birleştirilerek kullanılması açısından bir ilktir. Ayrıca, regresyon denklemleri içersinde bir değişken olarak bulunan ve kıyı şeklini temsil eden kıyı açısı da ilk kez bu çalışmada sunulmuştur. Kıyı açısı yalnızca kıyıdaki değil iç kısımdaki ölçüm istasyonları açısından da yağışın dağılımını etkileyen önemli bir parametredir.

1. INTRODUCTION

1.1 Importance of the Topic

The importance of considering spatial distribution of precipitation in many hydrological applications is well known. This importance becomes critical for mountainous regions where meteorological gauges are inadequate and non-uniformly distributed over the area. Moreover, these gauges are located in lower elevations or valley floors. For this reason, it is hard to understand precipitation variability on slopes. Like orographic effects, configuration of coastlines displays a dominant role in the regional distribution of precipitation. Interpolation algorithms of point-scale precipitation in topographically complex regions are unable to capture the influence of orographic lifting and coastline configuration on precipitation.

The scope of this study is to determine the accurate distribution of precipitation over the coastal part of Eastern Black Sea Region. For this purpose, a water balance approach is performed over the poorly gauged study area to figure out the orographic influence, then, the resulting map is combined to regression equations developed to represent coastline effects and precipitation variability on valleys.

1.2 Outline of the Study

This study is composed of ten chapters. Chapter 2 presents the literature review. Chapter 3 gives the information about the study area and data to be used. In the fourth chapter, the relationship between precipitation and geographical/topographical variables and the effect of the coastline configuration on precipitation is determined. These relationships are converted to regression equations in Chapter 5. By using regression equations and conventional methods, precipitation (isohyetal) maps are generated. The accuracy of isohyetal maps is checked by means of long-term runoff coefficients in Chapter 6, showing that precipitation is underestimated for the study area. This result points out to apply a different approach which is water balance method for true estimation of precipitation. For the application of water balance method, flow depth and evapotranspiration maps are delineated in Chapters 7 and 8,

respectively. Flow depth and evapotranspiration maps are combined to obtain the new isohyetal map in Chapter 9. The new map is corrected using regression equations which are found in Chapter 5. This correction is made to define the precipitation variability truly in the valleys. Because rain gauges are located mostly in the valley floors, and regression equations can obviously represent the precipitation in valleys. Consequently, it can be said that precipitation distribution on slopes is described by water balance and that on valleys by regression equations. The last chapter includes the conclusions of this study.

2. LITERATURE REVIEW

In this study, a number of hydrometeorological variables; precipitation, streamflow, evapotranspiration, are used together with the concepts such as hydrological mapping and runoff coefficient. Each of these variables and concepts has extensively been studied in literature. Therefore, literature review is provided for every concept separately in the following subchapters.

2.1 Literature Review for Precipitation

Different methods using point-scale precipitation data have been developed to predict the distribution of precipitation in hydrological basins. Daly et al. (1994) divided precipitation distribution methods into three major groups: graphical, numerical and topographical methods. Graphical methods include isohyet mapping and Thiessen polygon. Numerical methods are sometimes classified as deterministic and geostatistical methods (Johnston et al., 2003). Deterministic interpolation methods use mathematical functions to calculate the values at unknown locations based either on the degree of similarity (e.g. Inverse Distance Weighted) or the degree of smoothing (e.g. Radial Basis Function) in relation with neighboring data points. Geostatistical methods use both, mathematical and statistical methods to predict values at unknown locations and to provide probabilistic estimates of the quality of the interpolation based on the spatial autocorrelation among data points. Topographical methods, involve the correlation of point precipitation data with an array of geographical and topographical variables such as slope, exposure, elevation, location of barriers and wind speed and direction (Daly et al., 1994; Burrough and McDonnell 1998; Johnston et al., 2003).

Aforementioned methods have been used widely. Related studies mostly include comparisons of these methods. A detailed description of interpolation techniques such as Thiessen, polynomial, Inverse Distance Weighted (IDW), kriging were given, applied and compared using annual precipitation of 29 gauges in USA by Tabios and Salas (1985). Thiessen and different types of kriging were used and their results were compared and discussed by Pardo-Iguzquiza (1998). Ordinary and

Indicator kriging for mapping precipitation in Switzerland were used by Atkinson and Lloyd (1998). Dirks et al. (1998) and Tomczak (1998) used a simpler method like IDW to interpolate precipitation. Four forms of kriging and three forms of thin plate splines were discussed by Boer et al. (2001) to predict monthly mean precipitation in Jalisco State of Mexico. IDW and Kriging were in the study by Shi et al. (2007) for the purpose of obtaining the most suitable interpolation method for Ganjiang region in China.

For mountainous regions, Hevesi et al. (1992a, b) used multivariate geostatistics (cokriging) based on the significant precipitation-elevation relationship in Nevada and also compared it to alternative estimation methods such as IDW, kriging, regression. Ordinary kriging and modified residual kriging were applied to map annual maximum daily rainfall in the mountainous region of Scotland by Prudhomme and Reed (1999). Goovaerts (2000) investigated simple kriging, kriging with external drift, and cokriging methods to estimate the annual rainfall distribution based on measurements at 36 climatology stations in a 5000 km² area in Portugal. Simple kriging with local mean was determined as the best method in comparison with the inverse squared distance, linear regression with elevation, and Thiessen polygons. Sarangi et al. (2005) combined different kriging types to predict spatial variability of precipitation. Lloyd (2005) did the comparison between IDW, kriging and moving window regression on monthly precipitation data of Great Britain. Diodato (2005) applied geostatistical methods on annual and seasonal precipitation of Benevento mountainous region in southern Italy. In this study, in addition to ordinary kriging, cokriging was used with two auxiliary variables such as terrain elevation data and a topographic index. A comparative analysis of interpolation techniques like IDW, Polynomial, Splines, Ordinary Kriging and Universal Kriging was performed for Himalayas by Basistha et al. (2008). Fernandez and Bravo (2007) employed the geometric estimation methods such as triangulation and inverse distance and geostatistical estimation methods such as simple kriging, ordinary kriging, universal kriging, lognormal kriging, and cokriging for making annual precipitation maps of northwest of Spain. Saghafian and Bondarabadi (2008) examined four interpolation methods including weighted moving average, thin plate smoothing splines, and two kriging variants for estimating annual precipitation distribution in the southwest of Iran.

In Turkey, Tezcan and Arikan (1993), in order to estimate the spatial behavior of the orographic precipitation over the karstic areas in southern Turkey, used cokriging interpolation technique. Cetin and Tulucu (1998) determined the spatial variability of monthly precipitation of Eastern Mediterranean Region by means of kriging. Bostan and Akyürek (2007a, b) modeled precipitation distribution over Turkey using cokriging and geographically weighted regression. Keskiner (2008) produced precipitation maps of Seyhan River basin for 50%, 80% and 90% probability levels with the help of ordinary Kriging, Cokriging and multiple regression techniques.

In addition to graphical and numerical (deterministic and geostatistical) methods, in terms of topographical methods, different variables which affect the distribution of precipitation have been investigated in the literature. Some studies were carried out to understand the relationship between precipitation and geographical and topographical variables such as elevation (Osborn, 1984; Puvaneswaran and Smithson, 1991; Daly et al. 1994, Park and Singh, 1996; Marquinez et al., 2003; Naoum and Tsanis, 2004; Ranhao et al., 2008) or wind speed, wind direction, slope, orientation, exposure and distance from sea (Puvaneswaran and Smithson, 1991; Basist et al., 1994; Park and Singh, 1996; Richard et al., 2000; Marquinez et al., 2003; Ranhao et al., 2008) whereas others used latitude, and longitude (Agnew and Palutikof, 2000; Naoum and Tsanis, 2004; Ranhao et al., 2008).

Foregoing studies can be extended; nevertheless, the effect of coastline configuration on precipitation in coastal zones has not yet been extensively investigated (Hastenrath, 1967; Baker et al., 2001). Besides, although a few studies exist related to precipitation distribution of some regions of or over Turkey using geostatistical method, no investigation is made for Eastern Black Sea Region, particularly.

2.2 Literature Review for Runoff Coefficient

The runoff coefficient is a widely used and often reported parameter describing basin response from event-based scale to annual time scale. Annual runoff coefficients are total runoff over total precipitation, i.e. percentage of precipitation that is not lost by evapotranspiration, assuming storage as negligible at annual basis and groundwater outflow out of the catchment does not exist (Savenije, 1996; McNamara et al., 1998; Blume et al., 2007).

The runoff coefficient is quantitatively related to various interrelated factors such as precipitation types, e.g. orographic, in addition to seasonal distribution of precipitation, vegetation types and cover, transpiration rate, geological outcrops, infiltration rates, and finally, the topography of a catchment area (Kadioglu and Sen, 2001).

As summarized previously, long term runoff coefficients of the study area are used to validate precipitation map. The effect of orography on the study area can be identified by runoff coefficients.

No study directly using runoff coefficients for validation of precipitation maps is met; however a few studies are available involving runoff coefficients in terms of determination of orographic effects. In the study by Fekete et al. (2000), runoff ratios were simulated on a global 0.5° grid using a simple water balance model. The authors then used these runoff ratios and their gridded estimates of runoff (which are a composite of simulated runoff and observed streamflow distributed onto the watershed) to calculate a new precipitation value. Xia (2008) used an optimization algorithm which is minimizing the errors between observed and simulated annual runoff ratios in selected basins. Through this optimization process, optimal orographic scaling factors can be estimated, and then an optimal precipitation adjustment due to orographic effects can be calculated. Global scale datasets were used in the study by Fekete et al. (2000) while 24 basins over the world were selected by Xia (2008).

2.3 Literature Review for Flow Depth Mapping

A hydrological water balance approach is applied to develop an adjustment for underestimated precipitation which is proved by long term runoff coefficients for mountainous study regions. For this purpose, streamflow observations are distributed over basins of the study region thereby a flow depth map is obtained. Most of the observed streamflow has a 5% error and some has up to 10%–15% error in mountainous regions, however, precipitation errors are usually 30% or higher in cold regions, particularly (Milly and Dunne, 2002).

Generation of flow depth map for the study region is inspired from the study by Huang and Yang (1998). They defined flow depth as a regionalized phenomenon and used a centroid based method of regional analysis by applying Kriging to estimate

unregulated long-term streamflows corresponding to various exceedance probabilities over time and space. Gauged flow values were located at the centroids of the basins as previously used in Rochelle et al. (1989), Krug et al. (1990) and Bishop and Church (1992) for runoff mapping. This approach was also used by Merz and Blöschl (2005) for flood regionalization. The main idea in this study is that spatial proximity is a significantly better predictor of regional flood frequencies than are basin attributes.

The total area to be mapped can sometimes be divided into fundamental units by means of subdividing a larger drainage basin into sub-basins or into a regular grid network. The drainage basins can be approximated by points in space and during the mapping processes, the simplest method is to use an average of the flow from all the small basins which fall within a grid cell. A disadvantage of this method is that all cells contain observation points. Arnell (1995) applied this method and used Triangulated Irregular Network (TIN) technique (i.e. linear interpolation within the facets of the TIN defined by the gauging station considered as nodes).

Other studies are based on disaggregation and covariance approaches instead of geostatistical methods such as kriging. Sauquet et al. (2000) proposed an approach for mapping river runoff. The method is based on a hierarchical disaggregation principle and can assess runoff for elements of an arbitrary partition of a gauged drainage basin like sub-basins and grid cells. This procedure was extended and generalized by Sauquet (2006). The developed approach applied to mean annual runoff is based on geostatistical interpolation procedures coupled with empirical relationships and is illustrated by an application to assess water resources in France. The performance of the developed approach was tested against two other geostatistical methods (ordinary kriging and residual kriging). Skoien et al. (2006) presented Top-kriging, or topological kriging, as a method for estimating streamflow-related variables in ungauged catchments. The concept was built on the work of Sauquet et al. (2000) and extends it in a number of ways. Although they tested the method for the case of the specific 100-year flood for two Austrian regions, they also suggested that Top-kriging can be used for spatially interpolating a range of streamflow-related variables including mean annual discharge, flood characteristics, low flow characteristics, concentrations, turbidity and stream temperature.

2.4 Literature Review for Evapotranspiration

Evapotranspiration is hard to directly measure because of the difficulties in quantifying atmospheric evaporative demand and plant transpiration (Xing et al., 2008). However, estimates of evapotranspiration are necessary in many of hydrological studies.

Several studies are available to estimate evapotranspiration. For example, via pan coefficient (K_p), pan evaporation data are widely used to estimate reference or potential evapotranspiration (Doorenbos and Pruitt, 1977; Cuenca, 1989; Snyder, 1992; Raghuwanshi and Wallender, 1998; Conceicao, 2002; Gundekar et al., 2008). There are a number of methods for estimating evoptranspiration such as Thornthwaite, Blaney-Criddle, Penman-Monteith, Priest-Taylor, Hargreaves-Samani, Turc which were used by Lu et al. (2005); Summer and Jacobs (2005); Zhang et al. (2007); Xing et al. (2008); Weib and Menzel (2008). It is worth mentioning that water balance methods were is some cases used to predict actual evapotranspiration particularly (Menzel and Lang, 1998; Kolka and Wolf, 1998; Boronina et al., 2005).

As an alternative, satellite remote sensing has become a pragmatic approach for evapotranspiration estimation, with the availability of large amounts of remote sensing data and development of various modeling techniques. Because remotely sensed data have the advantage of large area coverage, frequent updates and consistent quality, remote sensing-based evapotranspiration estimation has been a subject of many studies (Kite and Pietroniro, 1996; Stewart et al, 1999; Irmak et al., 2007; Mu et al., 2007; Sobrino et al., 2007; Wang et al., 2007; Khan et al., 2010)

In addition to evapotranspiration estimates, spatial distribution of evapotranspiration is also another significant subject that should be taken into consideration. Geostatistics is applied to interpolate evapotranspiration (Dalezios et al., 2002; Li et al., 2003; Yue et al., 2003) as it is used in many previous cases such as precipitation, temperature, streamflow etc.

Satellite-based estimates of evapotranspiration in Gediz basin, western of Turkey were presented in Granger (2000), these estimates were also compared to a distributed hydrological model in the study by Kite et al. (2001). Another study related to evapotranspiration in Gediz basin was done by Karatas et al. (2006). They used SEBAL (Surface Energy Balance Algorithm for Land) model.

Evapotranspiration estimates which were obtained from remotely sensed data and conventional formulas separately were compared by Gokdemir and Arikan (2003) for Afyon-Akarcaý basin, located in Central Anatolia. A larger scale evapotranspiration estimation study for Turkey was done by Sahin et al. (2004). For nine agricultural regions covering 20 meteorological stations in total, daily evapotranspiration values were estimated by using different methods for time periods of 3 months, 8 months and a year.

2.5 Motivation of Study

The scope of this study is to determine the accurate distribution of precipitation over the coastal part of Eastern Black Sea Region. The selected study area in this study is a mountainous coastal area which means precipitation is influenced by both orography and humidity coming from sea along with winds. Additionally, weather gauges are non-uniformly distributed in valleys and there is no gauge available higher than a certain elevation. If foregoing causes are considered, it is obviously comprehended that inaccurate results arise due to direct use of available gauge data in determination of precipitation distribution. Instead, in this study, water balance approach is applied namely precipitation distribution is determined as an assessment of streamflow together with evapotranspiration at annual scale.

The aim and motivation of this study can be summarized as follows together with studies to be done.

- ✓ Although various investigations exists in the literature about relationship between precipitation and different variables, the effect of the coastline configuration on precipitation in coastal zones has not yet been extensively investigated in term of global and regional scale. Turkey is encircled by seas on three sides and configuration of coastlines displays a dominant role in the regional distribution of precipitation. Despite this, no investigation relevant the effect of coastlines on precipitation is made up till now. Furthermore, it is assumed that orographic effects may be seen in Eastern Black Sea Region but this idea is not proved yet. Besides, although a few studies are existing related to precipitation distribution of some regions of or over the entire Turkey using the geostatistical method, no investigation is made for Eastern Black Sea Region, particularly.

- ✓ Annual runoff coefficients are used to validate precipitation maps in this study. No study using runoff coefficients directly for validation of precipitation maps is met, however a few studies are available involving runoff coefficients in terms of determination of orographic effects.
- ✓ In order to determine spatial distribution of precipitation accurately, and to understand the effects of orography properly, precipitation is predicted inversely using streamflow and other losses based on the continuity equation. There are some examples about water balance-precipitation estimation, particularly at global scale. On the other hand, this approach can not be applied on any region of or over the entire Turkey.
- ✓ Studies on interpolation of flow depth have no such long past that the approach presented in this study is firstly applied on a region of Turkey. Even if the main purpose is to use flow depth map to be obtained for precipitation distribution, it can also be useful for flow estimation on ungauged locations in the Eastern Black Sea Region.
- ✓ Evapotranspiration rates are particularly required for many applications in agricultural management. Inland part of Eastern Black Sea Region cannot be accepted as an agricultural area due to its though topography, thus evapotranspiration measurements and studies for inland are limited. Most of pan evaporation data obtained from the inland meteorological gauges are missing. In this study, pan evaporation, potential and actual evapotranspiration estimations are carefully investigated for generating the most exact evapotranspiration map.
- ✓ This study is the first one that combined water balance-precipitation estimation and regression equations which is developed to define the relationships between precipitation and geographical/topographical variables and coastline configuration.
- ✓ In recent years, assessment of hydroelectrical potential energy is increasing in Turkey depending on energy demand and modified energy production laws. The study area, Eastern Black Sea is an efficiency region in terms of small hydropowers, because of its precipitation amount, surface water potential and high head. Current case motivates true estimation of surface water potential, therefore requires determination of precipitation distribution and prediction of point-scale precipitation over the entire study area.

3. STUDY AREA AND DATA USED

3.1 Study Area

The coastal part of the Eastern Black Sea Region which is located in the north east of Turkey, between the coordinates $40^{\circ} 31'$ - $41^{\circ} 24'$ North and $38^{\circ} 08'$ - $41^{\circ} 26'$ East is selected as study area. This coastal part of the region can be defined the area between the Eastern Black Sea Mountain chain and the Black Sea as seen in Figure 3.1. These high mountain ranges run parallel to the sea coast as the north boundary of the study area, and rise to more than 3000 m above mean sea level (MSL). The Black Sea Region has a steep rocky coast with some rivers that cascade through the gorges of the coastal ranges.

In the coastal area of the Eastern Black Sea Region, mild and humid climate dominates. Snowfall may be seen in winter. Yearly average temperature is about 14-15 °C in the coastline, however it decreases with increasing elevation. The average precipitation of the coastal area of this region is more than 1000 mm, for instance Rize receives approximately 2200 mm mean annual total precipitation (Agiralioglu et al., 2009).

3.2 Meteorological Data

3.2.1 Precipitation data

Mean annual precipitation observations are used in this study. Precipitation data were taken from 38 rain gauges of which 19 are located on the coastline of the area. As seen from Figure 3.1, rain gauges are numbered from 1 to 19 for the coast, and from 20 to 38 starting from west to east. Characteristics of the 38 grouped as coast and inland rain gauges are shown in Table 3.1. Gauges are generally established in valley floors, settlement areas. In the study area, no gauge is established higher than 1700 m. Namely, the elevations of the gauges which are used in the study range from 6 to 1700 m.

Table 3.1 : Characteristics of rain gauges.

Coastal					Inland				
No	Gauge No.	Operated by	Gauge name	Elev. (m)	No	Gauge No.	Operated by	Gauge name	Elev. (m)
1	1453	DMİ	Bulancak	10	20	22-018	DSİ	Sofulu	600
2	17034	DMİ	Giresun	38	21	22-001	DSİ	Tamdere	1700
3	1460	DMİ	Tirebolu	70	22	22-020	DSİ	Sinir	750
4	1299	DMİ	Gorele	20	23	1623	DMİ	Tonya	900
5	1300	DMİ	Eynesil	10	24	1624	DMİ	Duzkoy	850
6	1302	DMİ	Vakfikebir	25	25	22-017	DSİ	Guzelyayla	1250
7	17626	DMİ	Akcaabat	6	26	1626	DMİ	Macka	300
8	17037	DMİ	Trabzon	30	27	22-011	DSİ	Kayaici	1050
9	1471	DMİ	Arsin	10	28	1787	DMİ	Dagbasi	1450
10	1472	DMİ	Arakli	10	29	22-016	DSİ	Koknar	1218
11	1473	DMİ	Surmene	12	30	1801	DMİ	Caykara	264
12	1475	DMİ	Of	9	31	1962	DMİ	Uzungol	1110
13	17040	DMİ	Rize	9	32	1476	DMİ	Kalkandere	400
14	1312	DMİ	Cayeli	10	33	1803	DMİ	İkizdere	800
15	17628	DMİ	Pazar	79	34	22-003	DSİ	Sivrikaya	1650
16	1156	DMİ	Ardesen	10	35	1480	DMİ	Kaptanpasa	525
17	1015	DMİ	Findikli	100	36	22-009	DSİ	Hemsin	500
18	17042	DMİ	Hopa	33	37	22-013	DSİ	Meydan	1100
19	818	DMİ	Kemalpassa	75	38	22-019	DSİ	Tunca	500

DMI (State Meteorological Service), DSI (State Hydraulics Works) with Turkish acronym

This study used a common period of 46 years between 1960 and 2005. Data record length ranges from 10 to 46 years; however, there are some gaps in the data (Table A.1). To complete the gap in any gauge record, regression equations were developed using continuous data from the neighboring gauges. The homogeneity of the data was first checked out with the double mass curve method. Trend analysis was also made with the Mann-Kendall trend test. It was found that 27 gauges out of 38 are homogeneous and no trend is available. For the remaining 11 gauges, the non-homogeneity and/or the available trends were found insignificant such that the adjusted precipitation values were found not greater than 28% of the precipitation observed. Therefore, precipitation data observed in these 11 gauges are also used. The difference between observed and adjusted data is shown in Figure 3.2 with the results of available upward/downward trends.

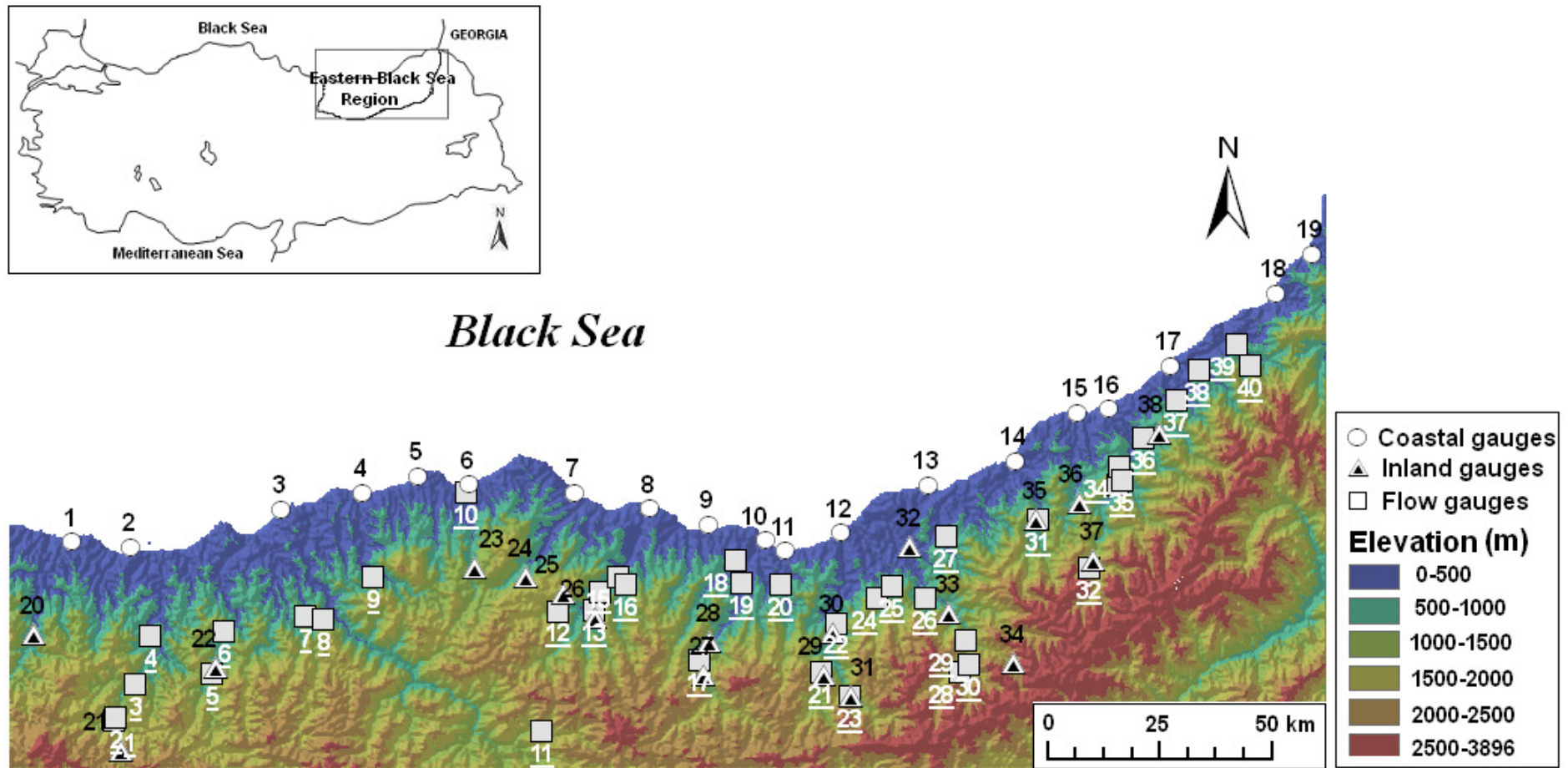


Figure 3.1 : Study area and locations of the rain and flow gauges.

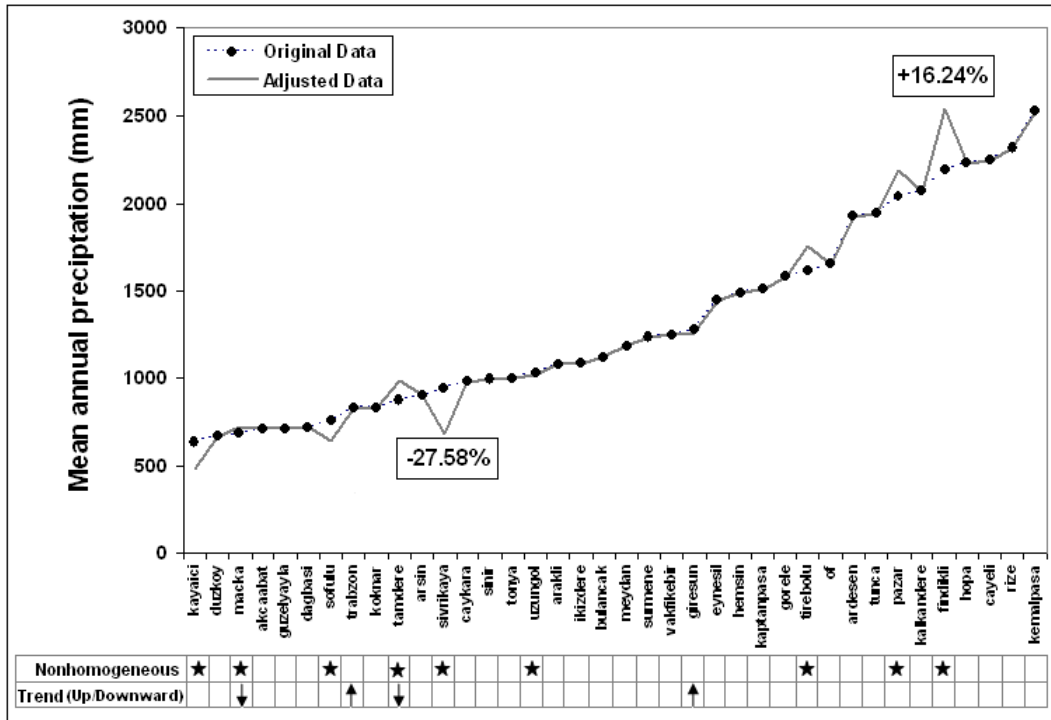


Figure 3.2 : Difference between observed and adjusted precipitation data.

In a previous study by Partal and Kahya (2006) in which Giresun, Trabzon and Rize were used as common gauges, no trend was found in Giresun and Trabzon whereas a trend was obtained in Rize. The beginning of the trend for Rize was determined as 1952. Note that the data record length in the study by Partal and Kahya (2006) ranges from 1929-1993, while in this study it covers only the years between 1960 and 2005. Giresun, Akcaabat, Trabzon, Rize, Pazar and Hopa gauges in Eastern Black Sea Region were used in the study by Gokturk et al. (2008) who found that precipitation data in the gauges were homogenous except for Giresun and Akcaabat. Sahin and Cigizoglu (2010) found Trabzon had inhomogeneous precipitation data covering period from 1974 to 2002.

3.2.2 Temperature and evaporation data

Temperature and evaporation data used in this study were obtained from DMI and DSI. Temperature data are recorded at monthly scale throughout the year whereas evaporation data are available for only eight months from April to November. Temperature and evaporation data availability is given in Table 3.2. The gauges operated by DSI only recorded evaporation data. Some gauges operated by DMI have only temperature data whereas the rest has both temperature and evaporation data.

Data record extends from 1975 to 2005; however gauges which have at least 5-year record are considered in this study.

Table 3.2 : Temperature and evaporation data availability and data range.

No	Gauge No	Gauge name	Operated by	Temperature Data	Data range	Evaporation Data	Data range
2	17034	Giresun	DMI	✓	1975-2005	✓	1975-2005
7	17626	Akcaabat	DMI	✓	1975-2005	✓	1975-2005
8	17037	Trabzon	DMI	✓	1975-2005	✓	1975-2005
13	17040	Rize	DMI	✓	1975-2005	✓	1975-2005
	17033	Ordu	DMI	✓	1975-2005	✓	1975-2005
	17624	Unye	DMI	✓	1975-2005	✓	1975-2005
6	1302	Vakfikebir	DMI	✓	1983-2005		
9	1471	Arsin	DMI	✓	1984-1995		
10	1472	Arakli	DMI	✓	1983-1996		
12	1475	Of	DMI	✓	1964-1989		
15	17628	Pazar	DMI	✓	1975-2005		
16	1156	Ardesen	DMI	✓	1984-1992		
17	1015	Findikli	DMI	✓	1989-2000		
23	1623	Tonya	DMI	✓	1976-1995		
24	1624	Duzkoy	DMI	✓	1986-2003		
26	1626	Macka	DMI	✓	1964-1997		
28	1787	Dagbasi	DMI	✓	1989-1998		
30	1801	Caykara	DMI	✓	1989-1998		
31	1962	Uzungol	DMI	✓	1983-2006		
33	1803	Ikizdere	DMI	✓	1975-1996		
20	22-018	Sofulu	DSI			✓	1983-2005
21	22-001	Tamdere	DSI			✓	1984-2004
22	22-020	Sinir	DSI			✓	1985-2005
25	22-017	Guzelyayla	DSI			✓	1980-2005
27	22-011	Kayaici	DSI			✓	1979-2002
34	22-003	Sivrikaya	DSI			✓	1980-1995
37	22-013	Meydan	DSI			✓	1980-2002
38	22-019	Tunca	DSI			✓	1984-2005

Temperature data recorded in 14 gauges are shown in Figure 3.3. To understand distribution of the data, they are drawn separately as coastal and inland gauges. As seen from Figure 3.3, coastal and inland gauges have similar temperature characteristics but inland gauges have lower temperature values than coastal gauges as expected due to topography.

Evaporation data recorded at eight gauges are depicted in Figure 3.4. These eight gauges are established in inland region of the study area. There are some gaps in the record particularly for April and November.

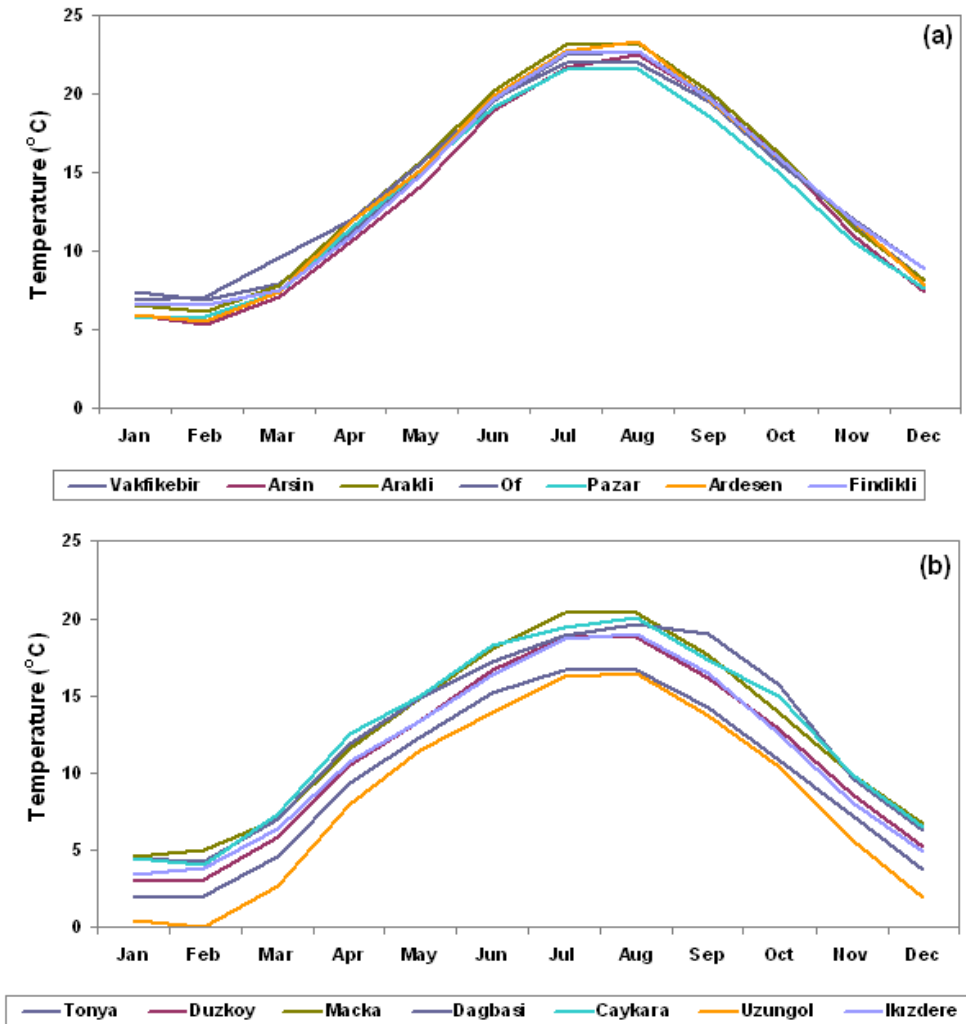


Figure 3.3 : Monthly average temperature data for (a) coastal, (b) inland region.

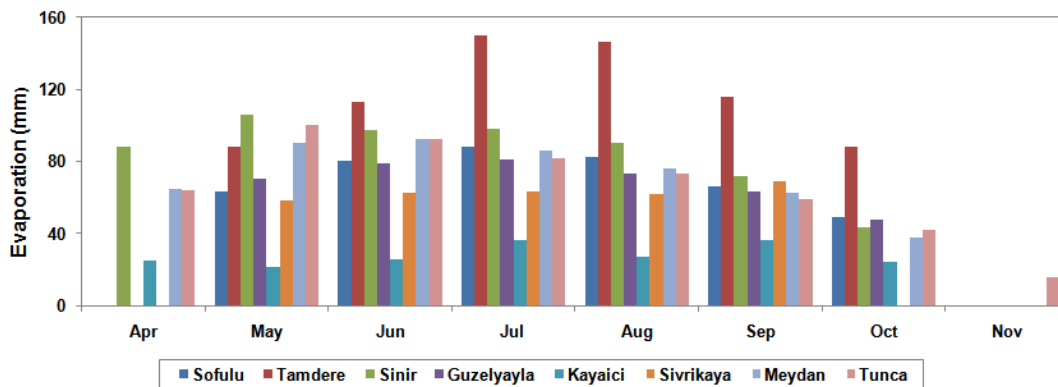


Figure 3.4 : Monthly average evaporation data for inland gauges.

The Giresun, Akcaabat, Trabzon, Rize, Unye and Ordu gauges have both temperature and evaporation data (Figure 3.5). Two gauges, Unye and Ordu, not covered by the study area are also considered. For the sake of determination of general evaporation characteristics of coastal region these gauges are used in the computations which will be explained in next chapters. As seen from Figure 3.5, the coastal gauges have almost the same temperature and evaporation characteristics.

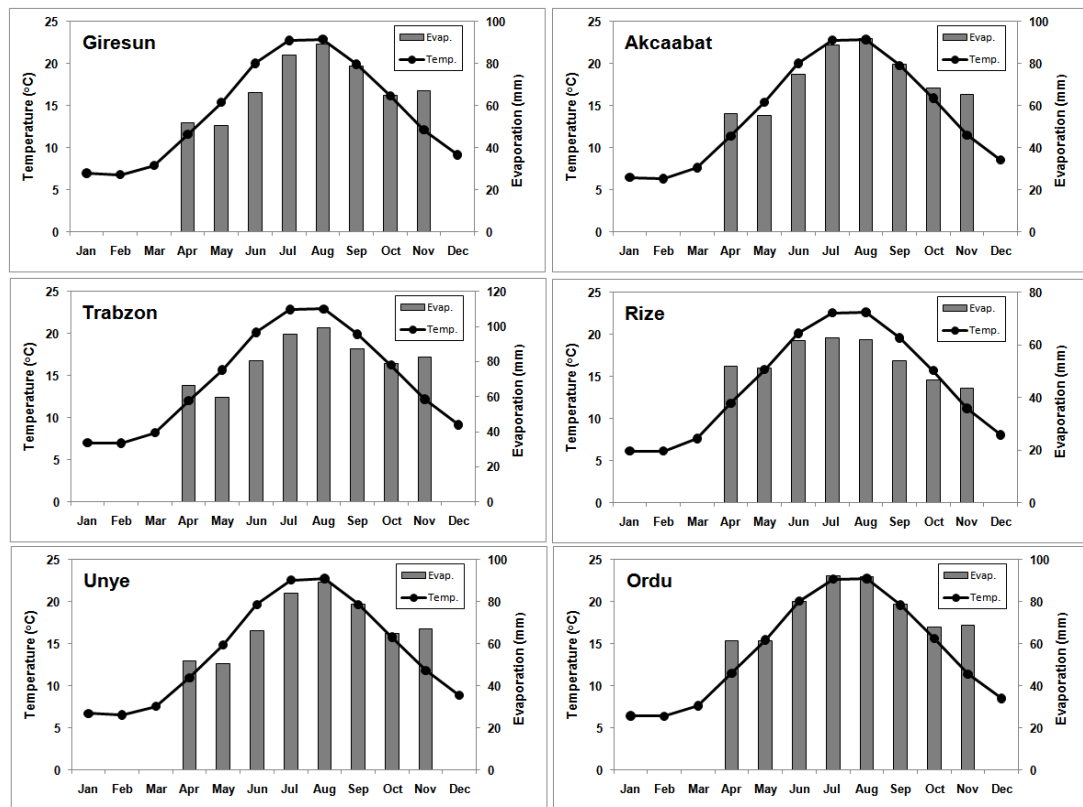


Figure 3.5 : Monthly average temperature and evaporation data for coastal gauges.

Detailed homogeneity and trend tests have been applied on temperature data of Turkey by Tayanc et al. (1998), Turkes et al. (2002), Sahin and Cigizoglu (2010) and Dikbas et al. (2010). Giresun, Trabzon and Rize gauges were used in the study by Tayanc et al. (1998) who found non-homogenous data covering the period of 1951-1990 in Giresun. Turkes et al. (2002) used Giresun, Trabzon, Rize and Hopa gauges together with other 8 gauges that these 12 gauges were defined as a region called BLS. They found that BLS had a cooling trend on annual mean temperature data which ranges from 1929 to 1999. Sahin and Cigizoglu (2010) found Giresun, Akcaabat and Hopa had inhomogeneous temperature data covering period from 1974 to 2002. Dikbas et al. (2010) detected homogeneous temperature data covering the years between 1968 and 1998 in 6 coastal gauges in the Eastern Black Sea Region.

3.2.3 Wind and Relative Humidity Data

The prevailing wind direction of the coastal part of Eastern Black Sea Region occurs between west and north part of the wind rose, mostly north and west directions (SHODB, 1991). The same information can be inferred from the number of direction in which maximum wind speed occurs. These data which are available in some coastal gauges was counted and summarized in Table 3.3. As seen from Table 3.3, the number of directions in which maximum wind speed occurs is mostly between north and west directions of the wind rose.

Table 3.3 : Number of directions in which maximum wind speed occurs.

No	Gauge No	Gauge name	Data range	Number of Max. Wind Direction															
				N	S	W	E	NW	NNW	WNW	NE	NNE	ENE	SW	WSW	SSW	SE	ESE	SSE
2	17034	Giresun	1975-2005	5	7	88		19	9	28	3	12	3	29	59	102	2		6
4	1299	Gorele	1998-1999					2						5				3	
5	1300	Eynesil	1989-1993	8	1	2	6	9			2			9				20	
6	1302	Vakfikebir	1983-1990 2000-2005	1	26	45	1	22			37			13				5	
7	17626	Akcaabat	1975-2005	2	23	100	18	31	7	94	8	3	7	24	13	12	6	7	15
9	1471	Arsin	1984-1995		20		4	84		1	7			2				9	
10	1472	Arakli	1983-1996	14	19	5	3	86						23				4	
12	1475	Of	1960-1978	16	23	8	4	153	2	1	2		1	44	1	3	30		
13	17040	Rize	1975-2005	1	6	83	3	37	14	125	1	8	1	5	50	25	1		12
16	1156	Ardesen	1984-1992		15	56								2					
17	1015	Findikli	1989-2000	2	23	5	2	5			7			32				32	
Total				49	163	392	41	448	32	249	67	23	12	188	123	142	112	7	33

Relative humidity together with the mean wind speed data are used to determine evaporation. Availability of relative humidity and mean wind speed data and data were given in Table 3.4. Among these gauges, Giresun (2), Akcaabat (7), Trabzon (8) and Rize (13) have also evaporation data. Data are available at monthly time interval. Relative humidity and wind speed data of eleven gauges are shown in Figure 3.6.

The homogeneity tests on relative humidity data of Ordu, Unye, Giresun (2), Akcaabat (7), Trabzon (8), Rize (13), Pazar (15), and Hopa (18) among 232 gauges over Turkey was studied by Sahin and Cigizoglu (2010) who found that Trabzon (8), Rize (13), Hopa (18) and Ordu had inhomogeneous relative humidity data.

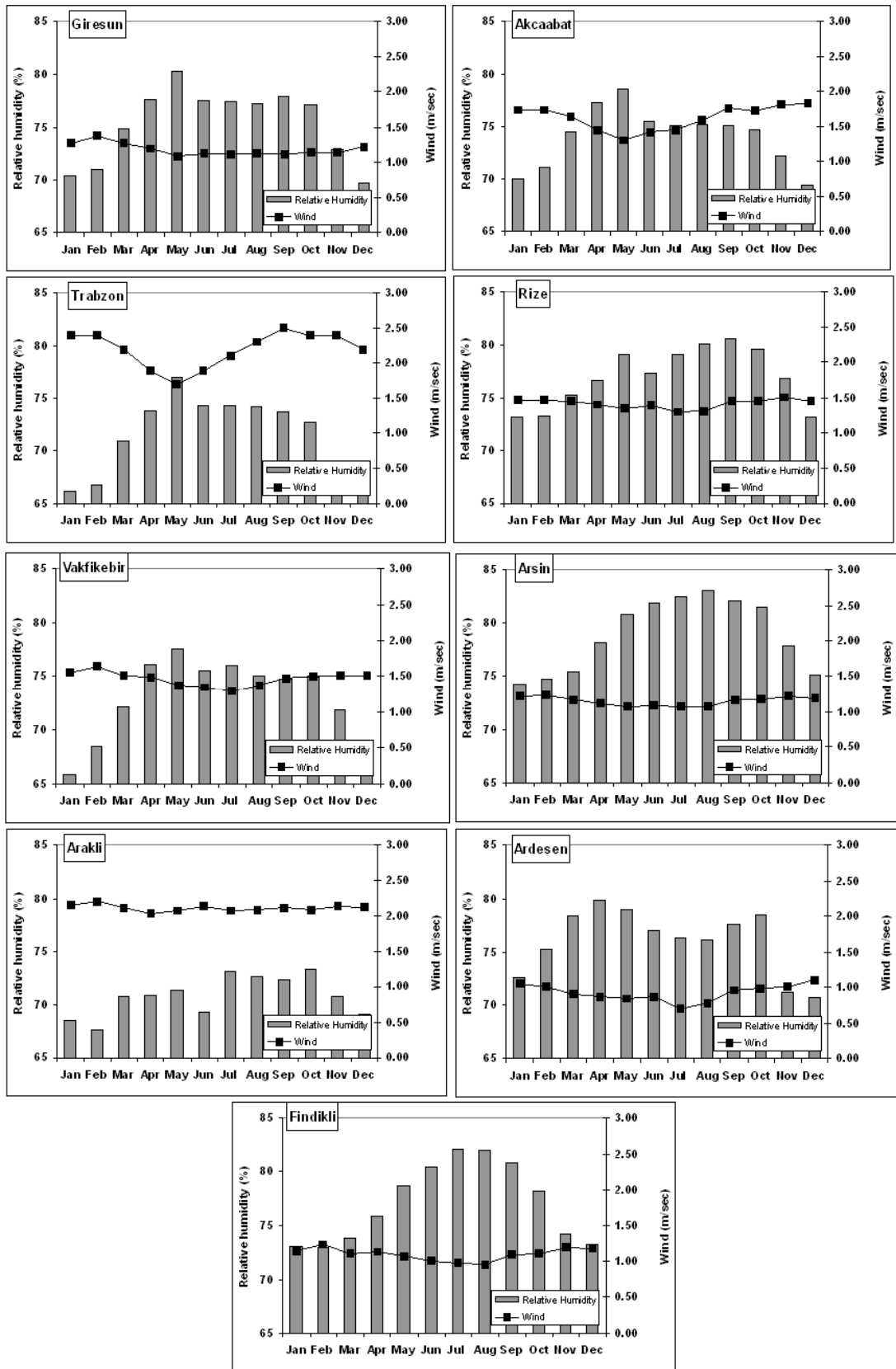


Figure 3.6 : Gauges which have relative humidity and wind speed data (Giresun, Akcaabat, Trabzon and Rize gauges have also evaporation data).

Table 3.4 : Mean wind speed and mean relative humidity data and data range.

No	Gauge No	Gauge name	Operated by	Data range	
				Mean wind speed	Mean relative humidity
2	17034	Giresun	DMI	1975-2005	1929-2005
6	1302	Vakfikebir	DMI	1983-1990,2000-2005	1983-1990,2000-2005
7	17626	Akcaabat	DMI	1975-2005	1975-2005
8	17037	Trabzon	DMI	1975-2005	1975-2005
9	1471	Arsin	DMI	1984-1995	1984-1995
10	1472	Arakli	DMI	1983-1996	1983-1996
12	1475	Of	DMI	1964-1994	1975-1994
13	17040	Rize	DMI	1975-2005	1929-2005
15	17628	Pazar	DMI	1961-2010	1975-2006
16	1156	Ardesen	DMI	1984-1986,1988-1992	1984-1986,1988-1992
17	1015	Findikli	DMI	1989-1995,1997-2000	1989-1995,1997-2000

3.3 Streamflow Data

Mean annual flow observations from 40 flow gauges are used in this study. Locations of the gauges are shown in Figure 3.1. Characteristics of the flow gauges are also given in Table 3.5. Number of the most right column of Table 3.5 corresponds to numbers on the map in Figure 3.1.

The flow record length ranges from 10 to 49 years between 1944 and 2006 with some gaps in the data (Table A.2). To complete the gap in any gauge record, regression equations were developed using continuous data from the neighboring gauges. The observed flow is not influenced by any upstream dam or water structure. Similar to precipitation data analysis, the homogeneity of the data was first checked out with the double mass curve method. Trend analysis was also made with the Mann-Kendall trend test. It was found that 22 gauges out of 40 were homogeneous and no trend was available. For the remaining 18 gauges, the non-homogeneity and/or the available trends were found insignificant. The most significant difference between the observed and the adjusted flow was found 17.45% in Kanlipelit (2206). All other gauges showed less significant differences such that mean annual flow recorded were used without any adjustment in these 18 flow gauges. The difference between observed and adjusted data is shown in Figure 3.7 together with the results of available upward/downward trends.

Table 3.5 : Characteristics of flow gauges.

Gauge No	Gauge name	Area (km ²)	Elevation (m)	Stream	Operated by	No
2202	Agnas	635.7	78	Kara	EIE	19
2206	Kanlipelit	708	257	Değirmendere	EIE	14
2213	Dereli	713.0	248	Aksu	EIE	4
2215	Derekoy	445.2	942	Camlidere	EIE	29
2218	Simsirli	834.9	308	Iyidere	EIE	26
2228	Bahadirli	191.4	17	Fol	EIE	10
2232	Topluca	762.3	233	Firtına	EIE	34
2233	Toskoy	223.1	1296	Toskoy	EIE	28
2236	Ikisu	317.2	1037	Aksu	EIE	1
22006	Koprubasi	156	60	Abuçağlayan	DSI	38
22007	Serah	154.7	1170	Haldizen	DSI	23
22013	Suttasi	124.9	188	Kavraz	DSI	8
22034	Findikli	258.6	258.6	Yanbolu	DSI	18
22044	Aytas	421.2	510	Kara	DSI	17
22049	Baskoy	186.2	75	Kapistre	DSI	39
22052	Ulucami	576.8	260	Solaklı	DSI	22
22053	Ortakoy	173.6	150	Surmene	DSI	20
22057	Alcakkopru	243	700	Ogene	DSI	21
22058	CucenKopru	162.7	240	Gorele	DSI	9
22059	Ciftdere	121.5	250	Galyan	DSI	16
22061	Ortakoy	261	380	Altn	DSI	13
22062	Konaklar	496.7	300	Hemsin	DSI	33
22063	Mikronkopru	239.2	370	Halo	DSI	35
22066	Cevizlik	115.9	400	Maki	DSI	25
22068	Yenikoy	171.6	470	Baltaci	DSI	24
22071	Ikisu	292.7	990	Aksu	DSI	2
22072	Arili	92.15	150	Arili	DSI	37
22073	Tuglacik	397.9	400	Yagli	DSI	6
22074	Cat	277.6	1250	Hemsin	DSI	32
22076	Kemerkopru	302.2	230	Durak	DSI	36
22078	Toskoy	284.3	1210	Toskoy	DSI	30
22080	Sinirkoy	296.9	650	Yagli	DSI	5
22082	Komurculer	83.3	250	Salarha	DSI	27
22084	Ikisu	149.6	1450	Korum - Yagli	DSI	11
22085	Kaptanpasa	231.2	480	Senoz	DSI	31
22086	Ogutlu	728.4	160	Degirmendere	DSI	15
22087	Hasanseyh	256.8	370	Gelevera	DSI	7
22088	Ormanustu	150	770	Macka	DSI	12
22089	Kucukkoy	66.37	310	Balli	DSI	40
22090	Alancik	470.2	700	Aksu	DSI	3

EIE (Electrical Power Resources Survey and Development Administration), DSI (State Hydraulics Works) with Turkish acronym

significant. No trend was found in 2213. It should be pointed out once again that the data period is between the years of 1968-1997.

3.4 Digital Elevation Model Data

Digital elevation model (DEM) is generated from Shuttle Radar Topographical Mission (SRTM) with about 90 m resolution. Universal Transverse Mercator (UTM) coordinate system which is a grid-based method of specifying locations on the surface and a practical application of a 2-dimensional Cartesian coordinate system (Url-1, 2010) is used in the study.

Elevation of both rain and flow gauges, flow direction and accumulation which are the requirements of stream network, drainage basin area of the flow gauges are delineated in Geographical Information System (GIS) environment.

Automated extraction of surface drainage, stream networks, drainage divides, drainage networks and associated topologic information, and other hydrography data from DEMs has advanced considerably over the past decade and is now routinely a part of most GIS software packages. The automated techniques are faster and provide more precise and reproducible measurements than traditional manual techniques applied to topographic maps (Johnson, 2009). The process of operations for extracting flow direction and accumulation, stream network and basins is illustrated in Figure 3.8.

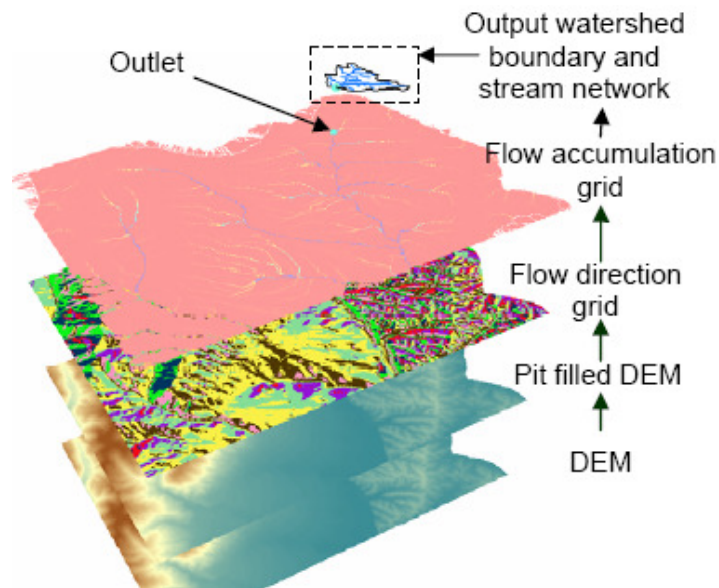


Figure 3.8 : Extracting flow direction and accumulation, stream network and basins (Chinnayakanahalli et al., 2006).

To conduct watershed analyses with a DEM, watershed surface must be hydrologically connected. In other words, every DEM cell must flow into the next downstream cell until the “water” flows off the edge of the grid. This connectivity within the DEM can be disrupted by “pits”. Pits are low elevation areas in DEMs that are surrounded by higher terrain that disrupts the flow path (Figure 3.9). Pits can naturally occur or simply artifacts of modeling the continuous surface of the earth. Filling pits creates a hydrologically connected DEM for watershed analyses (Chinnayakanahalli et al., 2006)

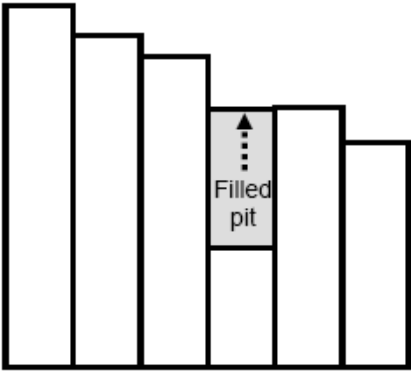


Figure 3.9 : Cross section of DEM surface.

Flow direction is the direction from each cell to its steepest down slope neighbor and calculated from the pit filled DEM (Figure 3.10).

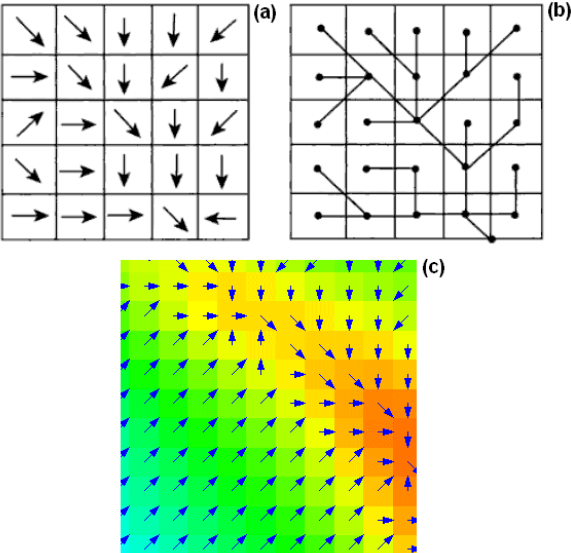


Figure 3.10 : Physical representation of flow direction grids (a) directional arrows, (b) flow network and (c) flow direction grid (modified from Maidment, 2002 and Url-2, 2010).

With the flow-direction grid, it is possible to sum the number of uphill cells that “flow” to any other cell. This summation can be done for all cells within a grid to create a “flow-accumulation” grid in which each cell-value represents the number of uphill cells flowing into it (Figure 3.11).

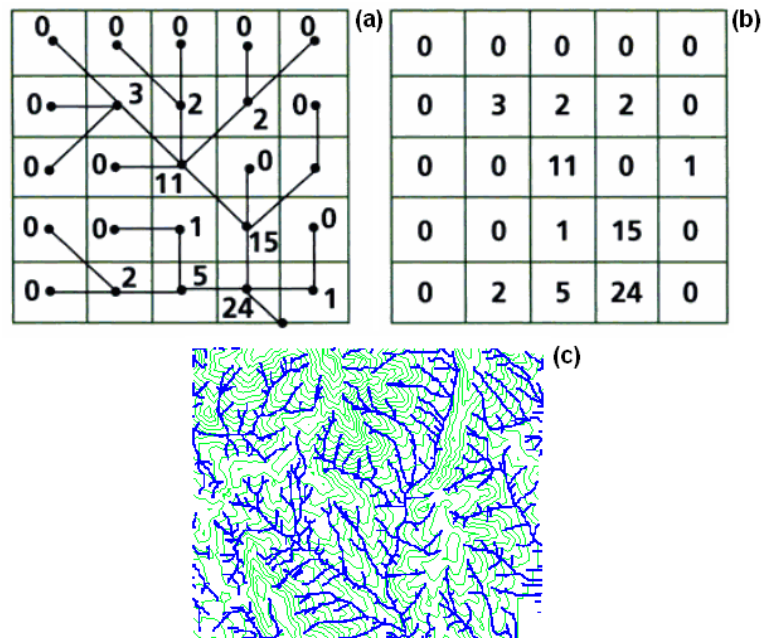


Figure 3.11 : (a, b) Number of cells draining into a given cell along the flow network and (c) flow accumulation grid (modified from Maidment, 2002 and Url-2, 2010).

A stream network can be created by querying the flow accumulation grid for cell values above a certain threshold (Chinnayakanahalli et al., 2006) which means that all cells whose flow accumulation is greater than the threshold value are classified as stream cells while remaining cells are considered the land surface draining to the streams (Maidment, 2002). The threshold value was chosen 500 in this study.

By following the flow direction grid backward, all of the cells that drain thorough a given outlets which corresponds to the flow gauge points for this study can be determined. These cells can then be selected and converted to a polygon representing the basin. Figure 3.12 shows the flow direction and flow accumulation map of the study area. The drainage basins using flow direction and accumulation grids can be seen in Figure 3.13.

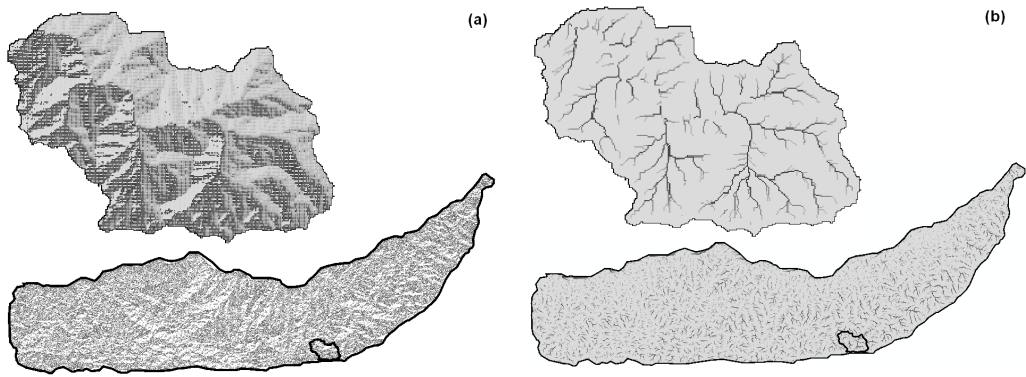


Figure 3.12 : Grids; (a) flow direction and (b) flow accumulation.

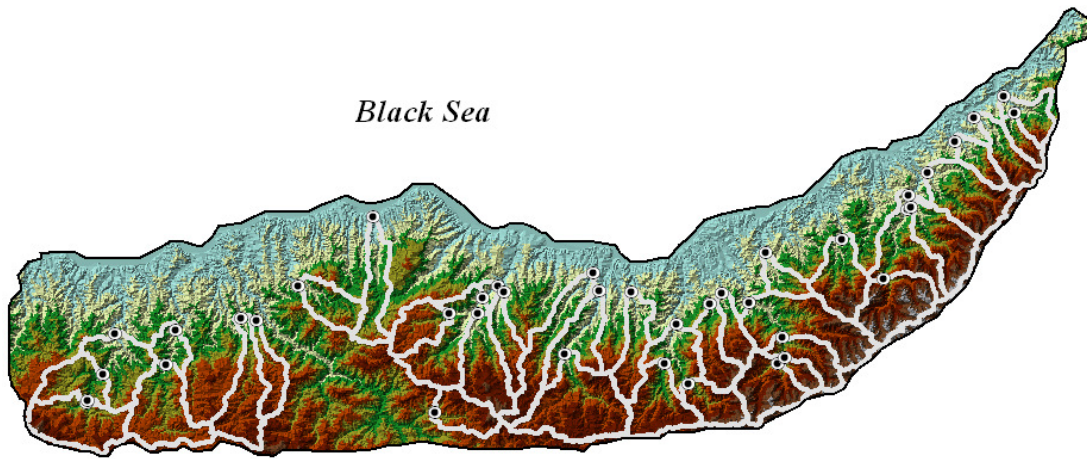


Figure 3.13 : Drainage basins of the flow gauges.

4. EFFECTS OF GEOGRAPHICAL/TOPOGRAPHICAL PARAMETERS ON PRECIPITATION DISTRIBUTION

In order to understand the spatial variability of precipitation, the relation between mean annual precipitation and topographical/geographical variables is investigated for the coastal area of the Eastern Black Sea Region. The variables are taken as longitude, latitude, distance from sea, elevation and coastline angle.

4.1 Effects of Geographical/Topographical Parameters

4.1.1 Effects of longitude

Mean annual precipitation versus longitude is evaluated and depicted in Figure 4.1 for the study area. Gauges are divided into two groups – coastal and inland – since coastal and inland gauges have similar precipitation-longitude variation but different precipitation amounts, as seen from Figure 4.1. In the study area, precipitation increases slightly with longitude. This increment can be explained by two reasons (i) location of the mountains, (ii) coastline configuration. From the west to east direction, the Eastern Black Sea Mountains become higher and closer to the coastline. Additionally, the Caucasus Mountain range, which occasionally reaches the altitude of about 5000 m, also follows the boundary of the Black Sea region. Humid air coming with the westerly and northerly winds is compressed between these two mountain chains and produces higher precipitation. Therefore, the eastern part of the study area, namely, coastal gauges such as Rize (13), Cayeli (14), Pazar (15), Ardesen (16), Findikli (17), Hopa (18), Kemalpasa (19) and inland gauges such as Kaptanpasa (35), Hemsin (36), Meydan (37), Tunca (38) receive greater precipitation than do those in the western part of the study area. Figure 4.1 also shows that the spatial distribution of mean annual precipitation of the coastal and inland gauges approximately forms the shape of the coastline. This clearly indicates the effect of the coastline configuration.

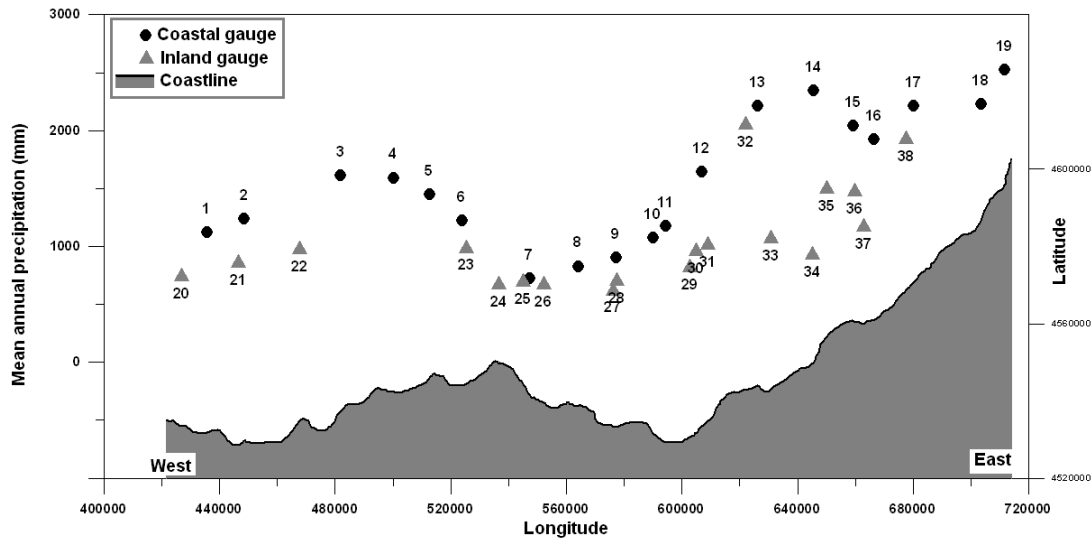


Figure 4.1 : Distribution of mean annual precipitation versus longitude.

4.1.2 Effects of latitude

The relationship between mean annual precipitation and latitude is investigated and depicted in Figure 4.2. Mean annual precipitation increases slightly with the latitude from west to east. The difference in precipitation characteristics for coastal and inland gauges can also be seen in this figure. The North-eastern side where Rize (13), Cayeli (14), Pazar (15), Ardesen (16), Findikli (17), Hopa (18), Kemalpasa (19) gauges are located, receives more precipitation than does the central zone of the study area, most probably because of the westerly and northerly prevailing wind directions.

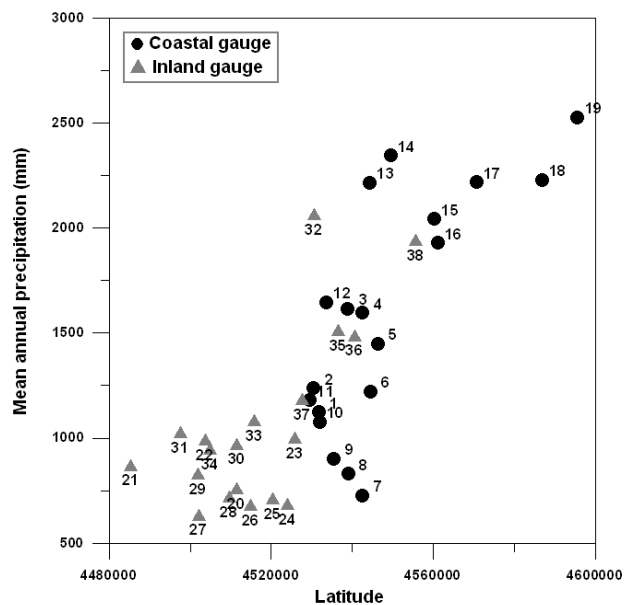


Figure 4.2 : Distribution of mean annual precipitation versus latitude.

4.1.3 Effects of distance from sea

In addition, the distance from the sea can be used as an indication of air humidity, which directly influences precipitation amount (Johansson and Chen, 2003). For the study area, the influence of the distance from the sea on mean annual precipitation is investigated and shown in Figure 4.3 for the inland gauges. It seems to indicate that the further from the sea, the smaller the precipitation.

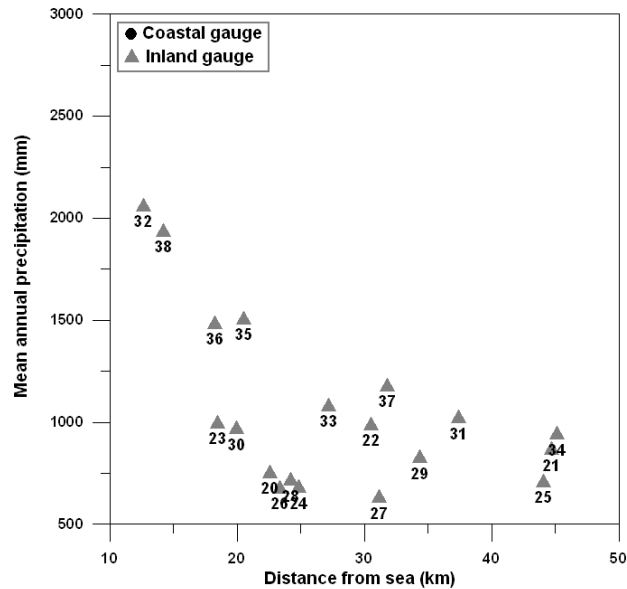


Figure 4.3 : Distribution of mean annual precipitation versus distance from sea.

4.1.4 Effects of elevation

The relationship between elevation and precipitation for all gauges is shown in Figure 4.4. As seen, precipitation seems to decrease with elevation. However, in the literature, for a mountainous area, precipitation typically increases with elevation (Daly et al., 1994; Park and Singh, 1996; Sevruk, 1997; Marquez et al., 2003; Naoum and Tsanis, 2004). In another study by Hastenrath (1967), an altitudinal belt of maximum precipitation below the 1000 m level was found in the large parts of the Central American mountains. In contrast to these common findings, the orographic, or altitudinal belt, effects cannot be seen for the Eastern Black Sea Region. The situation regarding precipitation-elevation in the vertical direction can be explained by the location of the gauges and height of the mountains. The mountains are located along the stream corridors and increase throughout the valleys. This topography may block moisture from the sea moving to the inner part of the region. Less moisture produces less precipitation for the gauges located in valley floors.

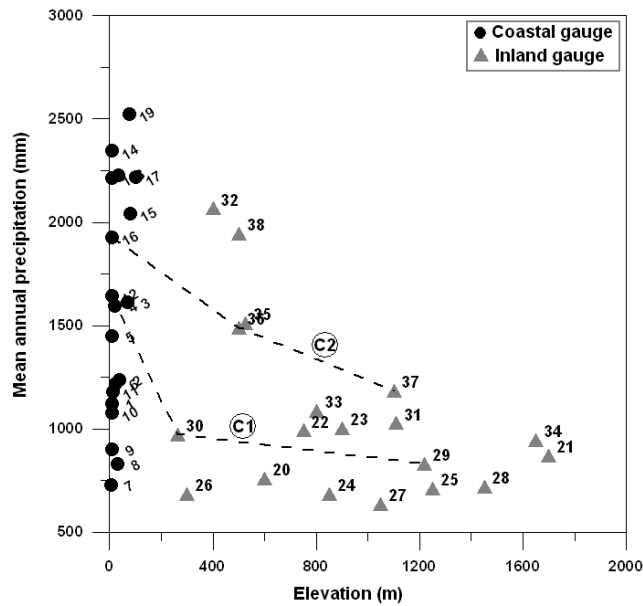


Figure 4.4 : Distribution of mean annual precipitation versus elevation.

For instance, for two different valleys, C1 and C2 (Figure 4.4), on which at least 3 gauges are located, the precipitation values are connected by curves. Gauges (12, 29, 30) and (16, 36, 37) belong to two separate basins representing curves (C1) and (C2), respectively. For both basins, precipitation amount decreases obviously. This condition is valid for other valleys, have only 2 gauges, such as (1)-(21) and (10)-(27). The precipitation distribution of two transects of valleys (C1, C2) represented by the previous curves before, is given in Figure 4.5.

The situation regarding precipitation-elevation on vertical direction can be explained with the height of the mountains. Mountains are located along the stream corridors and increase throughout the valleys. This topography may block moisture from the sea moving to inner part of the region. It can be said that less moisture produces less precipitation in this area. It should also be pointed out once again that, interpretation of the effect of elevation on precipitation for the study area comprises only the 0-1700 m range. No gauges are established on slopes; therefore no interpretation can be done for higher elevations.

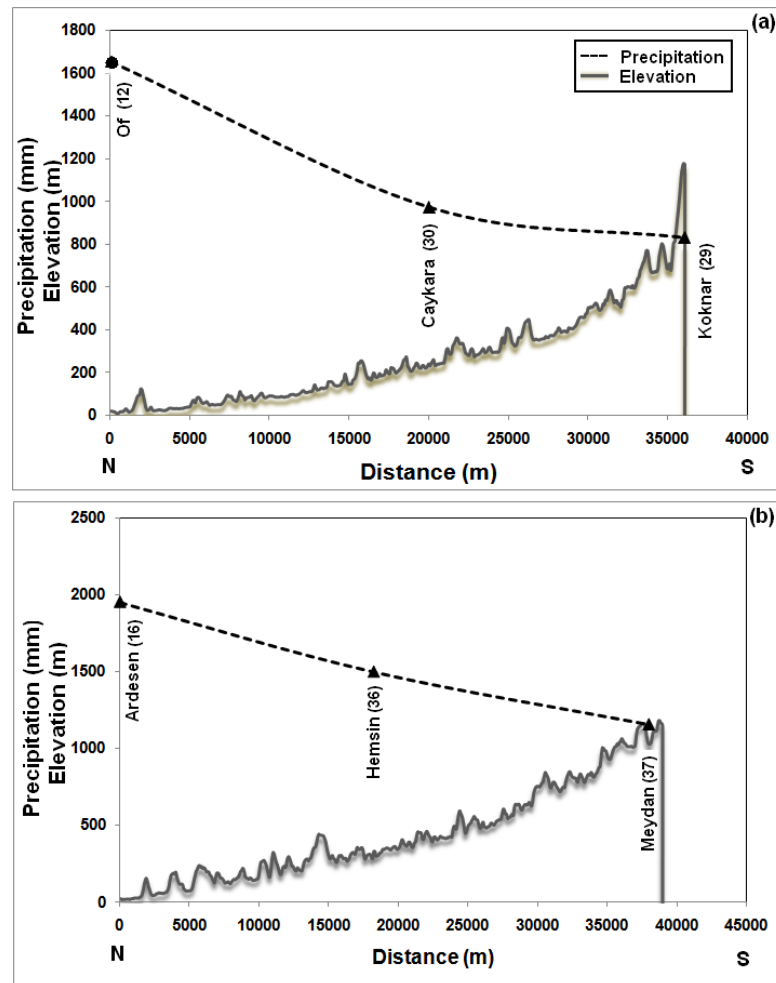


Figure 4.5 : Mean annual precipitation in a schematic transect from the two different valleys (a) valley C1; (b) valley C2 (for position of the cross-section see Figure 3.1).

4.2 Effects of Coastline Angle

Aforementioned graphical investigations for the study area indicated that one of the most effective variables of the geographical and topographical factors is coastline configuration. In many parts of coastal areas, the coastline configuration includes some headlands and bays and generally does not have any simple geometric shape. The coastline of the studied area is oriented roughly along the east-west direction and as seen Figure 3.1 some headlands and bays are present. This topography forms a natural obstacle to the predominant western and northern winds that carry moisture. Therefore, since the headland in the coastal area blocks western winds, the gauge in the eastern part of the headland receive less precipitation than do those in the western part.

In order to quantify the effect of the coastline configuration, a new variable, coastline angle is introduced. The coastline angle of a gauge (A) is defined as the angle between the north (N) and coastline direction which connect the gauge with the effect point (EP) on the western side of the coast as illustrated in Figure 4.6. The selection of the western side is based on the predominant wind direction in the study area. The coastline angle definition includes an effective area rather than a single gauge. If coastline angle (A) is less than 90 degrees (as indicated for A_2 in Figure 4.6), the gauge is blocked from the western and northern winds and receives less precipitation than those a gauge whose angle is greater than 90 degrees (as indicated for A_1 in Figure 4.6), or vice versa.

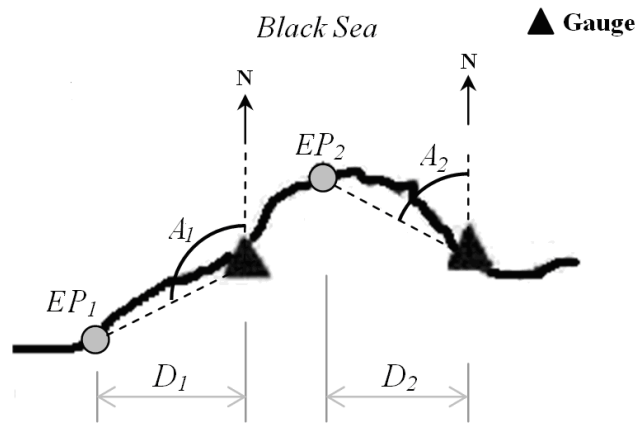
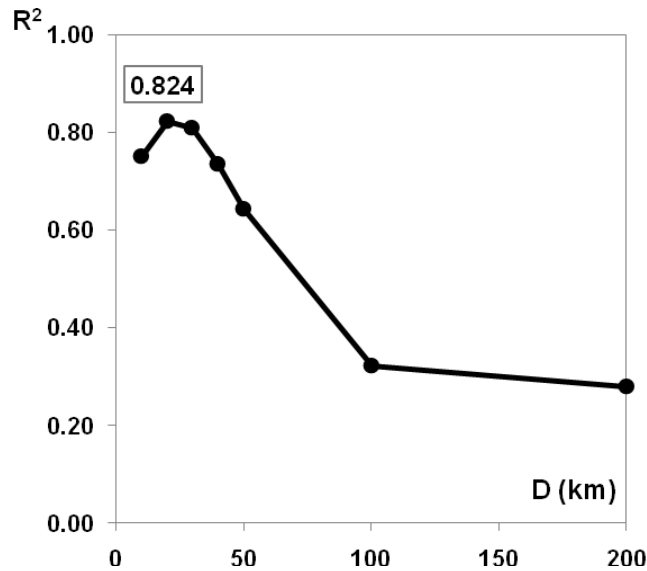


Figure 4.6 : Angle between the coast gauge and topographic obstacle (A ; coastline angle, EP ; effect point, D ; effective distance from a gauge).

The horizontal distance between the gauge and the effect point (EP) varies, based on the location of EP . This horizontal distance is assumed to be the effective distance in this study. To determine the most effective distance (D), angles for various distances (D_1, D_2, \dots) such as 10, 20, 30, 40, 50, 100 and 200 km were investigated. Determination coefficient (R^2) which measures the strength of relationship between two variables is used for the investigation. R^2 s between mean annual precipitations and angles were evaluated for given distances (Figure 4.7). In this study, the highest determination coefficient ($R^2=0.824$) was obtained for $D= 20$ km. The obtained coastline angle for each coastal gauge as well as for an inland gauge assumed to have the same angle as the coastal gauge in the same valley is shown in Table 4.1. The coastline angle values range from 65° to 129° .

Table 4.1 : Coastline angles of rain gauges.

Coastal				Inland			
No	Station number	Station name	Angle (degree)	No	Station number	Station name	Angle (degree)
1	1453	Bulancak	77	20	22-018	Sofulu	77
2	17034	Giresun	84	21	22-001	Tamdere	84
3	1460	Tirebolu	111	22	22-020	Sinir	111
4	1299	Gorele	112	23	1623	Tonya	95
5	1300	Eynesil	103	24	1624	Duzkoy	80
6	1302	Vakfikebir	95	25	22-017	Guzelyayla	65
7	17626	Akcaabat	80	26	1626	Macka	65
8	17037	Trabzon	65	27	22-011	Kayaici	77
9	1471	Arsin	81	28	1787	Dagbasi	77
10	1472	Arakli	77	29	22-016	Koknar	92
11	1473	Surmene	79	30	1801	Caykara	92
12	1475	Of	92	31	1962	Uzungol	92
13	17040	Rize	113	32	1476	Kalkandere	113
14	1312	Cayeli	110	33	1803	Ikizdere	113
15	17626	Pazar	123	34	22-003	Sivrikaya	113
16	1156	Ardesen	120	35	1480	Kaptanpasa	110
17	1015	Findikli	118	36	22-009	Hemsin	126
18	17042	Hopa	125	37	22-013	Meydan	120
19	818	Kemalpasa	129	38	22-019	Tunca	118

**Figure 4.7** : Determination coefficients (R^2) for various distances (D).

5. DERIVATION OF ISOHYETAL MAPS

5.1 Methods

Interpolation is the process of predicting the values of a certain variable of interest at ungauged locations based on measured values at points within the area of interest (Burrough and McDonnell, 1998). Interpolation methods can be classified into graphical, deterministic (numerical), geostatistical and topographical methods. Graphical methods include isohyetal mapping and Thiessen polygon. Deterministic interpolation methods use mathematical functions to calculate the values at unknown locations based either on the degree of similarity (e.g. Inverse Distance Weighted) or the degree of smoothing (e.g. Radial Basis Function) in relation with neighboring data points. Deterministic methods sometimes include geostatistical techniques, here; they are considered separately. Geostatistical methods use both, mathematical and statistical methods to predict values at unknown locations and to provide probabilistic estimates of the quality of the interpolation based on the spatial autocorrelation among data points. Topographical methods, involve the correlation of point precipitation data with an array of geographical and topographical variables such as slope, exposure, elevation, location of barriers and wind speed and direction (Daly et al., 1994; Burrough and McDonnell, 1998; Johnston et al., 2003).

Deterministic methods such as Inverse Distance Weighted (IDW), Radial Basis Function (RBF), geostatistical methods such as Kriging and topographical methods which include regression analysis will be mentioned in the following sub chapters.

5.1.1 Inverse distance weighted (IDW)

Inverse distance weighted (IDW), like a geostatistical method Kriging, depends on weighting neighboring data values in the estimation of $Z^*(x_o)$ which is the point value located at coordinates x, y to be estimated. The interpolated elevation (precipitation in this case), $Z^*(x_o)$ is calculated by assigning weights (λ) to precipitation values, $Z(x_i)$ found within a given neighborhood of the kernel:

$$\lambda_i = \frac{d_i^{-p}}{\sum_{i=1}^N d_i^{-p}} \quad (5.1a)$$

$$\sum_{i=1}^N \lambda_i = 1 \quad (5.1b)$$

$$Z^*(x_0) = \sum_{i=1}^N \lambda_i Z(x_i) \quad (5.2)$$

where $Z(x_i)$ is the precipitation value at point i in the point neighborhood N ; d is the distance from the kernel to point i ; and exponent p is the friction distance (mostly called as power value) ranging from 1.0 to 6.0 with the most commonly used value of 2.0 (Clarke, 1990). The negative sign of p implies that precipitation values closer to the interpolant are more important than those farther away. The closer the neighboring value $Z(x_i)$, the more weight it has in the interpolated elevation. Best results are obtained from sufficiently dense samples (Vieux, 2004). IDW is an exact interpolator which means that it predicts a value identical to the measured value at a sampled location (Johnston et al., 2003).

5.1.2 Radial basis function (RBF)

RBF methods are a series of exact interpolation techniques; that is, the surface must go through each measured sample value. There are five different basis functions:

- Thin-plate spline
- Spline with tension
- Completely regularized spline
- Multiquadric function
- Inverse multiquadric function.

Each basis function has a different shape and results in a slightly different interpolation surface. RBF methods are a form of artificial neural networks.

RBFs are used for calculating smooth surfaces from a large number of data points. The functions produce good results for gently varying surfaces such as elevation. The techniques are inappropriate when there are large changes in the surface values

within a short horizontal distance and/or when you suspect the sample data is prone to error or uncertainty.

The predictor is a linear combination of the basis functions,

$$Z^*(x_o) = \sum_{i=1}^n \omega_i \phi(|d_i - d_o|) + \omega_{n+1} \quad (5.3)$$

where, $\phi()$ is a radial basis function, Euclidean distance between the prediction location d_o and each data location d_i , and $\{\omega_i: i=1,2,\dots, n+1\}$ are weights to be estimated, ω_{n+1} is the bias factor.

The equivalent model of Equation (5.3) is assumed to be Equation (5.2) using untransformed data values and data weights λ_i . For clarity, the computation procedure is outlined as a series of steps using matrix notation below (Url-3, 2010).

- Computation of the $n \times n$ matrix, \mathbf{D} , of inter point distances between all (x,y) pairs in the source dataset.
- Application of the chosen radial basis function, $\phi()$, to each distance in \mathbf{D} to produce a new array Φ .
- Augmentation of Φ with a unit column and row vector, plus a single entry 0 in position $[(n+1), (n+1)]$. This augmented matrix is called \mathbf{A} .
- Computation the column vector \mathbf{r} of distances from the estimation point x_o to each of the source data points used to create \mathbf{D} .
- Application of the chosen radial basis function to each distance in \mathbf{r} to produce a new column vector and then creation of the $(n+1)$ column vector with a single 1 as the last entry. This augmented column vector is called \mathbf{c} .
- Computation of the matrix product $\mathbf{b} = \mathbf{A}^{-1}\mathbf{c}$. This provides a set of n weights to be used in the calculation of the estimated value at x_o .

The system of linear equations to be solved is of the matrix form:

$$\begin{bmatrix} \Phi & 1 \\ 1 & 0 \end{bmatrix} \begin{bmatrix} \lambda \\ \mu \end{bmatrix} = \begin{bmatrix} \psi \\ 1 \end{bmatrix} \rightarrow Ab = c \quad (5.4)$$

in which μ is the Lagrangian value. After the weights, λ_i , are computed based on the selected radial basis function, the estimated value $Z^*(x_o)$, at the point x_o can be determined. Each basis function results in a slightly different surface (Johnston et al., 2003). To pick any basis function, each of them can be tried separately and used based on its error values.

5.1.3 Kriging

Kriging was proposed by Matheron (1962) based on the master thesis written by Daniel Gerhardus Krige (1951). The basic idea of Kriging is to estimate the unknown attribute value at the unsampled location as a linear combination of the neighboring observations. Let x_1, x_2, \dots, x_n be the sample locations with given precipitation values of $Z(x_1), Z(x_2), \dots, Z(x_n)$ and x_0 is the unsampled location. Then the value of precipitation in the unsampled location, $Z(x_0)$, is estimated as a linear weighted combination of n known surrounding data, depending on distance from the unsampled location like IDW method in Equation (5.2) where the weights λ_i are determined such that $Z^*(x_0)$ is an unbiased estimate of $Z(x_0)$:

$$E[Z^*(x_0) - Z(x_0)] = 0 \quad (5.5)$$

and the estimation variance is minimum:

$$E[Z^*(x_0) - Z(x_0)]^2 \Rightarrow \min \quad (5.6)$$

where $E[.]$ is the expectation. Substituting equation (5.3) into equations (5.5) and (5.6) yields:

$$E\left[\sum_{i=1}^n \lambda_i Z(x_i) - Z(x_0)\right] = 0 \quad (5.7)$$

$$E\left[\sum_{i=1}^n \lambda_i Z(x_i) - Z(x_0)\right]^2 \Rightarrow \min \quad (5.8)$$

The optimal weights λ_i are solutions of the following linear system, called the Kriging system:

$$\sum_{i=1}^n \lambda_i C(x_i, x_j) + \mu = C(x_i, x_j) \quad (5.9a)$$

$$\sum_{i=1}^n \lambda_i = 1 \quad (5.9b)$$

where $C(x_i, x_j) = E[Z(x_i, x_j)]$ is the covariance and μ is a Lagrange multiplier which was employed to obtain the weights.

In the kriging system the estimation variance is written in terms of differences between two sample locations.

The minimization yields the replacement of $C(x_i, x_j)$ by $\gamma(x_i, x_j)$:

$$\sum_{i=1}^n \lambda_i \gamma(x_i, x_j) + \mu = \gamma(x_i, x_j) \quad (5.10a)$$

$$\sum_{i=1}^n \lambda_i = 1 \quad (5.10b)$$

which yields the semi-variogram equations:

$$\gamma(h) = \frac{1}{2} E[(Z(x+h) - Z(x))^2] \quad (5.11a)$$

or

$$\gamma(h) = \frac{1}{2} \text{var}(Z(x+h) - Z(x)) \quad (5.11b)$$

where $\gamma(h)$ is the semivariogram function, h is the distance between sample locations (also called the lag) and $\text{var}(\bullet)$ is the variance. The semi-variogram $\gamma(h)$ is a graph which relates the differences or increments of the regionalized variable Z to the distance h between the data points (Figure 5.1). In addition to the lag, the variogram is characterized by other three parameters: nugget, range and sill. The nugget is the variogram discontinuity at the origin (Figure 5.1) caused by a lag scale smaller than that of the sampling grid or by integration of error of measurements. The nugget represents variability at distances smaller than the typical sample spacing, including measurement error. The range of influence (Figure 5.1) designates the extent of distances, say a , beyond which autocorrelation between sampling sites is negligible. The sill (Figure 5.1) is defined by the semivariogram value at which variogram levels off.

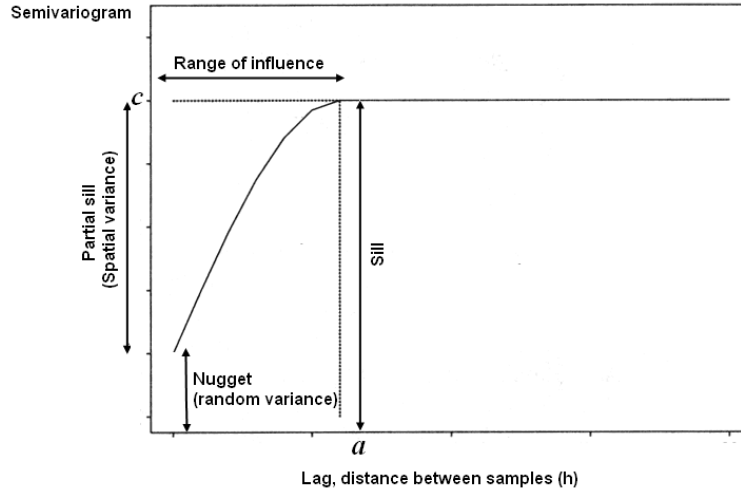


Figure 5.1 : Schematic presentation and notation of theoretical semivariogram.

An empirical (experimental) semivariogram, γ_e , can be calculated from the given set of observations by using the following numerical approximation:

$$\gamma_e(h) = 1/[2N(h)] \sum_{i=1}^{N(h)} (Z(x_i + h) - Z(x_i))^2 \quad (5.12)$$

where $N(h)$ is the number of pairs of points a distance h apart. For solving Equation (5.10), one of several common theoretical forms of Equation (5.11) must be used in order to visually fit γ to γ_e . Once the theoretical semivariogram has been chosen, four criteria can be used to determine the correctness of the model and to adjust its parameters (Karnieli, 1990):

(1) mean kriged estimation error:

$$1/n \sum_{i=1}^n [Z(x_i) - Z^*(x_i)] = 1/n \sum_{i=1}^n \varepsilon_i = 0 \quad (5.13)$$

where ε_i is the difference between the kriged and the known point value (this term should approach 0).

(2) mean standardized squared estimation error:

$$1/n \sum_{i=1}^n \left[\frac{Z(x_i) - Z^*(x_i)}{s_i^*} \right]^2 = 1/n \sum_{i=1}^n [\varepsilon_i / s_i]^2 = 1 \quad (5.14)$$

where s_i^* is the estimation standard deviation (this term should approach 1).

(3) sample correlation coefficient between the estimation values, Z^* , and the standardized estimation values, $(Z - Z^*)/s^*$, (this term should approach 0).

(4) sample correlation coefficient between the estimation values, Z^* , and the known values, Z , (this term should approach 1).

For simplicity and to illustrate the methodology of kriging, three known values, Z_1 , Z_2 , and Z_3 can be used to estimate an unknown value at point p , Z_p . Three weights must be determined λ_1 , λ_2 , and λ_3 , to make an estimate. The kriging procedure begins with the following four simultaneous equations with Lagrange multiplier (μ):

$$\lambda_1\gamma(h_{11}) + \lambda_2\gamma(h_{12}) + \lambda_3\gamma(h_{13}) + \mu = \gamma(h_{1p}) \quad (5.15a)$$

$$\lambda_1\gamma(h_{21}) + \lambda_2\gamma(h_{22}) + \lambda_3\gamma(h_{23}) + \mu = \gamma(h_{2p}) \quad (5.15b)$$

$$\lambda_1\gamma(h_{31}) + \lambda_2\gamma(h_{32}) + \lambda_3\gamma(h_{33}) + \mu = \gamma(h_{3p}) \quad (5.15c)$$

$$\lambda_1 + \lambda_2 + \lambda_3 + 0 = 1 \quad (5.15d)$$

Separating these equations into matrix form yields:

$$\begin{bmatrix} \gamma(h_{11}) & \gamma(h_{12}) & \gamma(h_{13}) & 1 \\ \gamma(h_{21}) & \gamma(h_{22}) & \gamma(h_{23}) & 1 \\ \gamma(h_{31}) & \gamma(h_{32}) & \gamma(h_{33}) & 1 \\ 1 & 1 & 1 & 0 \end{bmatrix} \bullet \begin{bmatrix} \lambda_1 \\ \lambda_2 \\ \lambda_3 \\ \mu \end{bmatrix} = \begin{bmatrix} \gamma(h_{1p}) \\ \gamma(h_{2p}) \\ \gamma(h_{3p}) \\ 1 \end{bmatrix} \quad (5.16)$$

This matrix equation is solved for the unknown coefficients, λ_i . The values in the matrix are taken from the theoretical semivariogram models. Once the individual weights are known, estimation can be calculated by following equation.

$$Z_p = \lambda_1 Z_1 + \lambda_2 Z_2 + \lambda_3 Z_3 \quad (5.17)$$

The semivariogram models used in the kriging process need to obey certain numerical properties in order for the kriging equations to be solvable. Using h to represent lag distance, a to represent (practical) range, and c to represent sill, the most frequently used models are summarized in Table 5.1. An example of empirical (experimental) and theoretical semivariogram models is shown in Figure 5.2.

To select the suitable theoretical semivariogram model, the cross validation technique can be used. Cross validation allows one to compare the impact of different models on interpolation results (Isaaks and Srivastava, 1989; Goovaerts, 1997). The idea consists of removing one datum at a time from the data set and re-

estimating this value from remaining data using the different semivariogram models. Estimated and actual values are compared and the model that yields the most accurate predictions is retained.

Table 5.1 : Frequently used variogram models.

Models	Variogram equation
Linear	$\gamma(h) = \frac{h}{c/a}$
Spherical	$\gamma(h) = \begin{cases} c \left(1.5 \left(\frac{h}{a} \right) - 0.5 \left(\frac{h}{a} \right)^3 \right) & \text{if } h \leq a \\ c & \text{otherwise} \end{cases}$
Exponential	$\gamma(h) = c \left(1 - \exp \left(\frac{-3h}{a} \right) \right)$
Gaussian	$\gamma(h) = c \left(1 - \exp \left(\frac{-3h^2}{a^2} \right) \right)$

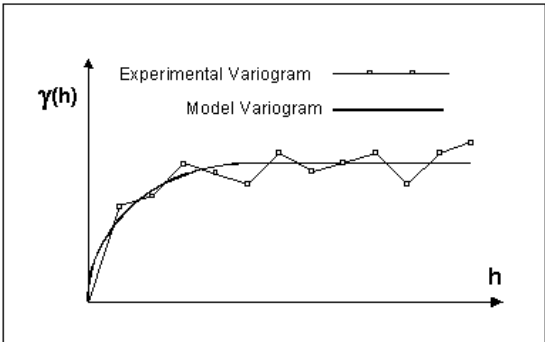


Figure 5.2 : An example of empirical (experimental) and theoretical semivariogram models.

For kriging, direction is not considered so far. The regionalized variable theory assumes that the variation of the variable under study is the same in all directions (Journel and Huijbregts, 2003). On the other hand, if the semivariogram (or covariance) functions change not only with distance but also with direction, a phenomenon called anisotropy occurs. Following the study by Goovaerts (2000) and due to the lack of data, only the omnidirectional (independent from direction) semivariogram is computed, and hence the spatial variability is assumed to be identical in all directions in this study.

Kriging method has different types such as Simple, Ordinary, and Universal etc. which pertain to the assumptions about the mean structure of the model. Ordinary type assumes a constant but unknown mean that may fluctuate among local neighborhoods within a study area and the sum of Kriging weights equals to one. As in this study the Ordinary type Kriging is used, Section 5.1.3 was devoted to a comprehensive explanation of this type of Kriging.

5.1.4 Multiple linear regression (MLR)

Regression analysis can simply be defined as determination of the relationship between continuous variables. Regression is performed to;

- (i) learn something about the relationship between the two variables, or
- (ii) remove a portion of the variation in one variable (a portion that is not of interest) in order to gain a better understanding of some other, more interesting, portion of the variation, or
- (iii) estimate or predict values of one variable based on knowledge of another variable, for which more data are available (Helsel and Hirsch, 2002).

If the relationship between one continuous variable of interest (response variable, dependent variable, predictant) and one more variable (explanatory variable, independent variable, predictor, regressor), it is called "simple linear regression" because one explanatory variable is the simplest case of regression models. Multiple linear regression (MLR) is the extension of simple linear regression (SLR) to the case of multiple explanatory variables. The goal of this relationship is to explain as much as possible of the variation observed in the response variable, leaving as little variation as possible to unexplained "noise" (Helsel and Hirsch, 2002; Wilks, 2006).

In the regression analysis, there are major assumptions that should be considered as follows (Montgomery et al., 2006).

- (i) the relationship between the response and the regressors is linear, at least approximately,
- (ii) the error term has zero mean,
- (iii) the error term has constant variance,
- (iv) the errors are uncorrelated,

(v) the errors are normally distributed.

A multiple linear regression model might describe the following relationship:

$$y = \beta_0 + \beta_1 x_1 + \beta_2 x_2 + \dots + \beta_n x_n + \varepsilon \quad (5.18)$$

where y denotes response variable (dependent variable, predictant), x_i ($i=1,2,\dots,n$) denotes explanatory variable (independent variable, predictor, regressor), ε is the error term, β_0 is the intercept and the parameters β_i ($i=1,2,\dots,n$) are regression coefficients. The method of least squares can be used to estimate regression coefficients.

In general, it would be liked to describe the system with as few regressors as possible (Montgomery et al., 2006), because a good model will explain as much of the variance of y as possible with a small number of explanatory variables (Helsel and Hirsch, 2002). To find the subset of variables to use in the final equation, it is natural to consider fitting models with various combinations of the candidate regressors but evaluating all possible regressions can be burdensome computationally. Because of this, various methods have been developed for evaluating only a small number of subset regression models by either adding or deleting regressors one at a time. These methods are generally referred to as stepwise-type procedures which can be classified into three categories: (i) forward selection, (ii) backward elimination, and (iii) stepwise regression.

To make automatic decisions for removal or inclusion in "stepwise" procedures, F or t tests are precisely used. The significance of the regression models and that of model parameters can be tested with F-test and t-test, respectively. If the F (or t) statistics calculated for each model (or parameter) is larger than the critical value, regression model is significant (or every explanatory variable is accounting for a significant amount of variation, and all should be present).

Forward selection; starts with only an intercept and adds variables to the equation one at a time. Once in, each variable stays in the model. All variables not in the model are evaluated with partial F or t statistics in comparison to the existing model. The variable with the highest significant partial F or t statistic is included, and the process repeats until either all available variables are included or no new variables are significant.

Backward elimination; starts with all explanatory variables in the model and eliminates the one with the lowest F statistic (lowest *t*). It stops when all remaining variables are significant.

Stepwise regression combines the ideas of forward and backward. It alternates between adding and removing variables, checking significance of individual variables within and outside the model. Variables significant when entering the model will be eliminated if later they test as insignificant (Helsel and Hirsch, 2002).

The determination coefficient (R^2) and standard error (SE) should be obtained for the MLR analysis. Determination coefficient is a measure of goodness of fit provided by the estimated regression equation, as mentioned before, and represents the proportion of explained variance. R^2 values close to one would imply that the model can explain most of the variation in the dependent variable and show how convenient the model is. Similarly, a model with the smallest SE is more agreeable (Willmott, 1982; Vicente-Serrano et al., 2003). $Adj-R^2$ is also used for better comparison, because R^2 increases when additional variables are used but $Adj-R^2$ compensates for the newly added explanatory variables.

Dependence of the residuals, one of the major assumptions in regression analysis, should also be verified by means of the Durbin-Watson statistic. The Durbin-Watson statistic changes in the range from 0 to 4. A value near 2 indicates non-autocorrelation; a value toward 0 indicates positive autocorrelation while a value toward 4 indicates negative autocorrelation (Durbin and Watson, 1950, 1951; Montgomery et al., 2006).

In the MLR analysis, it is very important to measure the multi-collinearity which is a condition where at least one explanatory variable is closely related to one or more other explanatory variables. It results in several undesirable consequences, for example; coefficients may be unrealistic in sign (a negative slope for a regression of precipitation), slope coefficients are unstable etc. Multi-collinearity can be measured by the variance influence factor (VIF) which was presented by Marquardt (1970). VIF value should be lower than 10. In the MLR analysis, to understand how variables contribute to the models developed, standardized regression coefficients can be used.

Detailed information related to MLR analysis and aforementioned tests can be found in Haan (2002), Helsel and Hirsch (2002), Ang and Tang (2006) and Montgomery et al. (2006).

5.2 Application

5.2.1 Isohyetal map using IDW

IDW assumes that each measured point has a local influence that diminishes with distance. The power value p in the general IDW formula (Equation 5.1a) is determined by minimizing the root mean square error (RMSE). The RMSE is the statistic that is calculated from cross-validation. To find optimum number of neighbors, RMSE is used once more. The most appropriate neighbor number is chosen based on the lowest RMSE value.

RMSE value can be calculated by following equation

$$RMSE = \left[\frac{1}{N} \sum_{i=1}^N (P_{est} - P_{obs})^2 \right]^{1/2} \tag{5.19}$$

where P_{est} , P_{obs} and N represent estimated, and observed precipitation and number of data, respectively. The RMSE and power values regarding the various numbers of neighbors are shown in Figure 5.3. Based on the lowest RMSE value, the number of neighbors and p value are chosen as 5 and 4.40, respectively. These values can be read from Figure 5.3.

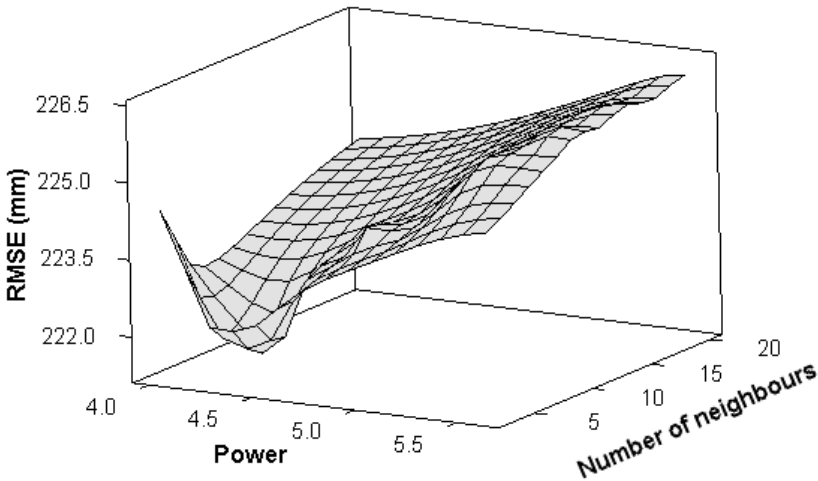


Figure 5.3 : RMSE and power values for different number of neighbors for IDW method.

Cross validation results, in other words, the scatter diagram of observed and estimated precipitation which is calculated by means of number of neighbors and p value is given in Figure 5.4.

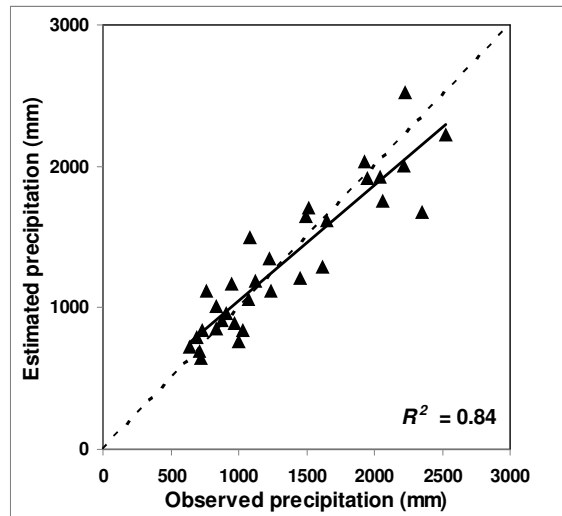


Figure 5.4 : Cross validation results of observed and estimated precipitation values for IDW method.

5.2.2 Isohyetal map using RBF

To select the most appropriate basis function, RMSE values are determined from the cross validation results. RMSE values for different basis functions are shown in Figure 5.5. As seen, Multiquadric function gives the lowest RMSE value for the annual data. Multiquadric function of RBF is already more popular and appropriate for various scattered dataset (Hardy, 1990; Buhmann, 2003). Multiquadric function is chosen to generate isohyetal maps for RBF method. Cross validation results of observed-estimated precipitation values for RBF method is given Figure 5.6. It is seen that RBF results are better than that of IDW when considering R^2 values.

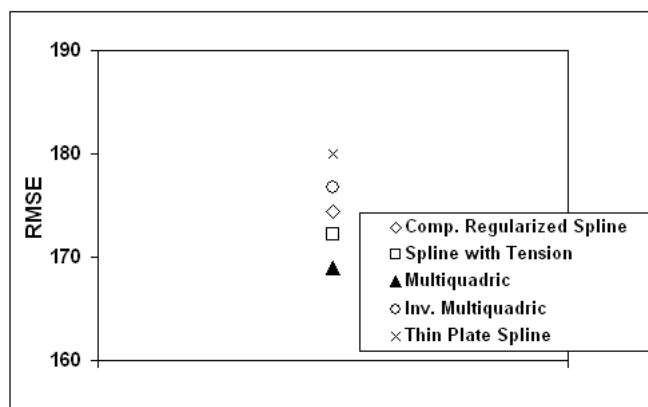


Figure 5.5 : RMSE values for different basis functions.

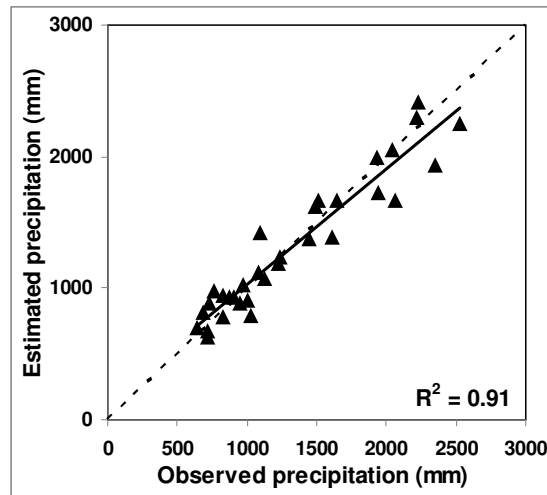


Figure 5.6 : Cross validation results of observed and estimated precipitation values for RBF method.

5.2.3 Isohyetal map using Kriging

Ordinary Kriging is used for precipitation interpolation. No anisotropy has been introduced in the data based on the study by Goovearts (2000). Because of the lack of data only the omnidirectional semivariogram was computed, and hence the spatial variability is assumed to be identical in all directions.

Cross-validation is used to compare different variogram models. The spherical model is the most widely used semivariogram model and characterized by a linear behavior at the origin (Goovearts, 2000) was chosen as theoretical variogram. Figure 5.7 shows the semivariogram of annual precipitation computed from the 32 rain gauges.

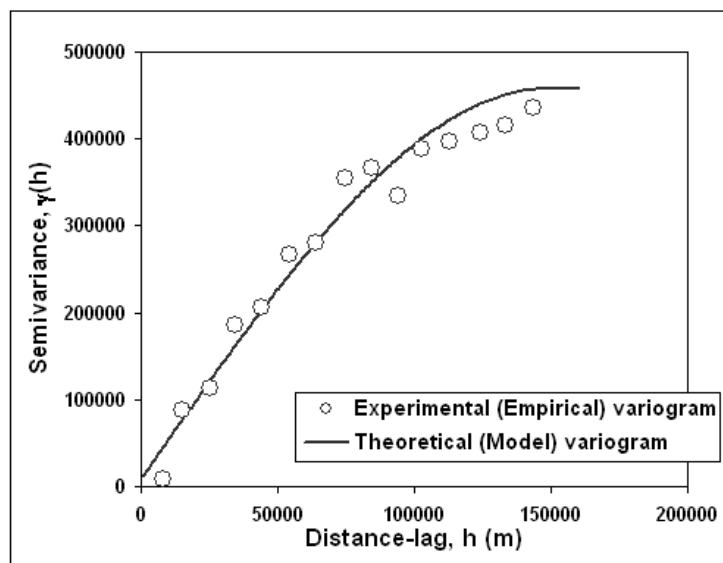


Figure 5.7 : Experimental variogram of the annual precipitation with spherical model fitted.

Semivariogram values increase with the separation distance, reflecting that two precipitation data close to each other on the ground are more alike, and thus their squared difference is smaller, than those that are further apart.

The corresponding parameters used in Ordinary Kriging are as follows (Table 5.2). Range, nugget and partial sill values can be comprehended from Figure 5.7.

Table 5.2 : Parameters of theoretical variogram for precipitation data.

Model	Range (m)	Lag Size (m)	Number of lag	Nugget (mm ²)	Partial Sill (mm ²)	Number of neighbor
Spherical	125400	9894	15	1000	412660	9

Lag size is chosen as uniformly distributed across the active lag distance that can be defined as the range over which autocorrelation will be calculated. In order to quantify the spatial autocorrelation, Moran's I technique (Moran, 1950) is used. Moran's I test statistic is a weighted product-moment correlation coefficient. The weights reflect geographic proximity and it is appropriate when data are randomly distributed in space. It shares some similarities with Pearson correlation coefficient such as it ranges from -1 to 1, which indicates negative and positive spatial correlation, respectively (Shekhar and Xiong, 2008). Moran's I values are determined using 148420 m active lag distance (which is the half or maximum point sampling distance) and shown in Figure 5.8. Maximum point sampling size is between Kemalpaşa (19) and Sofulu (20) gauges with the value of 296841 m which was calculated by Euclidean distance method (assumed as hypotenuse). Number of lag is chosen as 15. Active lag distance is uniformly distributed using this value and found to be 9894 m.

In the semivariogram definition (Equation 5.12), $N(h)$ represents the number of pairs separated by a distance h . Number of pairs is also shown in Figure 5.8 as Y -axis. If lag distance (h) increases, number of pairs decreases which causes difficulties to fit the theoretical variogram (Bargaoui and Chebbi, 2009). This case can be seen in Figure 5.8, namely no need to increase the value of 148420 m as active lag distance, it is appropriate to determine lag size. After the active lag distance is decided by considering Moran's I statistics and number of lags is selected, lag size can be reached.

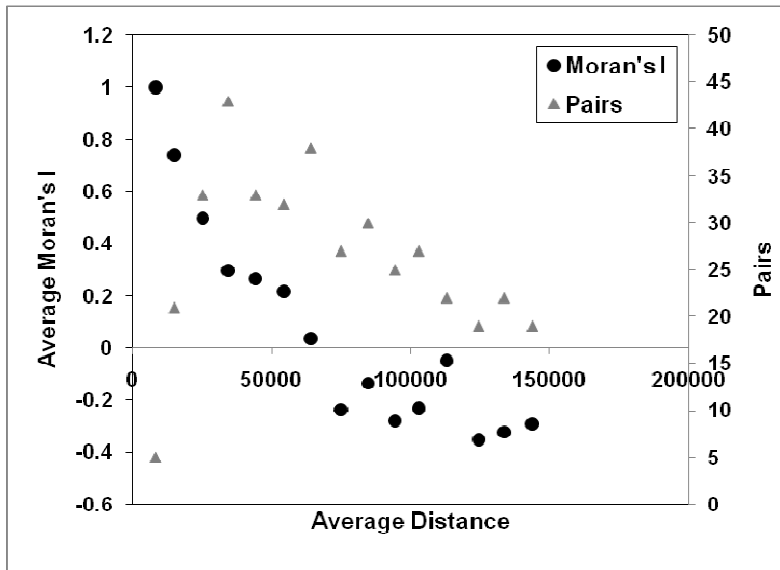


Figure 5.8 : Spatial autocorrelation (Moran’s I) of mean annual precipitation by sampling distance (h).

Detailed information about Moran’s I can be found in Lloyd (2010). Cross validation result of observed and estimated precipitation values for Kriging method is given in Figure 5.9.

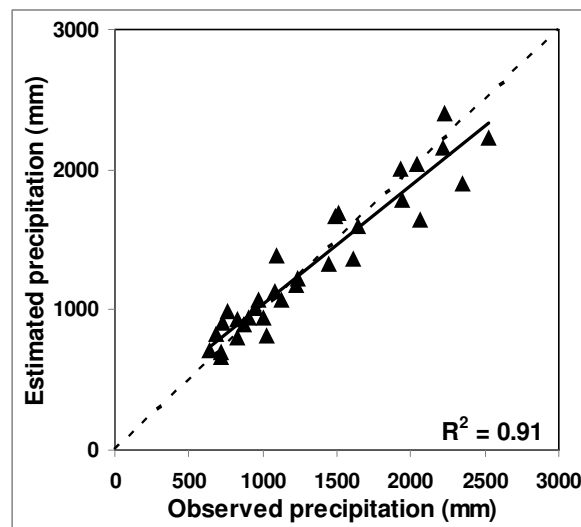


Figure 5.9 : Cross validation results of observed and estimated precipitation values for Kriging method.

5.2.4 Isohyetal map using MLR

MLR analysis is used to generate isohyetal map based on mean annual precipitation (P) and geographical/topographical characteristics of the Eastern Black Sea region such as longitude (X), latitude (Y), elevation (H), distance from sea (L) and coastline angle (A). Effects of these parameters on precipitation were comprehensively

explained in Chapter 4. Correlation coefficients for the relationships between precipitation and independent variables are shown Table 5.3. Statistically significant relationships at the 0.05 level are bolded.

Table 5.3 : Correlation coefficients of precipitation and independent variables.

	<i>P</i>	<i>X</i>	<i>Y</i>	<i>H</i>	<i>L</i>	<i>A</i>
<i>P</i>						
<i>X</i>	0.567					
<i>Y</i>	0.793	0.503				
<i>H</i>	-0.514	-0.072	-0.700			
<i>L</i>	-0.557	-0.236	-0.694	0.817		
<i>A</i>	0.778	0.591	0.544	-0.146	-0.279	

For the MLR analysis, stepwise regression which is a combination of forward selection and backward elimination procedures is used to find the best regression model. In this study, α for the critical value was set at 0.05.

While using the MLR analysis, the significance of the regression models and that of model parameters is tested with *F*-test and *t*-test, respectively. The Kolmogorov-Smirnov test is used to determine whether the regression residuals are normally distributed. The dependence of the residuals is also verified by means of the Durbin-Watson statistic. Multi-collinearity is measured by the variance influence factor (VIF). The determination coefficient (R^2), standard error (*SE*) and adjusted determination coefficient ($Adj-R^2$) are obtained for the MLR analysis.

Different models are performed for MLR analysis. Initially, a mathematical relationship is established for all data (Model 1). In Model 1, longitude (*X*), latitude (*Y*) and elevation (*H*) are used as explanatory (independent) variables. The best regression model, based on the stepwise approach, is the following:

$$P = \beta_0 + \beta_1 X + \beta_2 Y \tag{5.20}$$

where *P* is the mean annual precipitation; *X* and *Y* are the longitude and latitude, respectively. As seen from Equation (5.20), elevation (*H*) did not affect the prediction. Regression coefficients (β) are shown in Table 5.4 for Model 1.

For coastal gauges, another mathematical model is derived as Model 2. In addition to the longitude (*X*), latitude (*Y*) and elevation (*H*) variables, Model 2 also incorporates coastline angle (*A*), which affects the precipitation as mentioned before.

The quantification of coastline angles was given in detail in Chapter 4 together with their values for every gauge in Table 4.1.

The best prediction equation derived for the coastal gauges is the following:

$$P = \beta_0 + \beta_1 A \quad (5.21)$$

where P shows the mean annual precipitation and A is the coastline angle as defined previously. Equation (5.19) is a simple linear model, which includes only the coastline angle as an explanatory variable. Regression coefficients of Model 2 are also given in Table 5.4. It can be seen that the coefficient of the coastline angle (β_1) is very high.

Table 5.4 : Coefficients and regression statistics of calibration stage of the MLR models*.

	Model 1	Model 2	Model 3	Model 4
β_0	-67733	-1030.3	-44123.3	-48452.1
β_1	0.00201 (0.276)	26.25 (0.912)	0.00971 (0.574)	0.01063 (0.453)
β_2	0.01498 (0.638)	-	14.01 (0.395)	16.47 (0.553)
No. of gauges	32	16	16	32
R^2	0.653	0.831	0.735	0.799
$Adj-R^2$	0.629	0.819	0.694	0.785
SE	345.17	248.25	244.47	263.09
Durbin-Watson Test	0.87	1.31	1.90	1.25

*Coefficients in brackets are standardized

The MLR model developed for inland gauges (Model 3) is more complicated. In this case, the distance from sea (L) and the angle (A) are added, along with the variables, X , Y , H for the inland area. For the study area, precipitation-longitude variation of inland gauges are similar to the coastal gauges, but precipitation amounts of inland gauges are less than those of the coastal gauges (Figure 4.1). For instance, precipitation in the inland gauge Tunca (38) is related to precipitation recorded in the coastal gauge Findikli (17). Similarly Tonya (23) on the inland and Vakfikebir (6) on the coast can be paired. Due to topographical considerations, each inland gauge precipitation value can be paired with either precipitation value or angle of a coastal gauge located in the same valley as the inland gauge.

On the basis of this assumption, the best prediction equation derived for inland gauges (Model 3) is as follows:

$$P = \beta_o + \beta_1 Y + \beta_2 A \quad (5.22)$$

where P is the mean annual precipitation, A is the coastline angle of a coastal gauge that is located in the same valley as the inland gauge under consideration. Regression coefficients of Model 3 are given in Table 5.4.

In order to understand the effect of coastline configuration on precipitation for the entire study area (coastal and inland areas combined), Model 4 is developed using the coastline angle (A) together with the common variables (X, Y, H) previously used in Model 1. The best prediction function for the entire study area is the following:

$$P = \beta_o + \beta_1 Y + \beta_2 A \quad (5.23)$$

with variables defined as previously. Regression coefficients of Model 4 are given in Table 5.4. As seen from this table, the coefficient of the coastline angle (β_2) is higher than that of the latitude parameter (β_1).

Scatterplots of the mean annual precipitation estimated by the MLR models versus the actual observations are presented in Figure 5.10 for each model. Corresponding residuals (differences between estimated and observed precipitations) are plotted in Figure 5.11.

Only linear terms of the variables were used in the models. Models using squared and cubed terms of each variable were considered previously by Eris and Agiralioglu (2009).

To understand how variables contribute to the models developed, standardized regression coefficients are also computed and given in Table 5.4.

Both Model 3 and 4 include the coastline angle. Model 3 does not include distance from sea whereas it has northwest elevation as an explanatory variable instead of gauge elevation. Pairwise correlations have already shown that latitude (Y) and coastline angle (A) are more significant than are $X, H, \text{ or } L$ for Model 3 and 4 (Table 5.4).

In Model 2, the precipitation distribution can be explained by a simple linear function of only the coastline angle. Grouping the gauges as coastal and inland improves the results, particularly for the inland gauges.

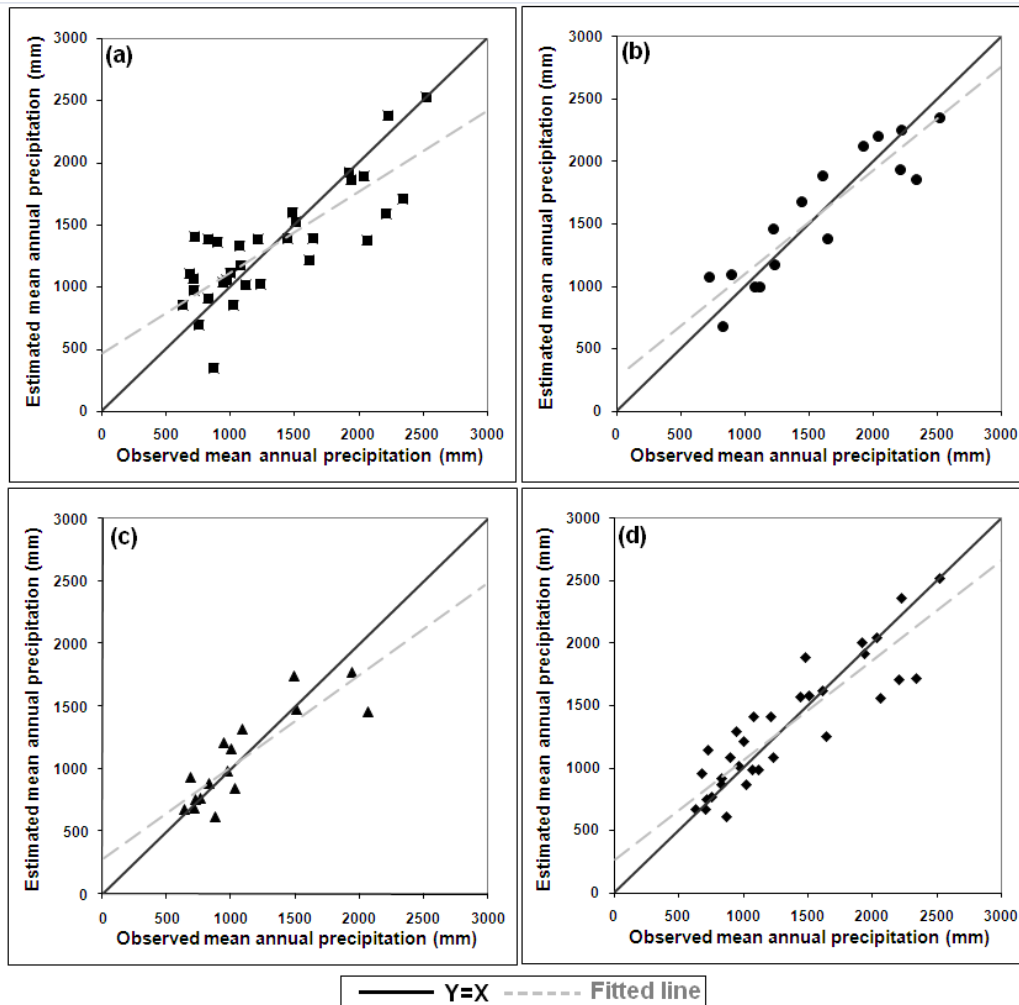


Figure 5.10 : Scatter diagrams of observed and estimated mean annual precipitation for the (a) all gauges (Model 1), (b) coastal gauges (Model 2), (c) inland gauges (Model 3), (d) all gauges (Model 4).

The calibration results of the MLR models are summarized in Table 5.4 from which it is seen that geographical and topographical variables explain 83% and 74% of the spatial variability of precipitation for the coastal (Model 2) inland gauges (Model 3), respectively. When the entire study area is considered (Model 4), 80% of the spatial variability in the precipitation is explained.

The models derived for all cases have few explanatory variables. The number of explanatory variables in any of the MLR models did not exceed 3; these are latitude, longitude, and the coastline angle. These models are parsimonious in that sense. A model is considered good when it explains as much of the variance of the dependent variable (precipitation in the case study here) as possible by using as small a number of explanatory variables as possible.

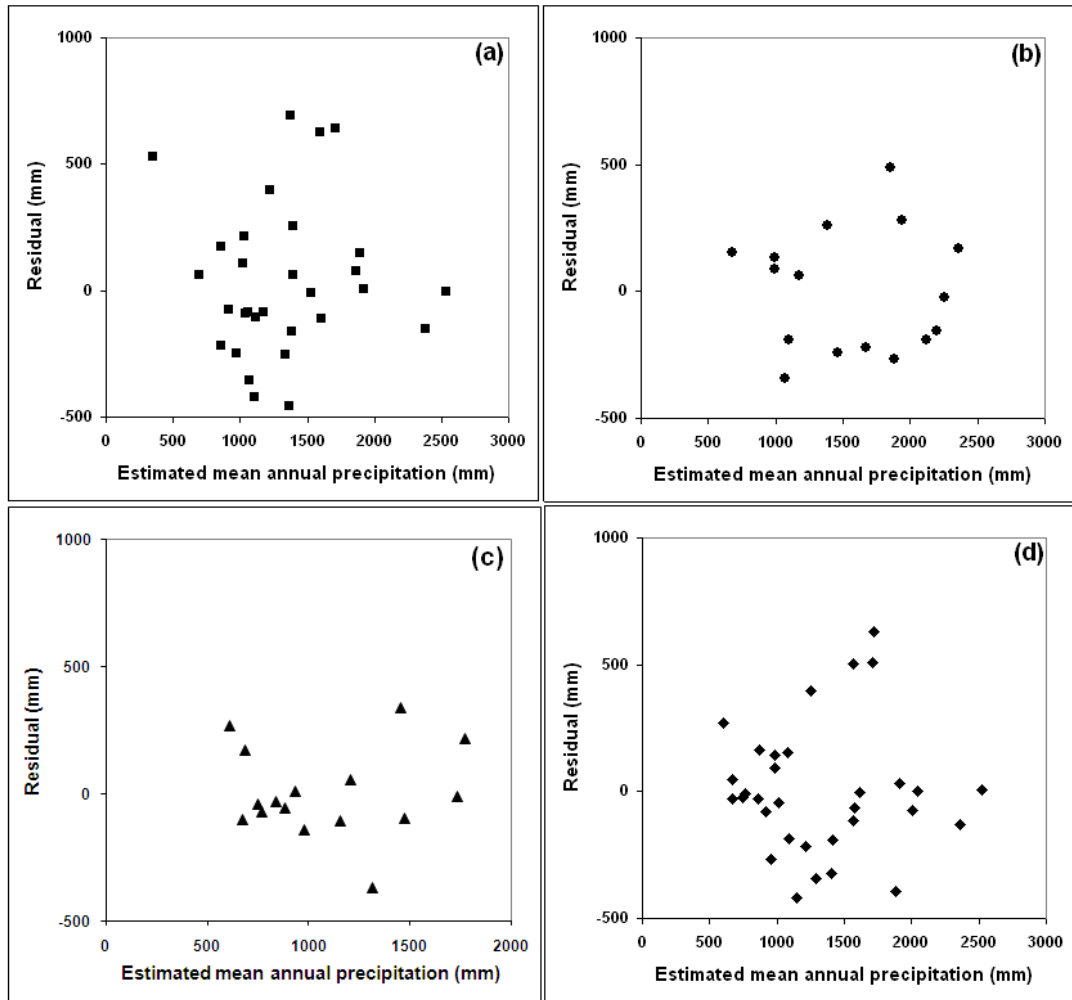


Figure 5.11 : Scatter diagrams of residuals for the (a) all gauges (Model 1), (b) coastal gauges (Model 2), (c) inland gauges (Model 3), (d) all gauges (Model 4).

Model residuals are found to be normally-distributed. The Durbin-Watson statistic varies from 0.87 to 1.90. The residuals do not present any systematic pattern (autocorrelation) with respect to the explanatory variables (Figure 5.11). The variance influence factor (VIF) values for Model 1, 3 and 4 are found to be lower than 10, meaning that none of the explanatory variables is closely related to the others. It should be noted that Model 2 is a simple linear regression equation for which computing VIF value is not required.

In order to test the validity of the models, a validation test with two randomly chosen subsets are used. Each subset includes 3 gauges from the coastal and inland groups, separately. Note that only 38 rain gauges are available and that the scarcity of validation subsets has been due to the low density of rain gauges over the area.

The validation results of randomly chosen gauges, based on MLR models, are summarized in Table 5.5. In this table, *EMAP* is the estimated mean annual precipitation and *RE* is the relative error. *RE* is computed using:

$$RE = \frac{P_{est} - P_{obs}}{P_{obs}} \times 100 \quad (5.24)$$

Table 5.5 : Validation results based on the MLR models.

Gauge type	Gauge name	No	Model 1		Model 2		Model 3		Model 4	
			EMAP (mm)	RE (%)	EMAP (mm)	RE (%)	EMAP (mm)	RE (%)	EMAP (mm)	RE (%)
Coastal	Gorele	4	1306.64	-18.10	1909.57	19.69			1673.71	4.91
	Surmene	11	1301.92	10.20	1043.36	-11.68			992.43	-15.99
	Findikli	17	2089.45	-5.77	2067.06	-6.78			2071.55	-6.58
Inland	Sinir	22	660.77	-33.47			1169.89	17.79	1245.04	25.35
	Macka	26	998.15	45.92			634.49	-7.25	606.49	-11.34
	Meydan	37	1411.11	19.05			1528.33	28.93	1647.63	39.00

The validation results appear satisfactory. Minimum and maximum relative errors are -33.47 and 45.92, respectively for Model 1, whereas these are -15.99 and 25.35 for Model 4. Validation results of Model 3 are better than those of Model 1 and Model 4.

5.3 Evaluation

In comparing the estimated spatial precipitation distribution obtained from the conventional and MLR models, both visual and arithmetic comparisons are established.

The results of cross validation which is similar to calibration stage of MLR models were given in previous chapters. Like MLR analysis, cross validation results of IDW, RBF and Kriging are grouped as coastal and inland gauges. Determination coefficient (R^2) and root mean square error (*RMSE*) and are determined and shown in Table 5.6. Since mean absolute error (*MAE*) is used as an indicator of overall performance of interpolator (Daly, 2006), in addition to *RMSE*, *MAE* is computed (Equation 5.25) and added into Table 5.6.

$$MAE = \frac{1}{N} \sum_{i=1}^N |P_{est} - P_{obs}| \quad (5.25)$$

where P_{est} , P_{obs} and N represent estimated, observed precipitation and number of data, respectively.

In MLR analysis, Model 2 and 3 are combined to generate a surface in ArcGIS environment. R^2 , $RMSE$ and MAE values are determined for Model 2 and Model 3, separately and given in Table 5.6. It can be seen that, R^2 values for Model 2 and 3 are slightly different from which were given in Table 5.4, before. This difference comes from the fact that isohyetal map (surface data) is used, instead of estimated precipitation data itself. Converting the combination of Model 2 and 3 to a surface increases the model performance for inland, particularly.

Table 5.6 : Comparison of models.

Gauge type	Statistics	IDW	RBF	Kriging	MLR
Coastal (16 gauges)	R^2	0.843	0.930	0.924	0.839
	$RMSE$	237.00	153.88	167.27	227.02
	MAE	175.36	107.12	118.02	198.43
Inland (16 gauges)	R^2	0.794	0.823	0.833	0.993
	$RMSE$	204.58	180.54	178.41	42.29
	MAE	168.73	148.42	144.63	20.96

The error statistics demonstrate that RBF performs better in the coastline than other methods. MLR results are similar to that of IDW and seem to be satisfactory for coastal gauges. The RMSE ranges from 153.88 to 237 represents from 9.8 and 15.1% of the observed mean annual precipitation in coastline. On the other hand, MLR is found to be the best suitable method for interpolation of precipitation for 16 inland gauges. This is followed by Kriging, RBF and IDW. The RMSE ranges from 42.29 to 204.58 which corresponds, respectively, 4 and 18.9% of the observed mean annual precipitation in inland.

For visual comparison, isohyetal maps are generated using aforementioned methods. Figure 5.12 shows isohyetal maps for IDW, RBF, Kriging and MLR, in sequence. In developing MLR isohyetal map, Model 2 and Model 3 are combined. The regression equation of Model 2 is used for coastline. Following coastline, for whole inland region, the equation of Model 3 is performed. MLR equations are applied on a grid system and converted to a surface.

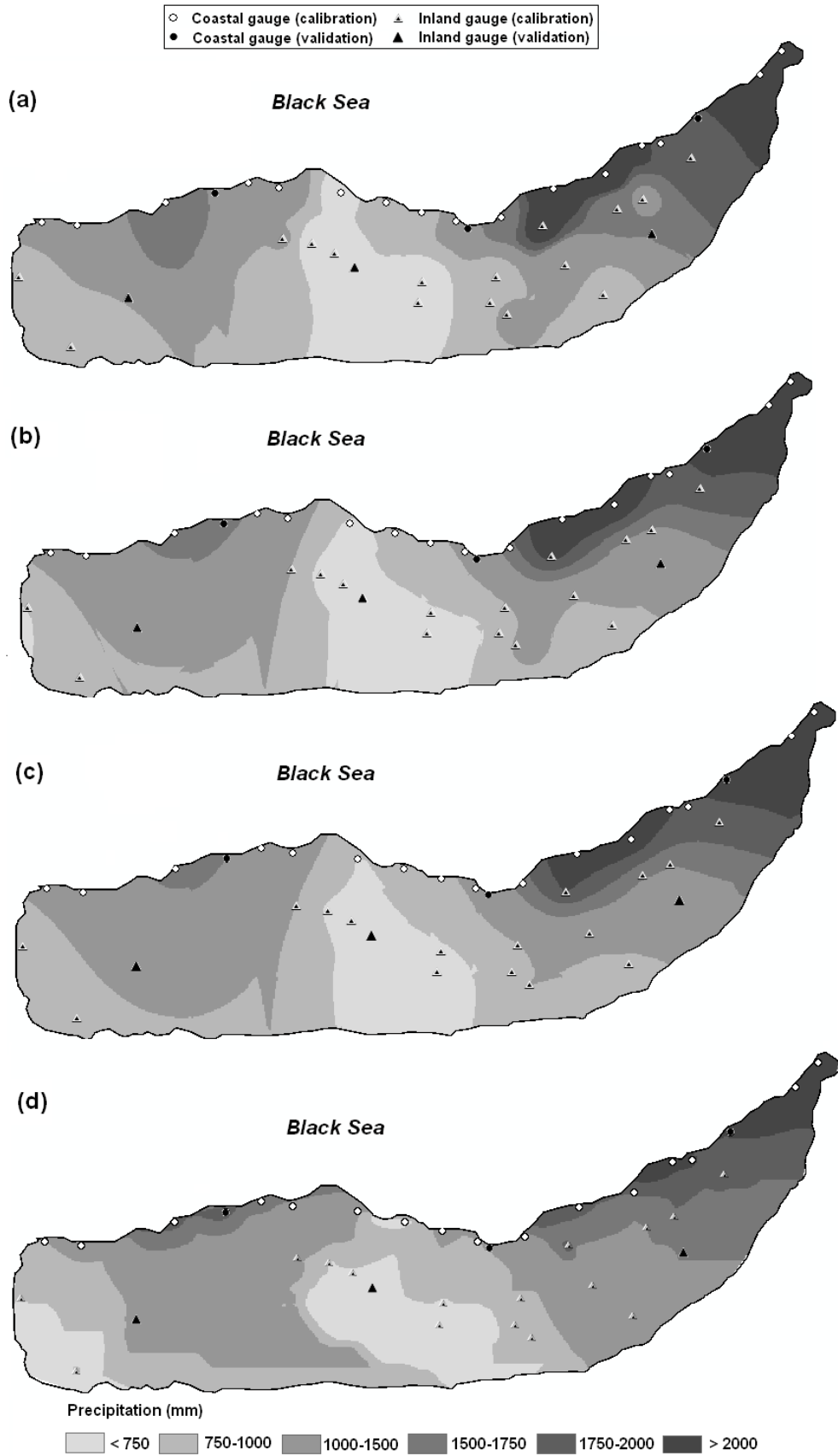


Figure 5.12 : Isohyetal maps generated from (a) IDW, (b) RBF, (c) Kriging and (d) MLR.

As seen from Figure 5.12, maps obtained by IDW, RBF, Kriging and even MLR are similar to each other. Effect of localization is obviously seen in IDW map. RBF and Kriging maps are more alike than others; in fact RMSE and MAE values of both are close to each other. In the MLR map, topographic characteristic of the region is more visible such as Harsit Valley (middle of the region with light grey color). Precipitation decreases through the inland in the whole maps as opposed to the elevation of the region that increases from coastline to inland. Orographic influence on precipitation can be seen in none of the isohyetal maps obtained from different methods.

One can realize that sharp passes were available on the left-hand side of the maps produced by IDW, RBF and Kriging (Figure 5.12 a, b, c). In order to improve the appearance of the contours in the maps, smoothing interpolation is employed, as an example, for isohyetal map derived using Kriging. The resulting smoothed isohyetal map is shown in Figure 5.13.

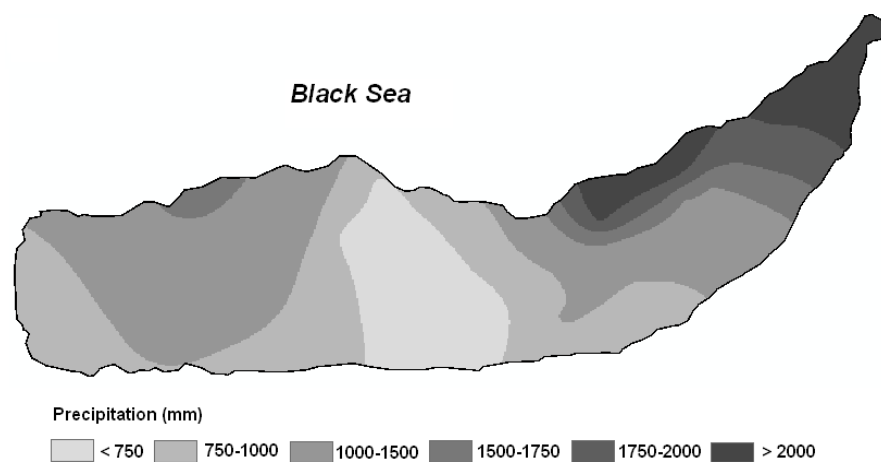


Figure 5.13 : Smoothed isohyetal map generated from Kriging.

Smoothing is not an exact interpolation; i.e., it is not possible to predict exact observed values at all gauged locations. Therefore, higher-order smoothness creates higher error term. For instance, RMSE value of smoothed isohyetal map generated from Kriging is 177 mm whereas RMSE value of the non-smoothed Kriging map is 172.9 mm. The non-smoothed maps are decided to use in the following chapters, due to the lower RMSE values.

The six (Gorele, Surmene, Findikli, Sinir, Macka and Meydan) gauges chosen before in the MLR analysis are used to validate the other models. Estimated precipitation for the coastal (Gorele, Surmene, Findikli) and inland (Sinir, Macka, Meydan)

gauges together with the observed precipitation values are shown in Figure 5.14. The validation results appear satisfactory for all methods except for MLR for Gorele, and MLR and IDW for Meydan gauges. For MLR, this can be explained by the distance between gauged locations and points on a 5x5 km grid system created for the MLR application (Figure 5.15).

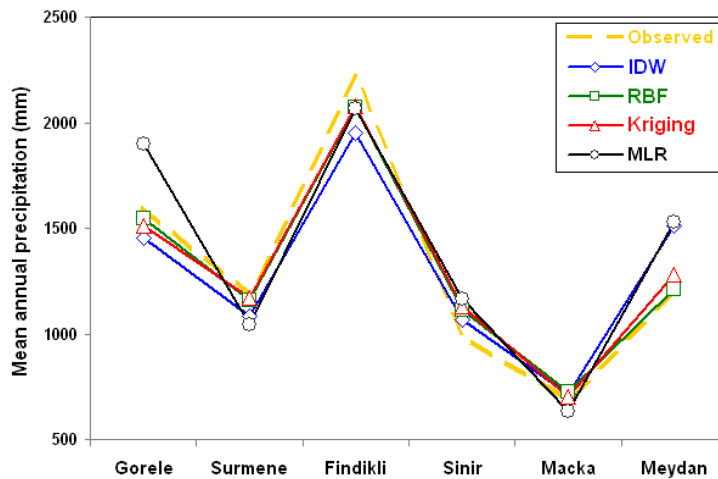


Figure 5.14 : Validation results of models.

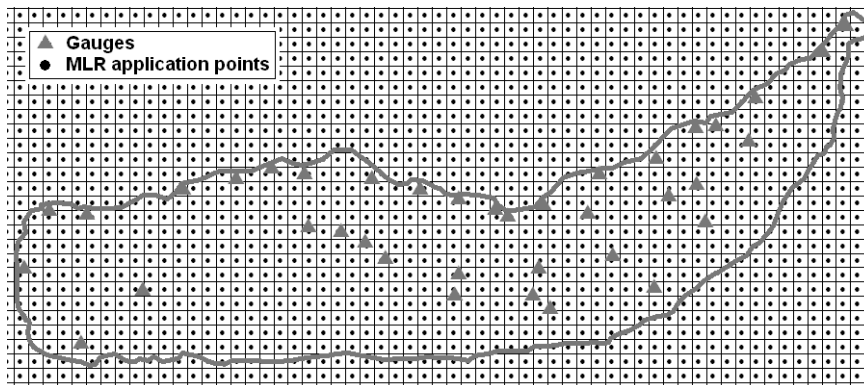


Figure 5.15 : Grid system used for MLR.

The accuracy of an interpolated surface depends on several factors: the number of observation points and the quality of the data at each point, the orientation and spacing of the observations, the distance between observations to be interpolated, and the spatial continuity of the variable under consideration (Armstrong, 1998). Developing accurate isohyetal maps can be a challenge because there are usually a limited number of rain gauges that have not a homogenous distribution on a mountainous terrain, particularly. In this context, only validation stage based on selected rain gauges will not be adequate to check the accuracy of isohyetal maps. Processes to validate maps will be mentioned in the following chapter.

6. VALIDATION OF ISOHYETAL MAPS

The weather stations are located at low elevations and are not generally representative for estimating basin-wide precipitation. When a watershed has a wide range of elevation, orographically induced precipitation is important (Chang, 2007). To avoid potential underestimation of precipitation, the isohyetal maps generated by means of different methods are validated by comparing the long term annual runoff coefficients estimated for each basin. It is known that, spatial distribution of precipitation over the basin had some effects on the degree of runoff (Leong and Abustan, 2006).

The runoff coefficient is defined as the ratio of flow depth to precipitation depth for annual time period. In the analysis, flow gauge at the outlet of each basin is used (Table 3.5). Mean annual streamflow is converted to runoff depths (millimeters) by dividing to the basin drainage area. The annual runoff coefficient is then calculated by Equation (6.1).

$$C = \frac{Q}{MAP} \quad (6.1)$$

where C , Q and MAP represents annual runoff coefficient, the height of mean annual flow in mm, and long term mean areal precipitation in mm, respectively. MAP is derived from the isohyetal maps for drainage area of each upstream gauge; namely, 40 runoff coefficients are obtained. The runoff coefficients considering isohyetal maps for each flow gauge are shown in Figure 6.1.

As seen from Figure 6.1, some of annual runoff coefficients are greater than one, which is theoretically unrealistic at annual scale. However, in a study by Akdogar (2006), annual runoff coefficient was given as 0.46, 0.83 and 1.07 for Giresun, Trabzon and Rize provinces, respectively. This information was obtained from a report by DSI (2005) (Onsoy, 2010).

Runoff coefficients greater than one might occur at monthly scale which can be explained with extraneous inflows such as groundwater and snowmelt contributing

runoff as delayed responses to precipitation (Mimikou and Ramachandra Rao, 1983; Kadioglu and Sen, 2001).

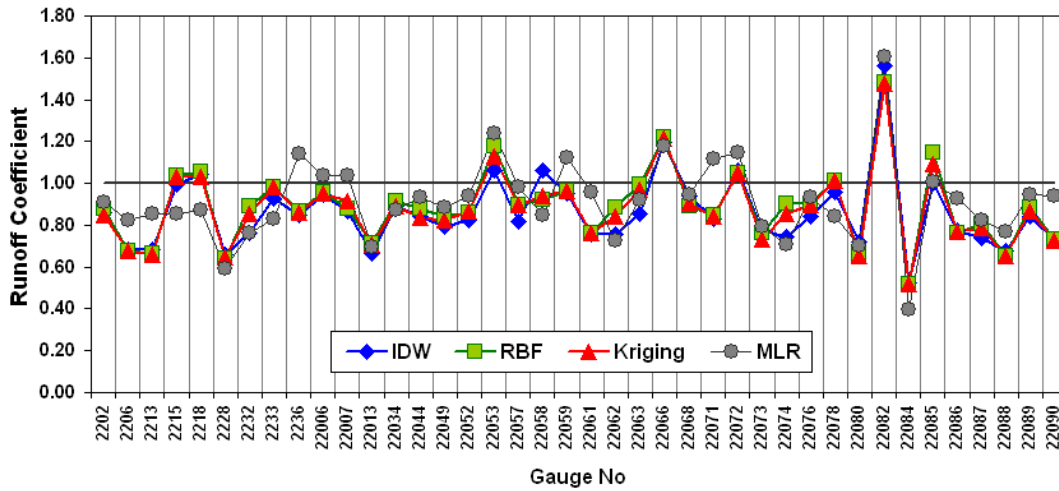


Figure 6.1 : Runoff coefficients for flow gauges.

Snowfall may be seen in winter in Eastern Black Sea Region. The ratio of precipitation in Uzungol (31) gauge to flow in Serah (22007) gauge is plotted in Figure 6.2. These gauges were located in almost the same place. As seen from Figure 6.2, flow is greater than precipitation from April to July. This clearly indicates contribution of snowmelt. Runoff coefficients approaching one can be explained by snow melting; however snowmelt is not considered to be reason of the higher runoff coefficients at annual scale since snowmelt cover is not permanent.

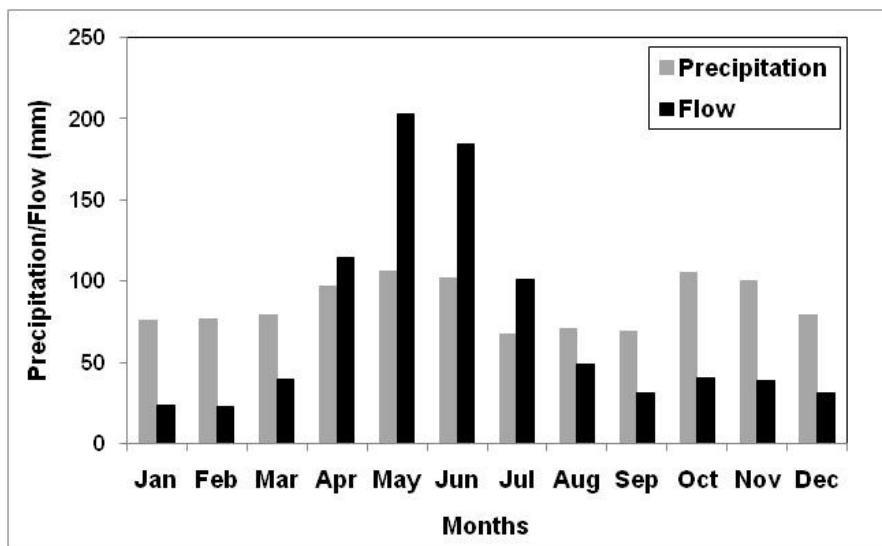


Figure 6.2 : Precipitation and flow data of Uzungol rain gauge and Serah flow gauge.

No doubt that, high runoff coefficients are reflections of the misrepresentation of spatial distribution of precipitation obtained from isohyetal maps.

Gauges tend to lie at low elevations relative to the surrounding terrain. For hydrologic modeling purposes, the resulting bias can result in serious underprediction of observed flows (Adam et al., 2006), which shows itself high runoff coefficients in this study.

Precipitation datasets that are constructed by the interpolation of point estimates to a coarse-resolution grid generally misrepresent (usually underestimate) precipitation in topographically complex regions due to an underrepresentation of gauge locations at high elevations (Adam et al., 2006). To determine “true” precipitation, in the next chapters, streamflow measurements will distribute onto basins and then performs water balance equation.

7. DERIVATION OF FLOW DEPTH MAP

7.1 Introduction

In the previous chapter, isohyetal maps generated with the help of various geostatistical methods and MLR was seemed to be appropriate for point scale precipitation estimation. However; these maps were validated by runoff coefficients which were found to be greater than one for some basins. This condition addresses orographic effects that could not be realized from gauge observations. In order to determine spatial distribution of precipitation more accurately, precipitation will be predicted inversely using streamflow and other losses based on the continuity equation.

The continuity equation applied to a basin is valid across all spatial and temporal scales:

$$\frac{dS}{dt} = P - ET - Q - G \quad (7.1)$$

where P , ET , and Q are the basin-average precipitation, evapotranspiration, and flow, respectively; G is the net discharge of groundwater out of the aquifer underlying the basin; and dS is the net change in storage for a given time increment, dt . For longer time periods in which the net change in storage is negligible (e.g., reservoir and aquifer storage effects are not significant), Equation (7.1) becomes

$$\bar{P} = \bar{Q} + \bar{ET} \quad (7.2)$$

where \bar{P} , \bar{Q} , and \bar{ET} are long-term mean annual basin average precipitation, flow, and evapotranspiration, respectively. Therefore, the precipitation climatology for a basin can be determined by distributing mean annual streamflow measurements \bar{Q} back onto the basin (Adam et al., 2006). Note that, streamflow data represents the most accurate information about terrestrial water cycle (Fekete et al., 2000)

In the next chapters, flow depth and evapotranspiration map will be determined sequentially, and then will be summed up to obtain precipitation distribution map for the study area.

7.2 Method

In order to generate flow maps, annual average values of flow have to be gathered over the study region. Ordinary kriging method which was applied to 10-day long runoff depth for a given exceedence probability by Huang and Yang (1998) is used for mapping annual flow depth.

It is well known that there is a relationship between flow and basin area as follows:

$$Q' = c(A)^n \quad (7.3a)$$

or

$$Q'/A = c(A)^{n-1} \quad (7.3b)$$

where Q' is flow volume for a given period at a site, A is basin area above this site, c and n are coefficients and (Q'/A) is runoff depth for a given period at the site.

The variable (Q'/A) can be regarded as a regionalized variable representing one realization of the runoff-depth random function. The mathematical expectation of this variable gives

$$E[Q'/A] = E\left\{ \left[c(A)^{n-1} \right] \right\} = f(A) \quad (7.4)$$

in which that as $n=1.0$ and $n \neq 1.0$ correspond to stationary and nonstationary conditions, respectively. In the latter, three cases are classified: (i) $n < 0.0$, where the flow decreases in the downstream direction in arid regions; (ii) $0.0 < n < 1.0$, where a gradual decline of runoff depth appears in the downstream direction and in such areas there may be a greater rainfall intensity in upstream regions; and (3) $n > 1.0$, where both flow and runoff depth increase in the downstream direction, indicating a great abundance of water resources in the basin.

Flow depth is uniformly distributed throughout the basin as $n = 1.0$, indicating a homogeneous basin where the increase in flow volume is proportional to

enlargement of the basin area. If the hypothesis of stationarity is valid, Ordinary Kriging is applicable (Huang and Yang, 1998).

The flow depth represents uniformly distributed effective precipitation over the area. Therefore the representative value of the flow depth is allocated on the centroid of the area (Huang and Yang, 1998). Therefore, after obtaining flow depth from the data, depth values are placed on centroid of the basins in the study area.

7.3 Application and Evaluation

To support the assumption that flow depth is distributed within a hydrologically homogenous area, namely to determine $n \approx 1$, the relationship between flows and basin areas are investigated. Mean annual flow data and basin areas are plotted on a logarithmic plane and shown in Figure 7.1.

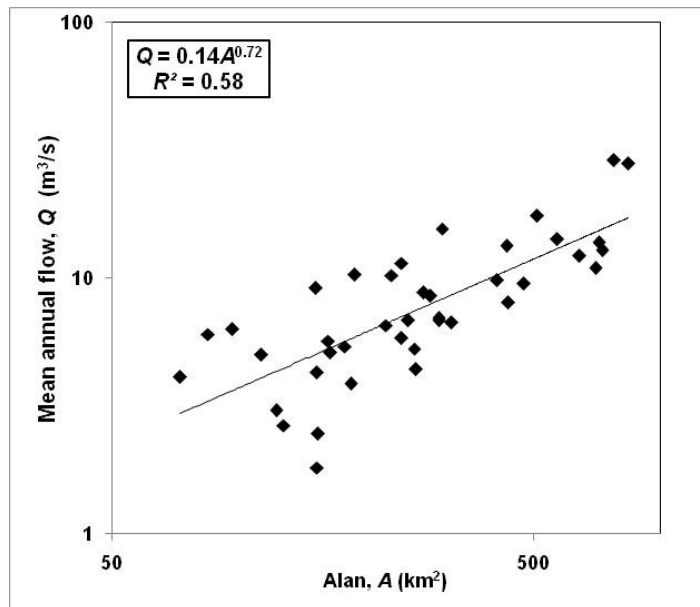


Figure 7.1 : Mean annual flow-area relationship.

As seen from Figure 7.1, obviously, there is a relationship between flow and basin area. The coefficient, n , was found to be 0.72 which is between the values 0 and 1, but closer to 1. To ensure for applicability of Ordinary Kriging, further analysis is performed. Regionalized variable (flow in this case) can be regarded as having 2 components such as drift which is sometimes called trend and residuals. The drift represents the systematic trend inherent in the data; the residual is the difference between the actual observations and the drift (Holdaway, 1996). The normality test

of residuals satisfies the stationary condition for kriging (Kholghi and Hosseini, 2009) which means Ordinary Kriging is applicable.

In this regard, a regression equation is derived from mean annual flow (Q , m^3/s) data as follows;

$$Q = -16.18 + 3.10^{-5} X + 0.024A \quad (7.5)$$

where X and A represents longitude (m) and basin area (km^2), respectively. The determination coefficient of this equation is 0.801, namely it can clearly explain the drift effect of the regionalized variable. The Kolmogorov-Smirnov test is used to determine the normality of residuals. At 95% level, residuals are found to be normal. Histogram of residuals and normal plot can be seen in Figure 7.2.

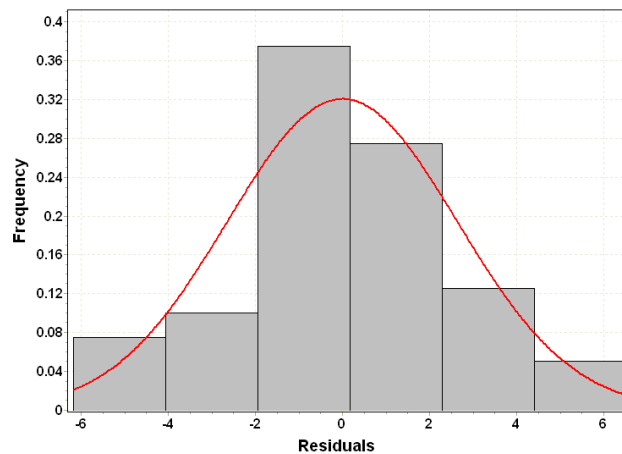


Figure 7.2 : Histogram of residuals and normal plot.

After stationarity of the data has been verified, centroid points of the basins are determined. For mapping flow depth, an appropriate theoretical variogram model must be determined. Cross-validation is used to compare different variogram models and chosen Gaussian type. Experimental and theoretical variograms for mean annual flow depth can be seen in Figure 7.3. The corresponding parameters used in the Ordinary Kriging were presented in Table 7.1. Cross validation results of observed and estimated flow depth values for Kriging method is given in Figure 7.4. Figure 7.5 shows the flow depth map generated from Ordinary Kriging method for coastal part of the Eastern Black Sea Region.

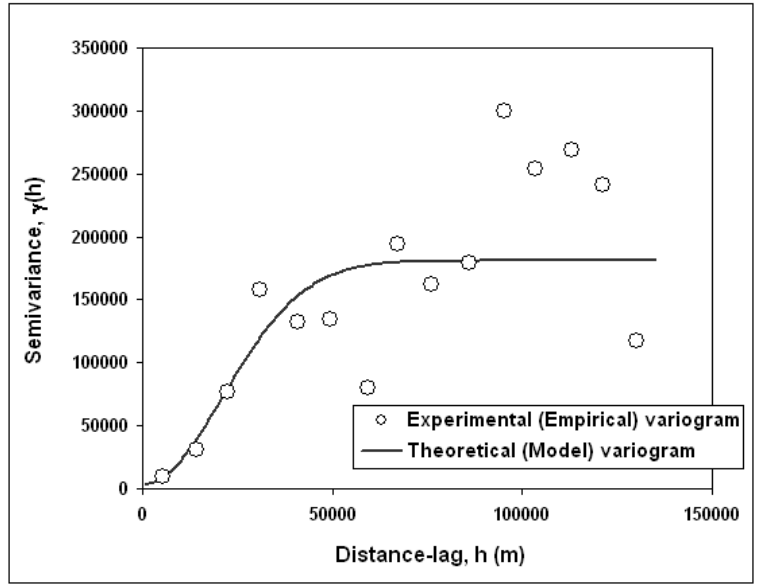


Figure 7.3 : Experimental variogram of the flow depth with Gaussian model fitted.

Table 7.1 : Parameters of theoretical variogram for flow data.

Model	Range (m)	Lag Size (m)	Number of lag	Nugget (mm ²)	Partial Sill (mm ²)	Number of neighbor
Gaussian	51860	9014	15	3513	177380	4

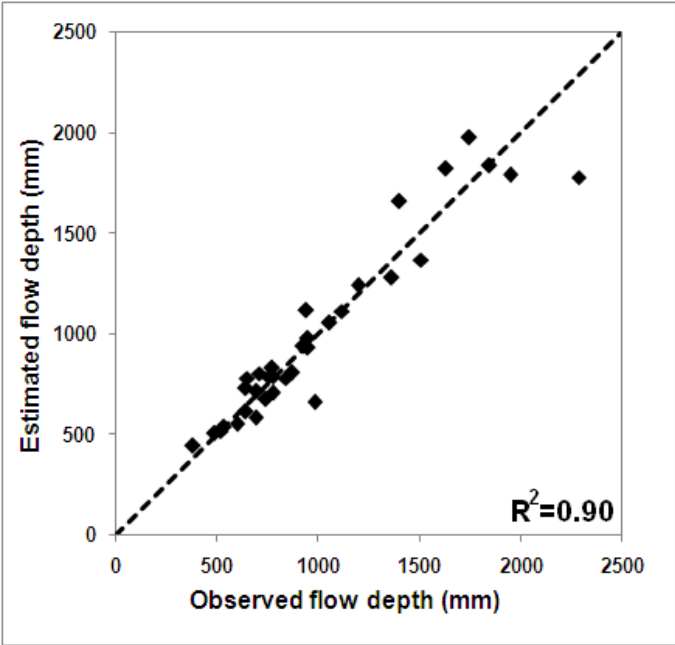


Figure 7.4 : Cross validation results of observed and estimated flow depth values.

Similar to the map given in Figure 5.13, flow depth map in Figure 7.5 can be smoothed. However, the map was not smoothed as the non-smoothed map were decided to use due to their lower RMSE values.

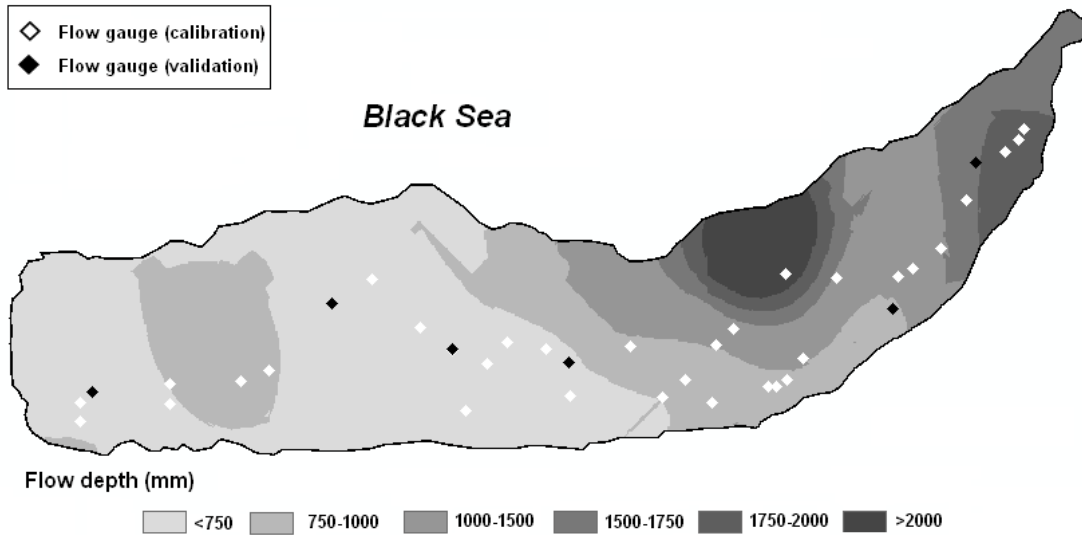


Figure 7.5 : Flow depth map for the study area.

In order to test the validity of the flow depth map, 6 among 40 flow gauges are randomly chosen. Figure 7.5 also shows the gauges used in the calibration and validation processes. The validation results of randomly chosen gauges are summarized in Table 7.2 where *OMAF* and *EMAF* denote the observed and estimated mean annual flows; respectively; *RE* shows the relative error (Equation 5.22).

Table 7.2 : Validation results based on flow depth map.

Gauge no	Gauge name	<i>OMAF</i> (m ³ /s)	Estimated flow depth (mm)	<i>EMAF</i> (m ³ /s)	<i>RE</i> (%)
2202	Agnas	12.20	702.57	14.16	16.09
2213	Dereli	13.80	640.43	14.48	4.93
22058	Cucenkopru	5.68	651.27	3.36	-40.80
22072	Arili	6.32	1722.26	5.03	-20.33
22074	Cat	8.79	965.31	8.50	-3.36
22086	Ogutlu	12.85	504.50	11.65	-9.30

8. DERIVATION OF EVAPOTRANSPIRATION MAP

8.1 Introduction

In order to determine the precipitation distribution of coastal part of the Eastern Black Sea Region, in addition to spatial distribution estimation of streamflow depth map, evapotranspiration should be also determined.

Evapotranspiration is a collective term for all the processes by which water in liquid or solid phase at or near the land surfaces becomes water vapor (Dingman, 2008). Two main concepts related to evapotranspiration are potential and actual evapotranspiration. Losses that occur when sufficient water is available in the soil are called potential evapotranspiration (*PET*), while actual evapotranspiration (*AET*) is limited by the water in the soil (Bayazit, 2001). Several characteristics of the surface have a strong influence on evapotranspiration such as albedo, the maximum leaf conductance, presence or absence of intercepted water etc. Because of these surface effects, Penman (1956) redefined *PET* as “amount of water transpired...by a short green crop, completely shading the ground, of uniform height and never short of water”, and the term reference crop evapotranspiration (*ET_o*) is increasingly used as a synonym for *PET* (Dingman, 2008). There are approximately 50 methods or models available to estimate *PET* (*ET_o*), but these methods or models give inconsistent values due to their different assumptions and input data requirements, or because they were often developed for specific climatic regions (Grismar et al., 2002; Lu et al., 2005). On the other hand, in many areas, the necessary meteorological data are lacking, and simpler techniques are required. Reference (or potential) evapotranspiration (*ET_o*, *PET*) is often estimated from evaporation pan data as they are widely available and of longer duration than more recently available micrometeorologically based *ET_o* estimates (Grismar et al., 2002).

The relation between evaporation rate from class “A” evaporation pan (*E_{pan}*) and reference evapotranspiration (*ET_o*) is given as follows (Snyder, 1992):

$$K_p = ET_0 / E_{pan} \quad (8.1)$$

where K_p is the pan coefficient, that depends on the prevailing upwind fetch distance, average daily wind speed, and relative humidity conditions associated with the sitting of the evaporation pan (Doorenbos and Pruitt, 1977).

As mentioned briefly before, actual evapotranspiration includes evaporation from water and soil and transpiration from the vegetation of a specific region; whereas potential evapotranspiration includes the maximum quantity of water capable of being evaporated from the soil and transpired from the vegetation of a specific surface (Zhang et al., 2007). Actual evapotranspiration (AET) is a function of precipitation, temperature, solar radiation, soil water storage, wind, canopy and understory interception, and growth rates. Few methods for measuring AET directly are available. Although field studies using lysimeters and air-monitored tents have been somewhat successful in measuring AET in agricultural or open situations, AET cannot be measured directly within forested systems by any practical field method (Brooks et al., 1991; Kolka and Wolf, 1998). Another way to estimate AET is an empirical relation consists of precipitation and PET , proposed by Turc (1954) and Pike (1964) which is used in this study.

In the next chapters, calculation of PET (ET_o), E_{pan} and AET values by different methods is discussed for both coastal and inland gauges. PET and E_{pan} values to be calculated are used to compare to AET values. Consequently, AET values are used to evapotranspiration mapping.

8.2 Estimation of Potential Evapotranspiration

8.2.1 Method

As indicated before (see chapter 3.2.2), some meteorological gauges have both temperature and evaporation data, rest recorded only one of these data. Evaporation records of some gauges include only 8 months of the year (from April to November), the rest have even less. To estimate the non-existing E_{pan} data in the gauges, and extend the data period to whole year temperature-based Thornthwaite method is used.

Thornthwaite method was originally developed as an index for classifying climate. It is based on the assumption that air temperature represents the integrated effects of radiation and other control mechanisms such as wind, humidity, vegetation etc. The Thornthwaite basic formula for computing monthly PET is (Thornthwaite, 1948):

$$PET = 16C(10T_m / I)^a \quad (8.2)$$

where PET ; monthly potential evapotranspiration (mm), C ; daylight coefficient which can be obtained from Table 8.1, T_m ; monthly mean temperature ($^{\circ}C$), I ; a heat index which can be calculated from Equation 8.3, a is an exponent derived from the heat index (I) using Equation (8.4).

$$I = \sum_1^{12} (T_m / 5)^{1.51} \quad (8.3)$$

$$a = (67.5 \times 10^{-8} I^3) - (77.1 \times 10^{-6} I^2) + (0.179 I) + 0.492 \quad (8.4)$$

Table 8.1 : Daylight coefficient (C) for Thornthwaite formula.

Latitude (degree)	Jan	Feb	Mar	Apr	May	June	July	Aug	Sep	Oct	Nov	Dec
60 N	0.54	0.67	0.97	1.19	1.33	1.56	1.55	1.33	1.07	0.84	0.58	0.48
50 N	0.71	0.84	0.98	1.14	1.28	1.36	1.33	1.21	1.06	0.90	0.76	0.68
40 N	0.80	0.89	0.99	1.10	1.20	1.25	1.23	1.15	1.04	0.93	0.83	0.78
30 N	0.87	0.93	1.00	1.07	1.14	1.17	1.16	1.11	1.03	0.96	0.89	0.85
20 N	0.92	0.96	1.00	1.05	1.09	1.11	1.10	1.07	1.02	0.98	0.93	0.91
10 N	0.97	0.98	1.00	1.03	1.05	1.06	1.05	1.04	1.02	0.99	0.97	0.96
0	1.00	1.00	1.00	1.00	1.00	1.00	1.00	1.00	1.00	1.00	1.00	1.00
10 S	1.05	1.04	1.02	0.99	0.97	0.96	0.97	0.98	1.00	1.03	1.05	1.06
20 S	1.10	1.07	1.02	0.98	0.93	0.91	0.92	0.96	1.00	1.05	1.09	1.11
30 S	1.16	1.11	1.03	0.96	0.89	0.85	0.87	0.93	1.00	1.07	1.14	1.17
40 S	1.23	1.15	1.04	0.93	0.83	0.78	0.80	0.89	0.99	1.10	1.20	1.25
50 S	1.33	1.19	1.05	0.89	0.75	0.68	0.70	0.82	0.97	1.13	1.27	1.36

8.2.2 Estimation of Evaporation and Potential Evapotranspiration for Coastal Zone

Coastal gauges, Vakfikebir (6), Arsin (9), Arakli (10), Of (12), Pazar (15), Ardesen (16), Findikli (17) record temperature, mean wind speed and relative humidity but no evaporation. In addition to foregoing observations, evaporation data from April to November are recorded in Giresun (2), Akcaabat (7), Trabzon (8), Rize (13), Ordu, Unye. A relationship can be developed between pan evaporation and mean wind speed, relative humidity and temperature data of the coastal gauges (2, 7, 8, 13 including Ordu and Unye) for 8 months of the year. Thus, this relation can be used to estimate E_{pan} in the coastal gauges (6, 9, 10, 12, 15, 16, and 17) which no E_{pan} data exist for the same period. A multiple linear regression (MLR) equation is derived to reflect this relation as follows:

$$E_{pan} = \beta_0 + \beta_1(WS) + \beta_2(T) + \beta_3(RH) \quad (8.5)$$

where, WS , T and RH represent mean wind speed (m/sec), temperature ($^{\circ}C$) and relative humidity (%), respectively. Regression coefficients (β) and statistics are shown in Table 8.2, scatter diagram of observed and estimated E_{pan} is given in Figure 8.1.

Table 8.2 : Regression coefficients and statistics.

	Coefficients	Standardized Coefficients
β_0	263.36	-
β_1	8.986	0.246
β_2	2.463	0.690
β_3	-3.330	-0.593
Statistics		
Number of data	32	
R^2	0.926	
$Adj-R^2$	0.918	
SE	4.343	

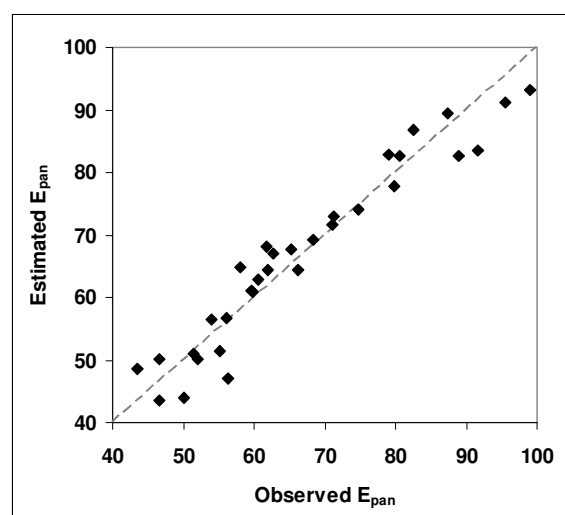


Figure 8.1 : Scatter diagram of observed and estimated E_{pan} values.

This equation was established by means of the data recorded in the gauges (2, 7, 8, 13 including Ordu and Unye) to use in estimating evaporation values in the coastal gauges (6, 9, 10, 12, 15, 16, and 17) for the period extending from April to November. Estimated E_{pan} values are shown in Figure 8.2 with dark grey color.

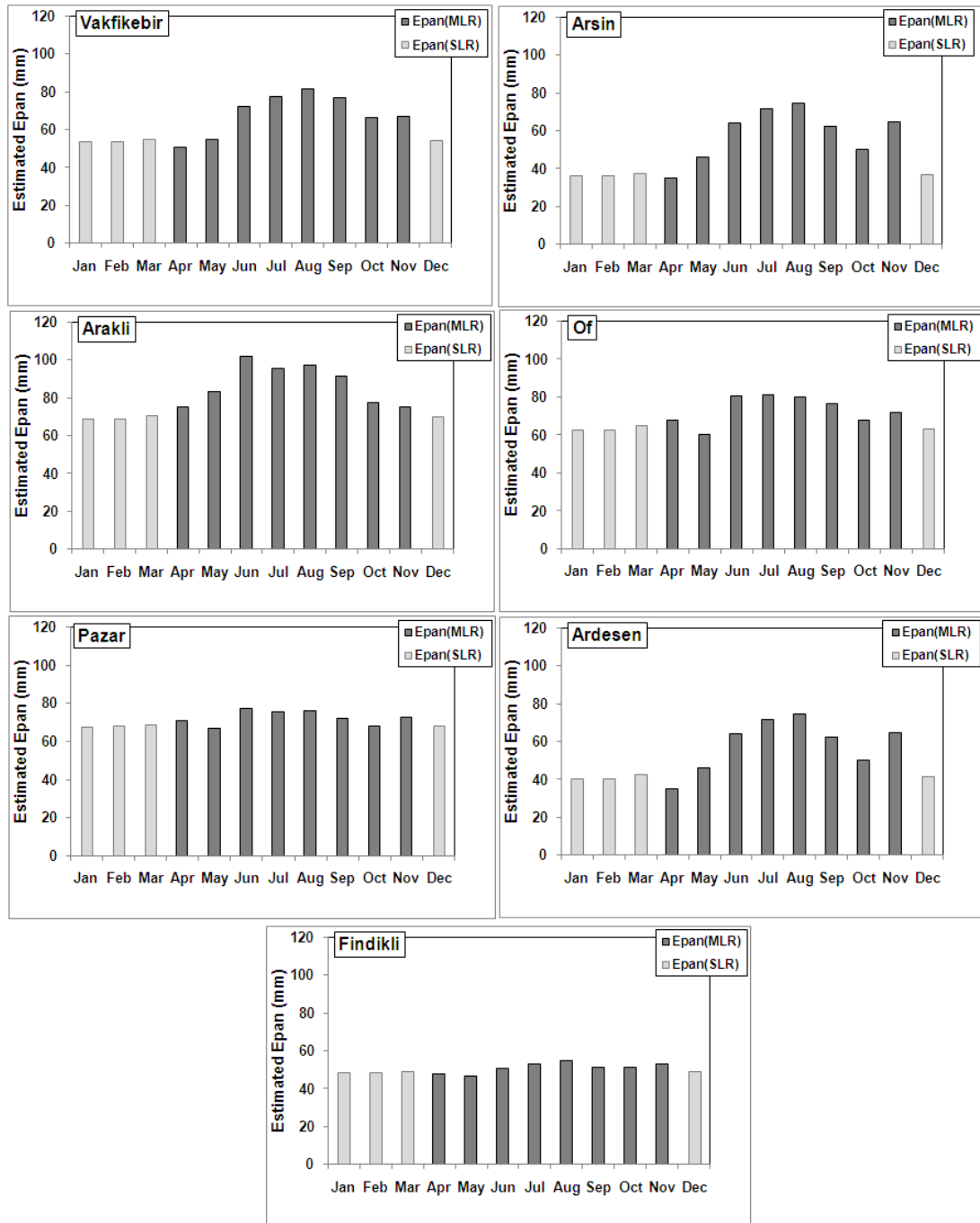


Figure 8.2 : E_{pan} values estimated from MLR equation and PET values for coastal gauges (6, 9, 10, 12, 15, 16, and 17).

Pan evaporation records in Turkey cover only the 8-month period, from April to November. Therefore, E_{pan} values from December to March are not available neither in coastal gauges Giresun (2), Akcaabat (7), Trabzon (8), Rize (13), Ordu, Unye nor in Vakfikebir (6), Arsin (9), Arakli (10), Of (12), Pazar (15), Ardesen (16), Findikli (17). For completion of these values, first, PET values of aforementioned gauges are calculated with help of Thornthwaite method. A simple linear regression (SLR)

equation between calculated PET values and observed/estimated E_{pan} values is then generated for each coastal gauge. It should be recalled that, E_{pan} values in the gauges (6, 9, 10, 12, 15, 16, and 17) are not observations but estimations. The SLR equation developed using PET values and observed/estimated E_{pan} values covering the months April-November for each coastal gauge can be extended to the period from December to March (Equation 8.6).

$$E_{pan} = \beta_o + \beta_1(PET) \quad (8.6)$$

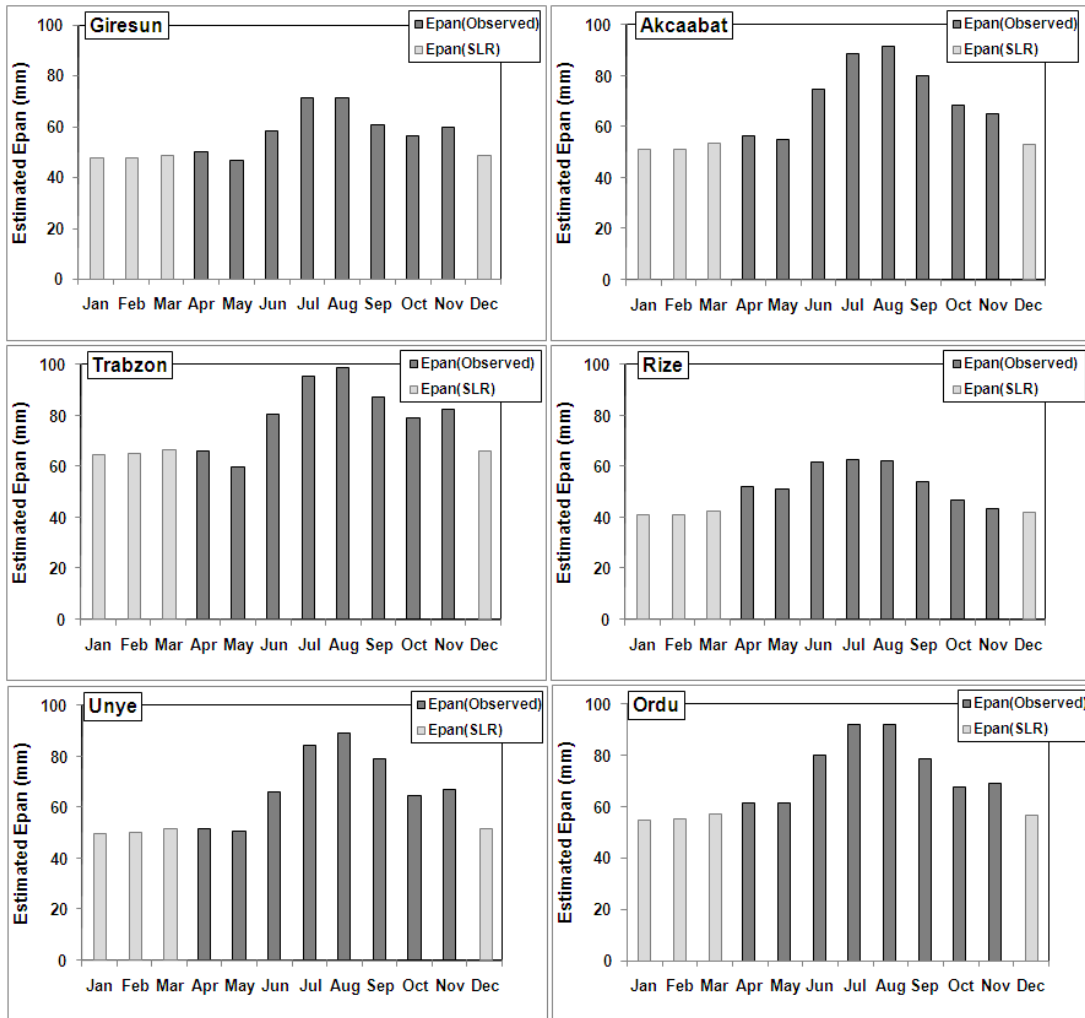


Figure 8.3 : E_{pan} values, observations and estimations from simple linear regression equation using PET values for gauges (2, 7, 8, 13 with Ordu and Unye).

E_{pan} values which are not observed from December to March are obtained using SLR equation for each coastal gauge. Note that, temperature data of all coastal gauges are available so that PET values of these gauges can be calculated. E_{pan} values from December to March for the gauges (6, 9, 10, 12, 15, 16, and 17) are also shown Figure 8.2 with a light grey color. Observed and estimated E_{pan} values for the gauges

(2, 7, 8, 13 with Ordu and Unye) are depicted in Figure 8.3. Consequently, E_{pan} values were calculated for the coastal gauges with partial observations (from April to November) or no observation at all, thus annual totals were obtained.

8.2.3 Estimation of Evaporation and Potential Evapotranspiration for Inland Zone

Determination of E_{pan} values in inland is more complicated than that in the coastal ones. Because inland gauges which have evaporation data, have no temperature data recorded. Besides, evaporation records are irregular, available data length ranges from 5 to 8 months of the year. For filling the gaps, following procedure shown also as a flow chart in Figure 8.4 can be applied and. All computations are based on the PET values and E_{pan} observations of the 6 coastal gauges Giresun (2), Akcaabat (7), Trabzon (8), Rize (13), Ordu, Unye and E_{pan} observations of the 8 inland gauges Sofulu (20), Tamdere (21), Sinir (22), Guzelyayla (25), Kayaici (27), Sivrikaya (34), Meydan (37) and Tunca (38).

1. Available E_{pan} observations of above inland gauges and coastal gauges are averaged separately independent from the record period. Thus, coastal average and inland average E_{pan} are calculated.
2. Inland average E_{pan} is divided to coastal average E_{pan} . This is the ratio of inland E_{pan} to coastal E_{pan} and it is called K_{Epan} .
3. PET values of 6 coastal gauges are averaged for each month (j represents each month from January to December). These 12 values can be assumed as PET curve of coastal zone.
4. K_{Epan} is multiplied with monthly PET values of coastal gauges. Similar to the coastal zone, these values can be presumed as the monthly PET curve of inland ($\overline{PET}_{inland}(j)$).
5. Available E_{pan} observations of each inland gauge are averaged (i represents individual inland gauge)
6. Average E_{pan} value of each inland gauge is divided to the inland average E_{pan} , called $k_{Epan}(i)$. Thus, 8 $k_{Epan}(i)$ values are obtained for 8 inland gauges. It can be said that these ratios show the difference between evaporation values for each gauge and the inland average E_{pan} .

7. For each month, each $k_{E_{pan}}(i)$ is multiplied with monthly $\overline{PET}_{inland}(j)$ which was calculated in Step 4. These are PET values of each inland gauges from January to December.
8. For 8 inland gauges, a simple linear regression equation is derived between PET and E_{pan} for data-available months which vary from April or May to October or November.
9. Non-available E_{pan} values for months from October or November to March or April are obtained from the regression equations in Step 8 using PET values computed in Step 7.

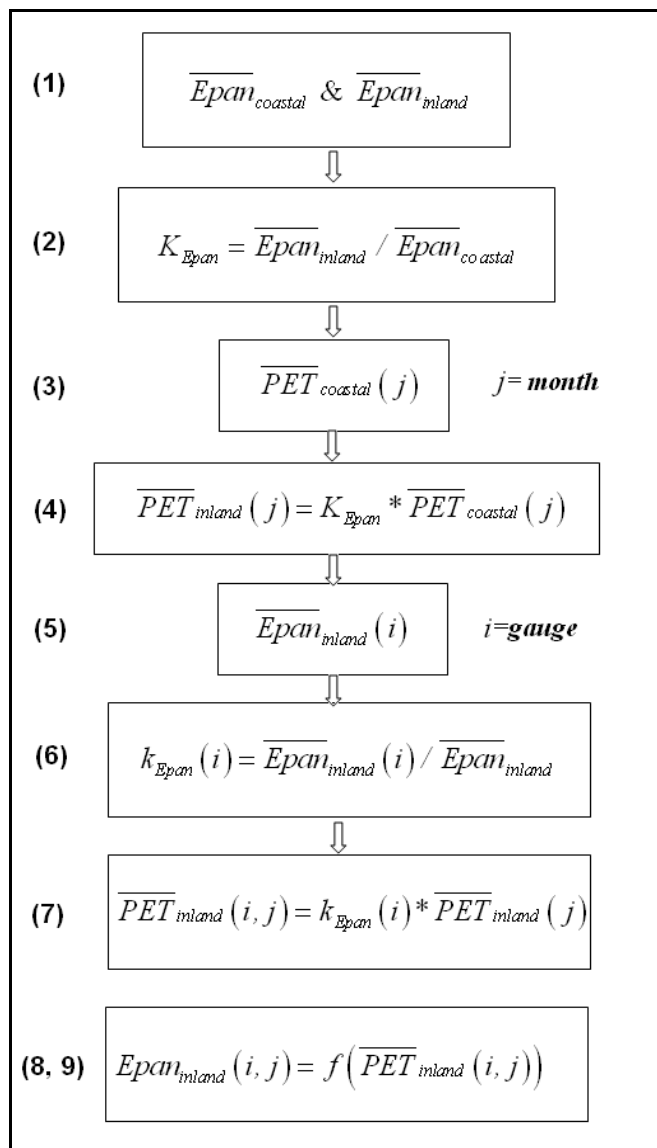


Figure 8.4 : Flow chart of estimation of evaporation for inland zone.

Eight inland gauges, Sofulu (20), Tamdere (21), Sinir (22), Guzelyayla (25), Kayaici (27), Sivrikaya (34), Meydan (37) and Tunca (38), have only evaporation data for a specified period. To complete E_{pan} values, aforementioned way is applied. Results are shown with light grey color in Figure 8.5 together with observed E_{pan} data. E_{pan} values were calculated for the inland gauges which have partial E_{pan} observations (from April to November) and thus annual totals were obtained.

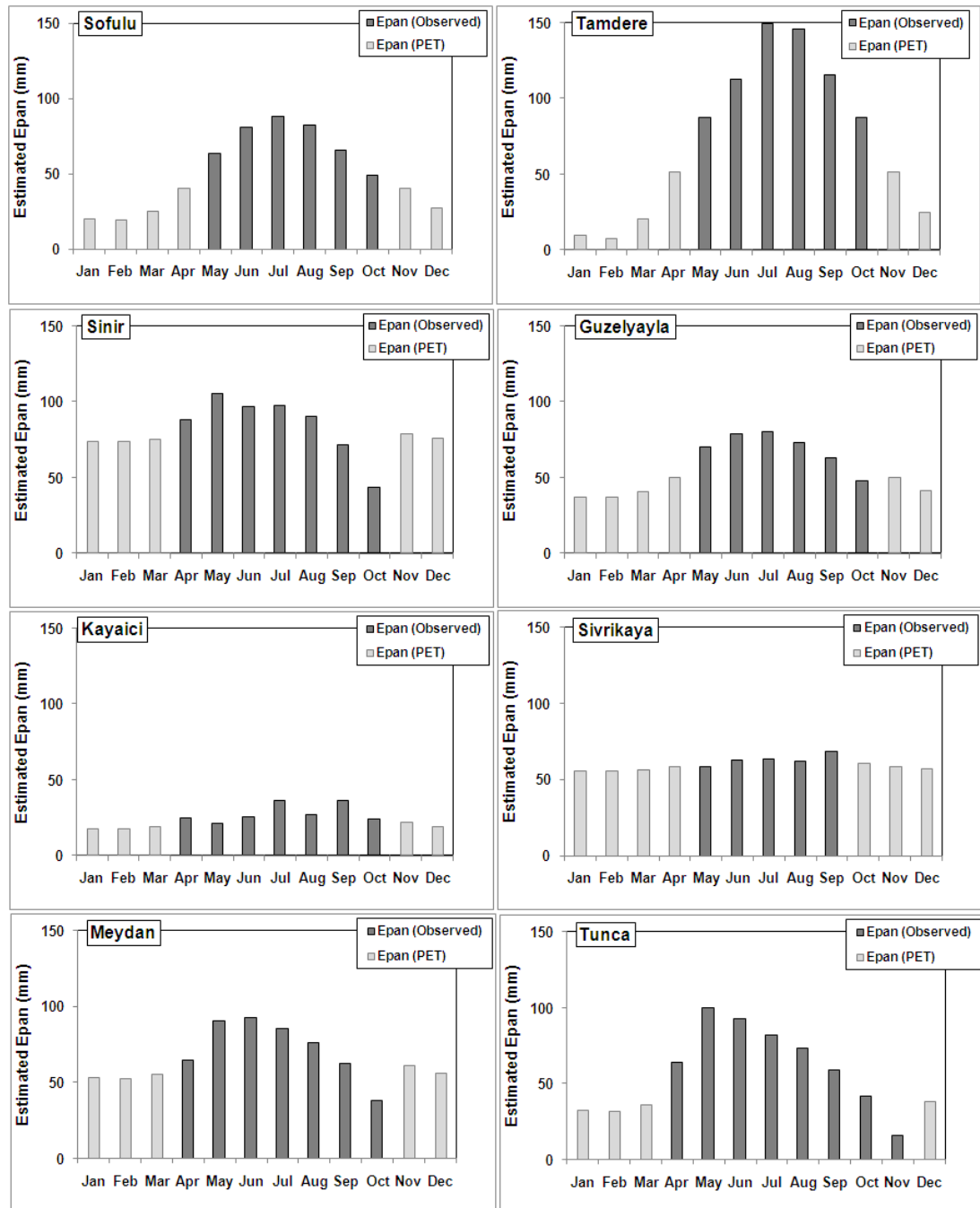


Figure 8.5 : E_{pan} values, observations and estimation by the method shown in Figure 8.4 for gauges (20, 21, 22, 25, 27, 34, 37 and 38).

8.3 Estimation of Actual Evapotranspiration

8.3.1 Method

Long-term actual evapotranspiration is estimated using an equation developed by Turc-Pike (1964). Turc (1954), using annual sums of annual precipitation, annual means of runoff and temperature from 254 drainage basins covering different climates in Europe, Africa, America and Asia, has derived a formula for the calculation of annual actual evapotranspiration (Parajka and Szolgyay, 1998). This approach was modified by Pike (1964) (Turc-Pike method). The Turc-Pike model is a quasi 'physically based' annual model because it uses precipitation and potential evapotranspiration (PET) to compute a ratio between actual evapotranspiration and potential evapotranspiration (Figure 8.6). Hotter, more arid regions plot to the left of the figure as PET is high and colder, more humid regions will plot to the right (Yates, 1997).

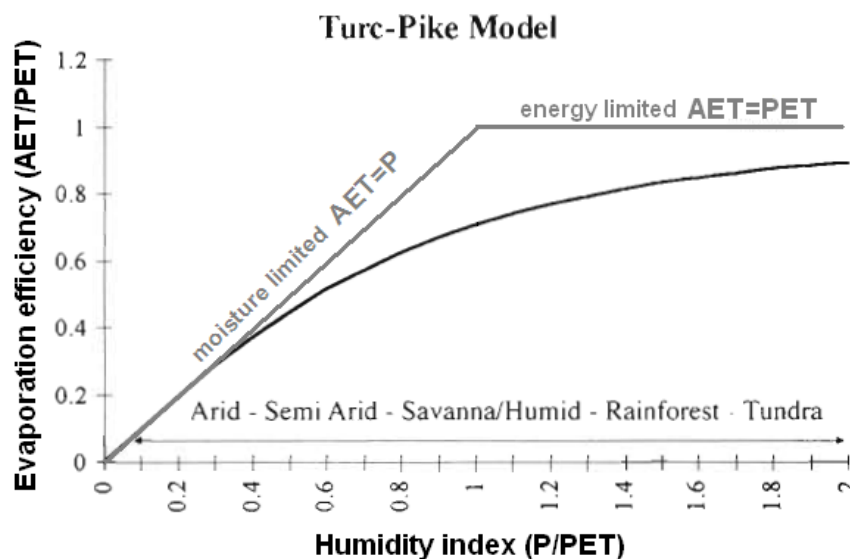


Figure 8.6 : Plot of Turc-Pike model.

The Turc-Pike actual evapotranspiration model can be written as:

$$\frac{AET}{PET} = \frac{(P/PET)}{\sqrt{1 + \left(\frac{P}{PET}\right)^2}} \quad (8.7)$$

where PET and AET represents potential and actual evapotranspiration, respectively; P is precipitation.

The difficulty in using this approach is the need to estimate *PET*. In the previous chapter, *PET* values have already been calculated by means of Thornthwaite method. Thus, mean annual *PET* values and precipitation data are available to predict *AET*.

8.3.2 Estimation of Actual Evapotranspiration for Coastal and Inland Gauges

Temperature data are available in 13 coastal gauges Giresun (2), Vakfikebir (6), Akcaabat (7), Trabzon (8), Arsin (9), Arakli (10), Of (12), Rize (13), Pazar (15), Ardesen (16), Findikli (17), Ordu and Unye and 7 inland gauges Tonya (23), Duzkoy (24), Macka (26), Dagbasi (28), Caykara (30), Uzungol (31) and İkiizdere (33). *PET* values were estimated for the coastal gauges using Thornthwaite formula before. These values are also calculated for inland gauges. *AET* values are determined from *PET* values and precipitation data using Turc-Pike equation. *AET* values are shown in Figure 8.7.

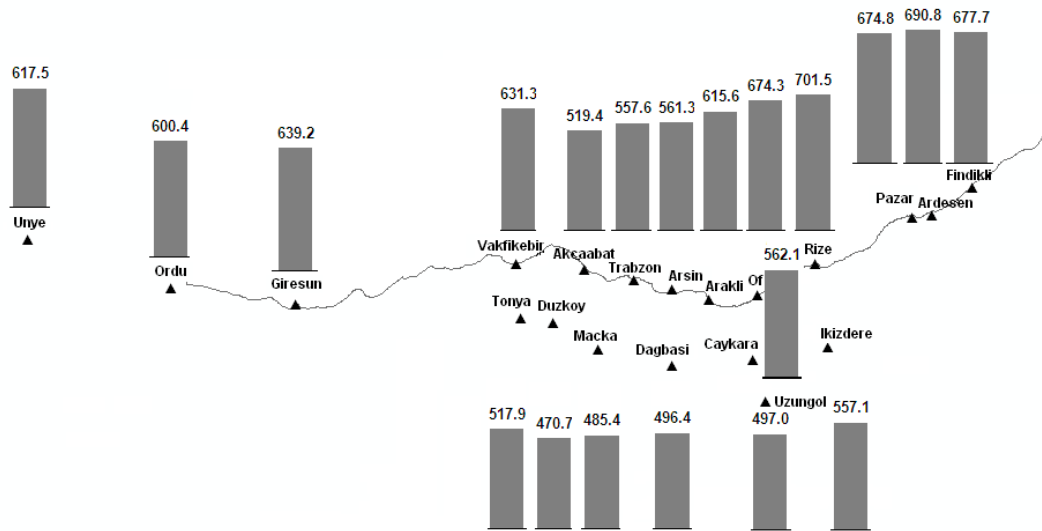


Figure 8.7 : *AET* values estimated using Turc-Pike method.

8.4 Application and Evaluation

Potential evapotranspiration (*PET*), evaporation (E_{pan}) and actual evapotranspiration (*AET*) values have been estimated for the study area, so far. The estimated values are used to identify the characteristics of evapotranspiration and evaporation of the study area, before mapping *AET*. All these values are summarized in Figure 8.8. Precipitation values are greater than E_{pan} , *PET* and *AET* for most gauges. Precipitations of Akcaabat (7), Trabzon (8) and Tamdere (21) gauges are lower than E_{pan} . Remember that gauges (7 and 8) have the lowest precipitation values among the coastal gauges, because of the obstacle located before these gauges (See Figure 4.1).

Tamdere (21) is the innermost gauge, even observed E_{pan} data of which are higher than that of other inland gauges (See Figure 8.5). E_{pan} is generally greater than PET (Sumner and Jacobs, 2005), they are related to each other with pan coefficient (K_{pan}).

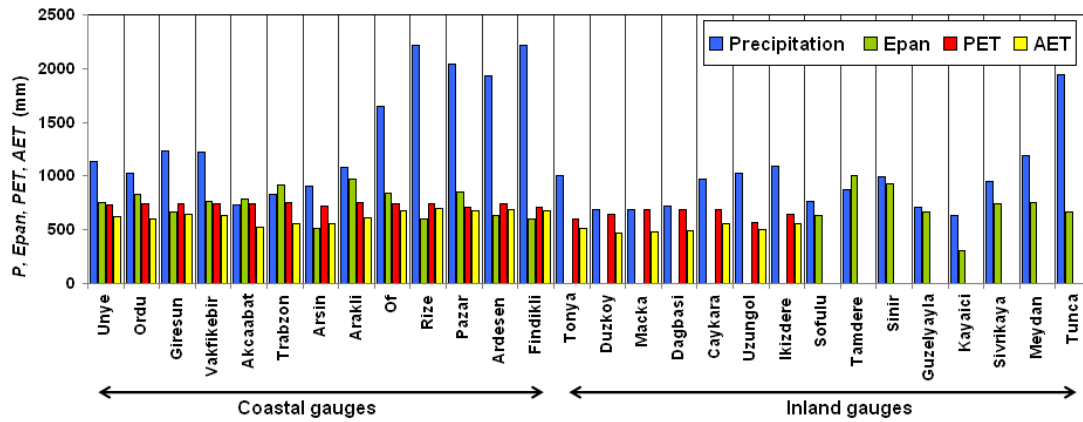


Figure 8.8 : Annual values of precipitation (P), evaporation (E_{pan}), potential evapotranspiration (PET) and actual evapotranspiration (AET).

Annual values of E_{pan} in Giresun (2), Arsin (9), Rize (13), Ardesen (16), Findikli (17) are lower than that of PET . Evapotranspiration increases when air temperature increases or when humidity decreases (Haque, 2003). Temperature of coastline is approximately $14\text{ }^{\circ}\text{C}$ and coastal gauges have almost the same temperature characteristics. On the other hand, relative humidity of the gauges (2, 9, 13, 16 and 17) is generally higher than the average relative humidity of all coastal gauges (Figure 8.9). Lower E_{pan} values may be associated to the higher relative humidity of these 5 coastal gauges. AET values of all gauges are lower than that of PET , as expected.

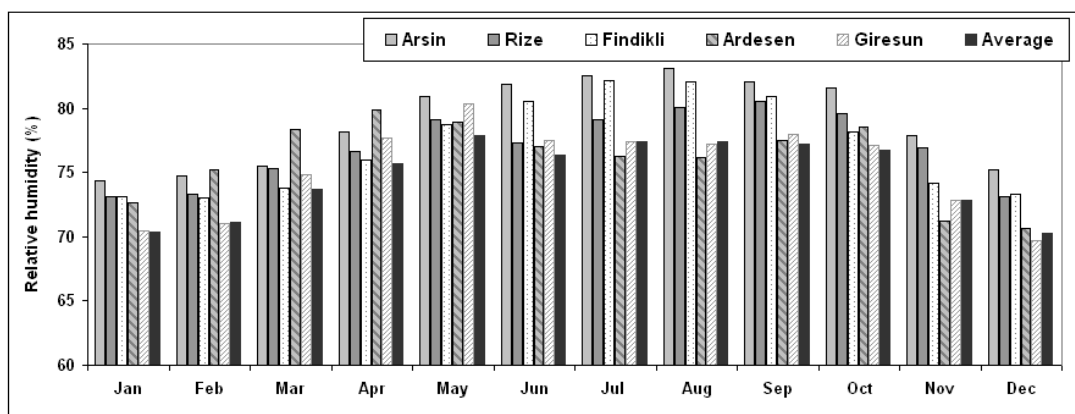


Figure 8.9 : Relative humidity of the gauges (2, 9, 13, 16 and 17) and average relative humidity of coastline.

In the study by Sahin et al. (2004), the daily *PET* value for the Trabzon (8) gauge was found to be approximately 2.5 mm for annual period as an averaging of nine different estimation methods such as Penman, FAO-24, Kimberly-Penman, Penman-Monteith. In this study, total annual *PET* for Trabzon (8) gauge was obtained as 752 mm (Figure 8.8) which corresponds to about 2.1 mm at daily scale.

For mapping evapotranspiration depth, an appropriate variogram theoretical model must be determined. Cross-validation is used to compare different variogram models and chosen Spherical type. Experimental and theoretical variograms for actual evapotranspiration can be seen in Figure 8.10.

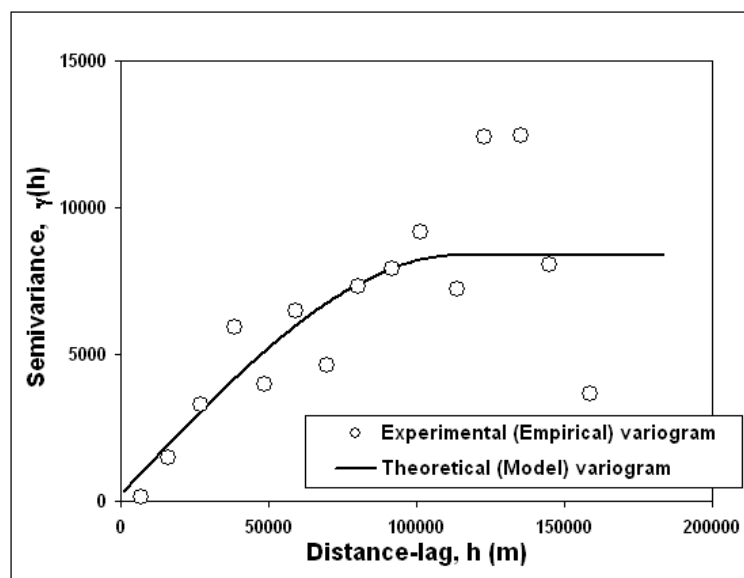


Figure 8.10 : Experimental variogram of AET with Spherical model fitted.

The corresponding parameters used in Ordinary Kriging are shown in Table 8.3. Cross validation results of observed-estimated *AET* values for Kriging method is given in Figure 8.11. The *X* axis was named as “observed *AET*”; however, these *AET* values are certainly not measured, they were calculated by using Turc-Pike method, as defined before.

Table 8.3 : Parameters of theoretical variogram for actual evapotranspiration data.

Model	Range (m)	Lag Size (m)	Number of lag	Nugget (mm ²)	Partial Sill (mm ²)	Number of neighbor
Spherical	114453	10796	17	235	8146	4

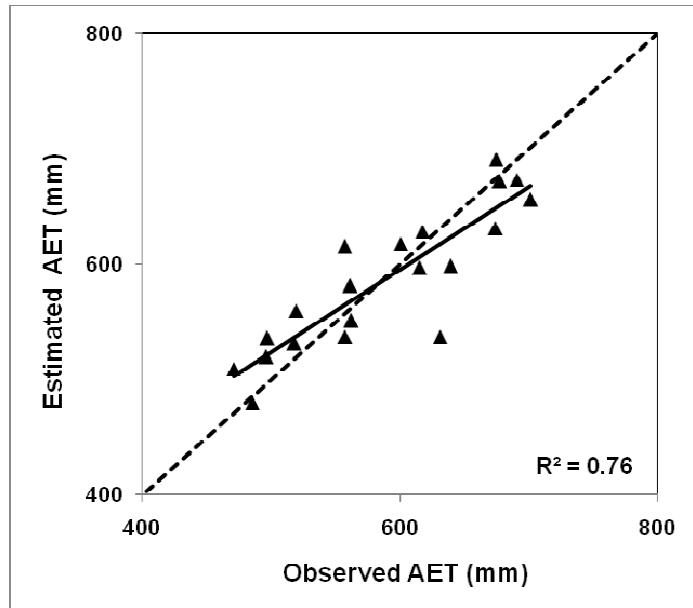


Figure 8.11 : Cross validation results of observed-estimated *AET* values.

Figure 8.12 shows the evapotranpiration map generated from the Ordinary Kriging method for the coastal part of the Eastern Black Sea Region. Also shown in Figure 8.12 are the gauges in the study area (except for Unye and Ordu gauges).

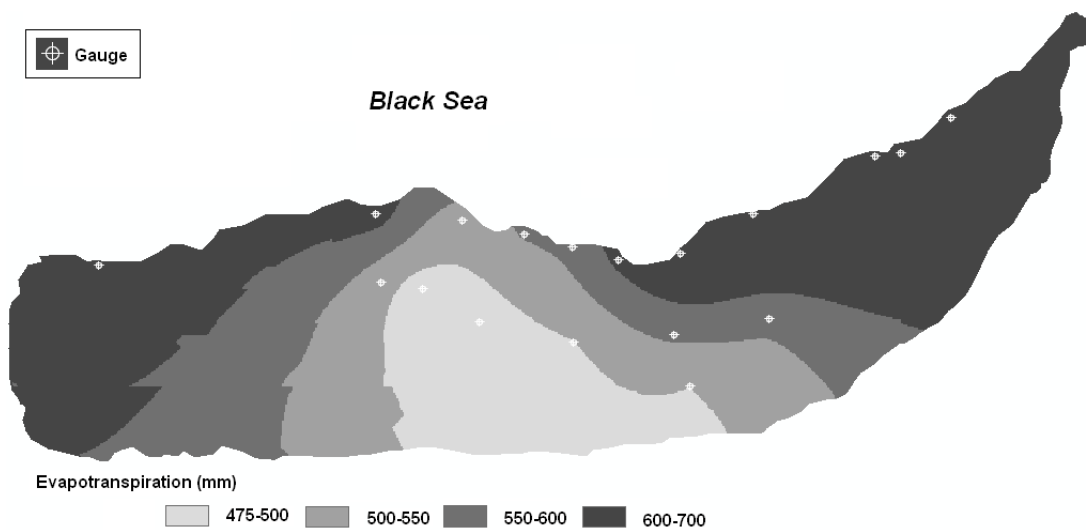


Figure 8.12 : Evapotranspiration map for the study area.

9. DETERMINATION OF PRECIPITATION FROM STREAMFLOW AND EVAPOTRANSPIRATION DATA

9.1 Introduction

Runoff coefficients depicted that spatial distribution of precipitation over the study area was unrealistic due to location of the rain gauges. For an accurate distribution of precipitation, streamflow can be distributed over the basin considering orographical influence on the basin in a water balance model. Flow depth and evapotranspirations maps to be generated are then summed up to derive isohyetal map as a final step. This procedure is carried out in GIS environment.

9.2 Method

A raster represents a surface as a rectangular grid of evenly spaced square cells (Kennedy, 2009). Raster layers can be combined in some ways. The values of a raster are added to that of other one on a cell-by-cell basis. The arithmetic combining of the values in multiple rasters are illustrated in Figure 9.1. This type of summation can only be done with multiple rasters.

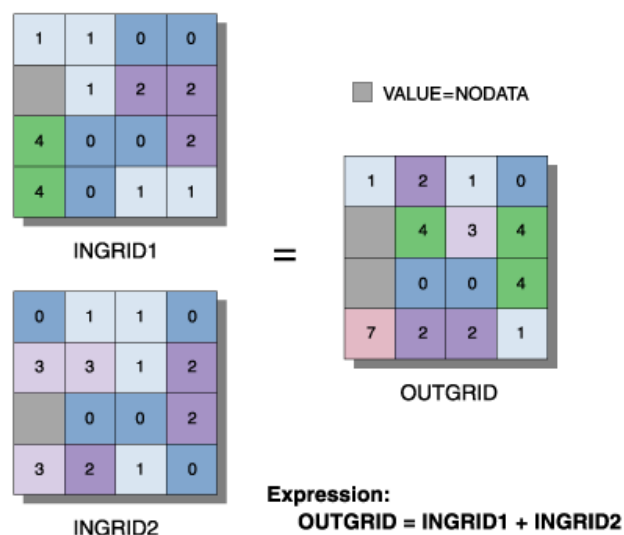


Figure 9.1 : Illustration of combining two different raster data.

Alternatively, a surface can be generated from points using interpolation techniques. Most widely used interpolation methods from point data are inverse distance weighted, radial basis function, kriging and regression about which detailed information was provided in previous chapters. Differ from aforementioned interpolation methods; natural neighbor technique can be used to generate the surface. This technique can be used for both interpolation and extrapolation and generally works well with clustered scatter points. This method can efficiently handle large input point datasets (Childs, 2004) and where input points are distributed with uneven density (Forkuo, 2008). It will be seen in next chapters that a combination is achieved from two different large point datasets. One is obtained from the combined raster of flow depth and evapotranspiration map, while the other consists of points on which MLR equations are applied. The points are high in number and irregular. Therefore, natural neighbor technique will be used.

9.3 Application and Evaluation

The evapotranspiration map is added on the flow depth map, resulting isohyetal map is shown in Figure 9.2. As anticipated, no actual precipitation observations were used. This gives an opportunity to compare observed precipitation to its estimated values to be extracted from the isohyetal map generated. Scatter diagrams of observed and estimated precipitations of 38 rain gauges are shown in Figure 9.3 for coastal and inland gauges separately, and for whole gauges combined.

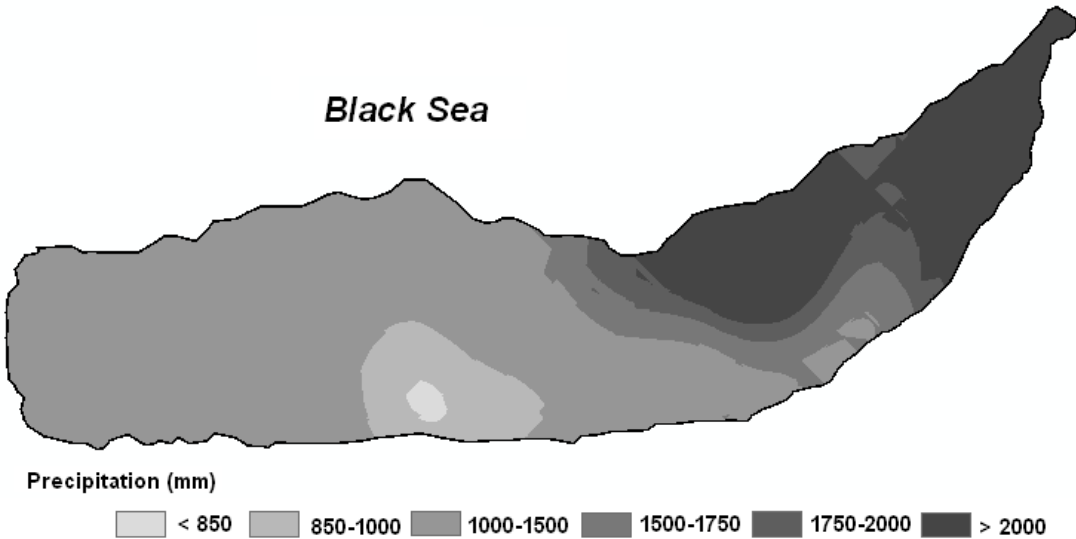


Figure 9.2 : Isohyetal map from water balance.

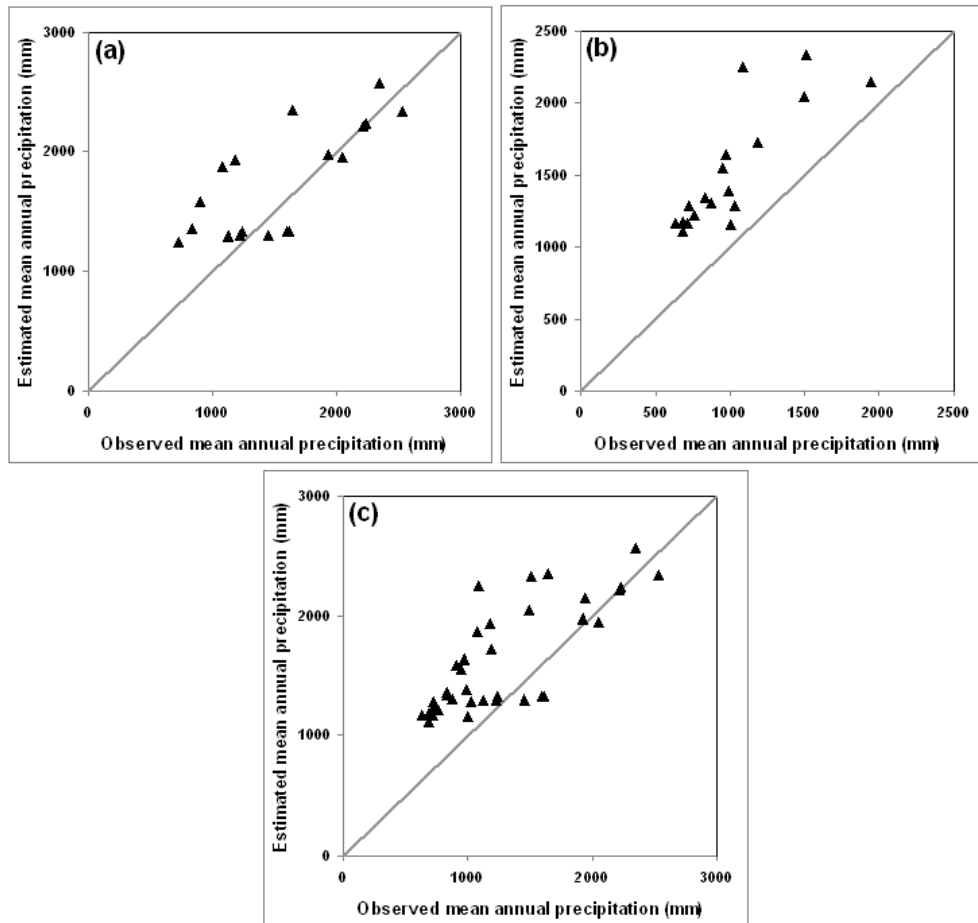


Figure 9.3 : Scatter diagrams of observed and estimated mean annual precipitations from water balance method for (a) coastal, (b) inland and (c) whole gauges.

As seen from Figure 9.3, the observed and estimated precipitations seem to be quite dispersed. Precipitation was overestimated, particularly for inland gauges. These facts are reflected in the statistics of prediction errors given in Table 9.1 in which minimum, maximum and mean precipitation values were found 74.5%, 20% and 29.1% greater than their observed counter parts, respectively.

Table 9.1 : Statistics of prediction errors.

	Min Precip. (mm)	Max Precip. (mm)	Mean Precip. (mm)	MAE (mm)	RMSE (mm)	R ²
Observed	636.69	2525.69	1322.42	-	-	-
Isohyetal Map	1110.99	3031.01	1707.24	384.82	517.89	0.63
Adjusted Isohyetal Map	686.33	2364.39	1358.92	36.50	222.25	0.84

This case indicates that a correction should be applied during the combination process of flow depth and evapotranspiration raster layers. Results based on point-scale data of observation sites pointed out that precipitation decreases from coastline through the inland region. As the number of rain gauges is limited and they are mostly established in the valley floors, the distribution of precipitation in the valleys is precisely known. For the gauges located in the valley floors, MLR analysis was performed before and different equations were derived for inland (Model 3, in Chapter 5). The same way was followed for the coastline (Model 2, in Chapter 5). Consider that the study area is divided into subbasins, developed regression equations can briefly represent distribution of precipitation on the points which can be placed in valleys and coastlines with any desired number. On the other hand, for any number of boundary points on the subbasins, namely slopes, precipitation values can be extracted from the isohyetal map generated by water balance method. Thus, two types of point dataset are available, one of these is for valleys/coastlines and the other for subbasin boundaries. A surface on which distribution of precipitation increase from valley floors through the slopes up to water divides of the subbasins can be now interpolated.

In Figure 9.4, Serah basin is chosen as an example to describe the method. As seen from figure, the circles represent the valley points whereas triangles the boundary of the basin. Throughout the valley, the MLR equation for inland (referred to as Model 3 in Chapter 5) and the MLR equation for coastline (referred to as Model 2 in Chapter 5) are applied on circle points, separately. On the other hand, triangles located at boundaries of the basin are extracted from a raster which is the isohyetal map obtained by water balance. Thus, a point dataset made of circles and triangles is obtained. The Natural neighbor technique can now be performed to precipitation mapping by using this point dataset.

Consequently, isohyetal map using water balance method is developed by MLR equations and referred hereafter to as adjusted isohyetal map shown in Figure 9.5. Scatter diagram of precipitation observed in the rain gauges with estimated from adjusted isohyetal map can be seen in Figure 9.6. The statistics of prediction errors are also given in Table 9.1. As seen from Figure 9.6 and Table 9.1, the results of adjusted isohyetal map are more satisfactory than preceding map. One can realize that these results actually represent the performance of the MLR equations.

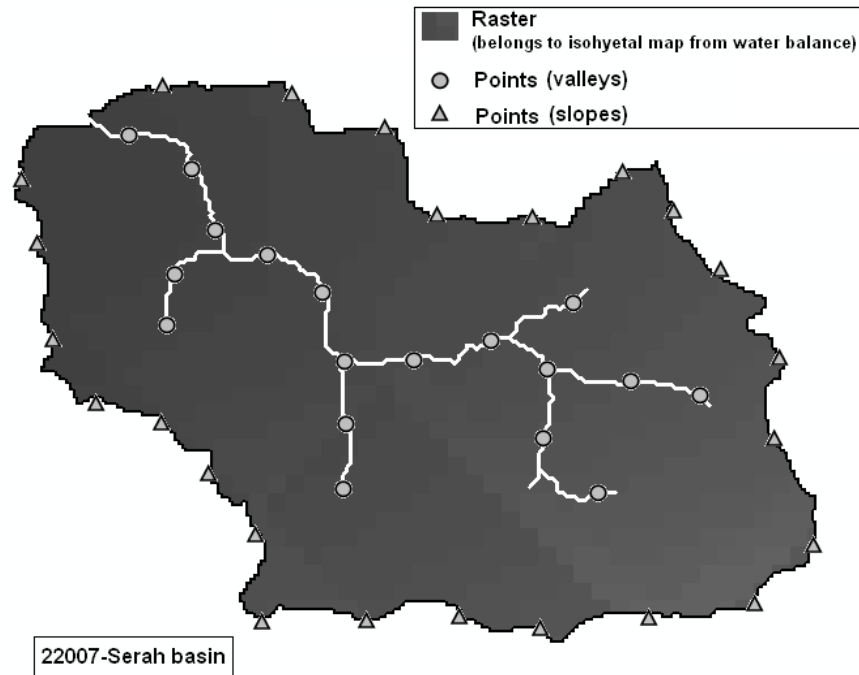


Figure 9.4 : An example of points using in combination raster data and MLR analysis equations.

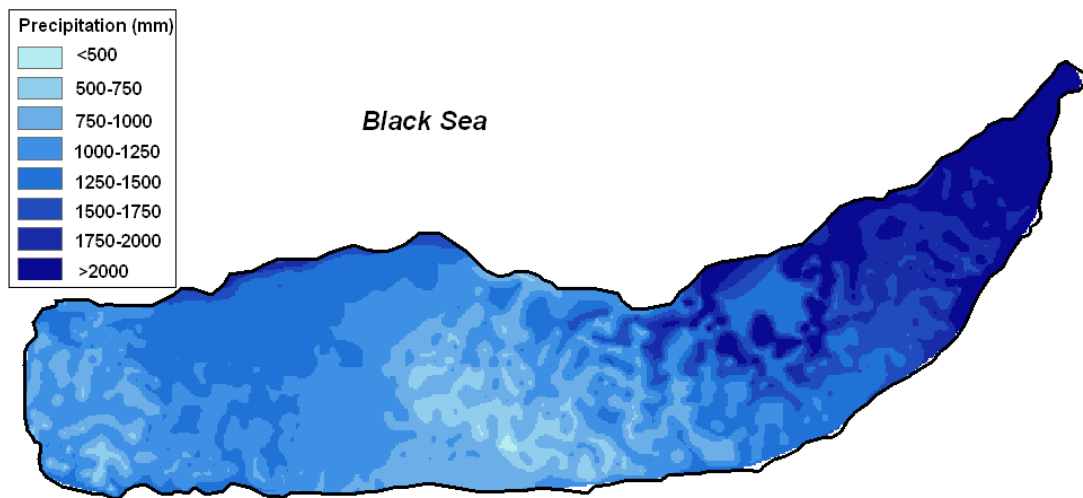


Figure 9.5 : Adjusted isohyetal map for the coastal part of the Eastern Black Sea Region.

In order to validate adjusted isohyetal map, long term runoff coefficients are calculated again. The runoff coefficients of isohyetal map and adjusted isohyetal map are shown in Figure 9.7. Almost all coefficients are lower than 1, except for the gauge Komurculer (22082) that covers an area of 83.3 km². Komurculer (22082) is located very close to the rain gauges Rize (13) and Kalkandere (32), annual precipitation amounts of which are 2215 and 2067 mm, respectively. It should also be noted that, this particular gauge was found non-homogenous (Chapter 3).

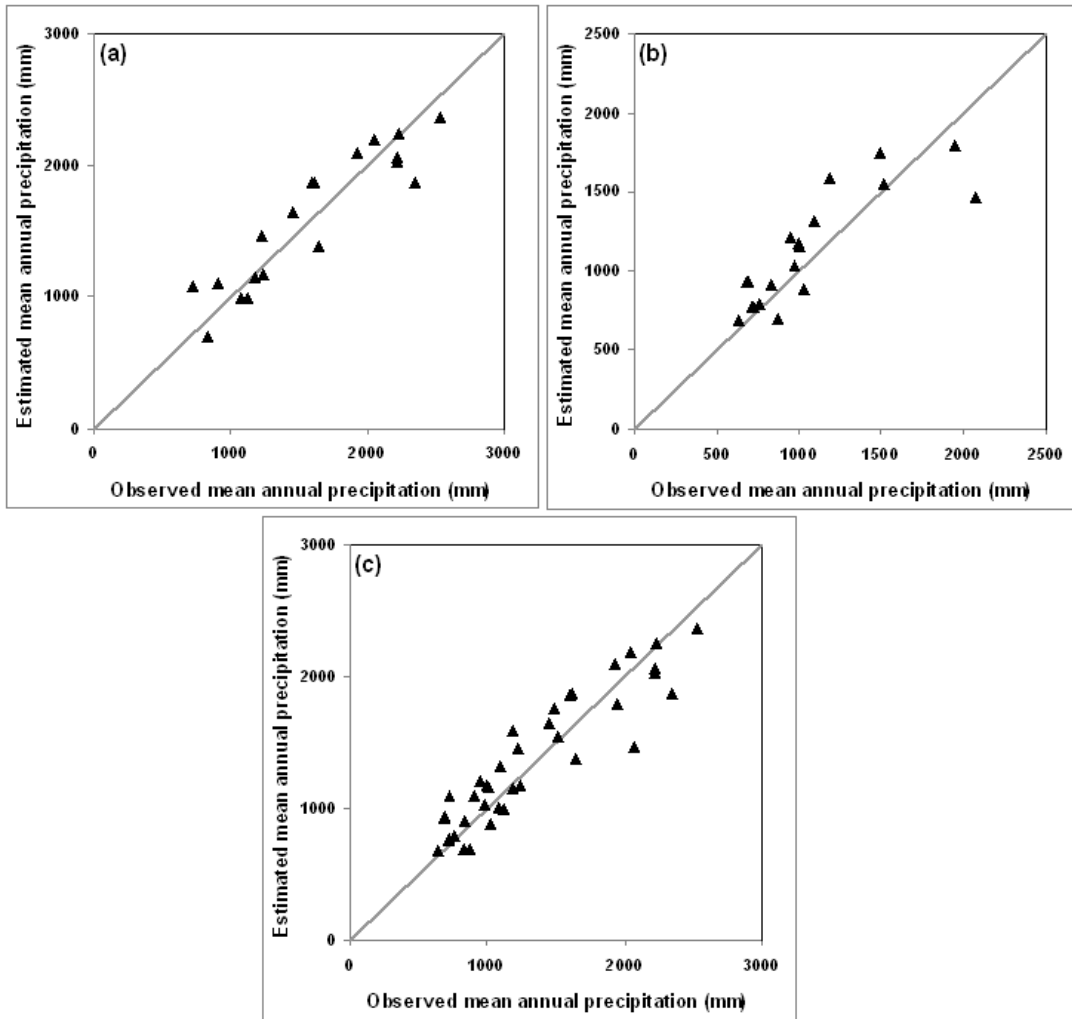


Figure 9.6 : Scatter diagram of observed and estimated precipitations from adjusted isohyetal map for (a) coastal, (b) inland and (c) whole gauges.

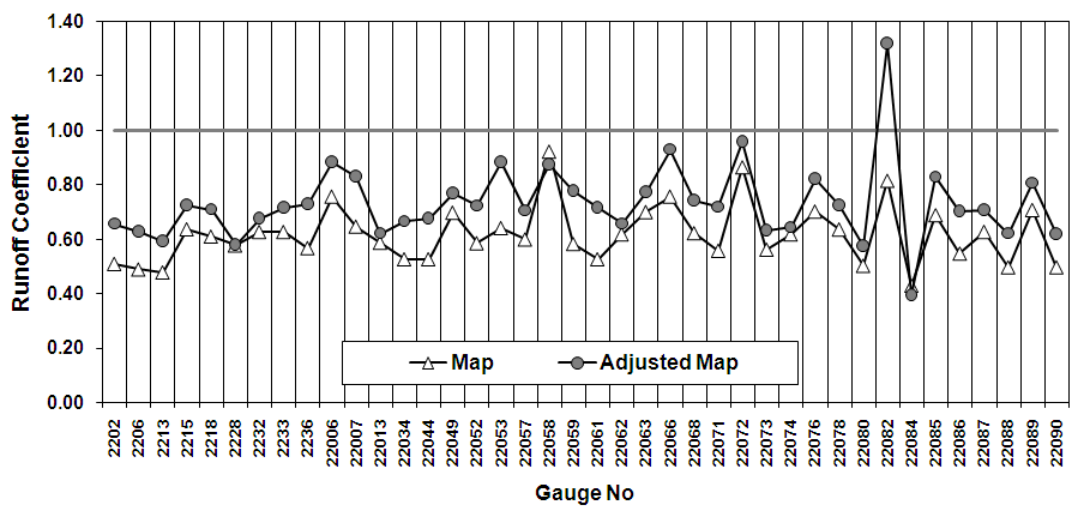


Figure 9.7 : Annual runoff coefficients determined from adjusted isohyetal map for flow gauges.

The spatial distribution of runoff coefficient is depicted in Figure 9.8. For the study area, a weighted runoff coefficient is calculated as 0.70 by using basin runoff coefficients in Figure 9.8. Based on DSI Statistical Bulletin of 1985, Bayazıt (2001) provided the runoff coefficient as 0.43 for the Eastern Black Sea Region. This value was 0.57 in the National Environmental Action Plan based on a DSI study in 1996 (Burak et al., 1997). In the Eastern Black Sea Region Development Plan, runoff coefficient was 0.47 based on the study of DSI and Japan International Cooperation Agency (JICA, 2000). It should be noted that different areas were considered in the aforementioned studies (Table 9.2 and Figure 9.9).

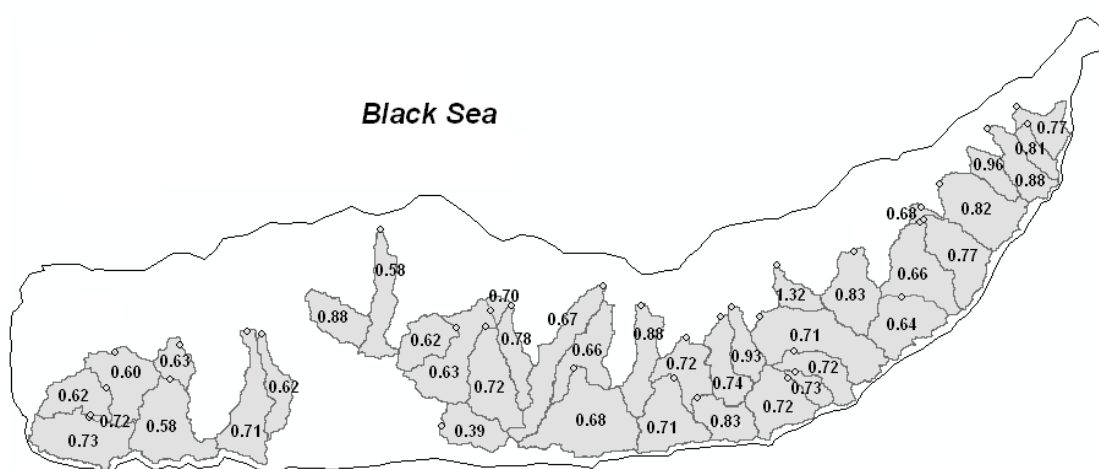


Figure 9.8 : Spatial distribution of runoff coefficients.

Table 9.2 : Comparison of the runoff coefficients.

Study	Area (km ²)	Annual Runoff Coefficient
Burak et al. (1997)	24022	0.57
JICA (2000)	39201	0.47
Bayazıt (2001)	24077	0.43
This study*	7560	0.70

**Runoff coefficient is calculated based on the total drainage areas of the flow gauges.*

The isohyetal map obtained by using the Kriging method in Chapter 5 and the adjusted isohyetal map are compared, a correction ratio map is developed for the study area (Figure 9.10). Correction ratio shows the ratio of precipitation taken from the adjusted isohyetal map to precipitation taken from isohyetal map by the Kriging method.

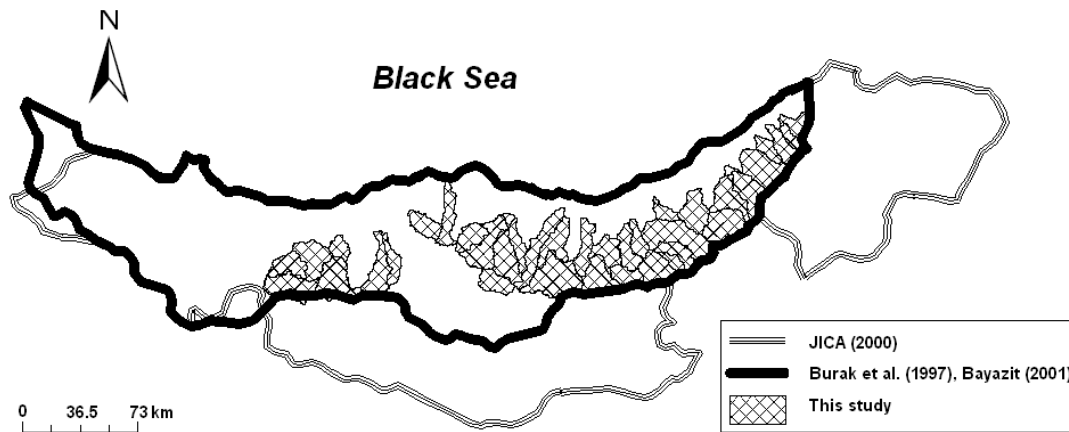


Figure 9.9 : Areas used in the runoff coefficient determination studies.

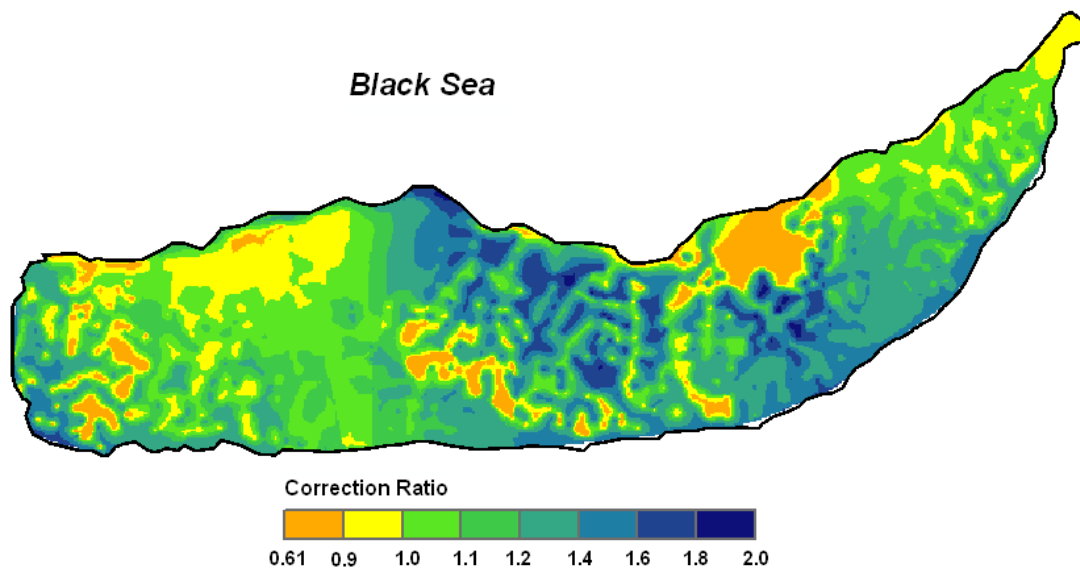


Figure 9.10 : Correction ratio for the study area.

Correction ratios in Figure 9.10 are comparable to those calculated by Adam et. al. (2006) for 357 mountainous river basins worldwide. The map shown in Figure 9.11 has grids of 0.5° grid corresponding to 55 km and it shows correction ratios for all global land areas. In spite of its low scale, it can be understood that the ratio ranges from 1.0 to 1.8 for the northeastern part of Turkey. This range can be mostly seen from Figure 9.10, as well. In a very small part of the study area, correction ratios were found less than 1 such as southwest, mid-south and mid-northeast which is around the gauge of Kalkandere. The reason of lower correction ratio around Kalkandere may be explained by the mean annual precipitation values of its surrounding rain gauges (Figure 9.12). Because precipitation in surrounding gauges

and even in the coastal gauge Of ranges from 974-1646 mm which is quite different from the precipitation value of Kalkandere. This might be the reason for correction ratio is lower than 1 on this area.

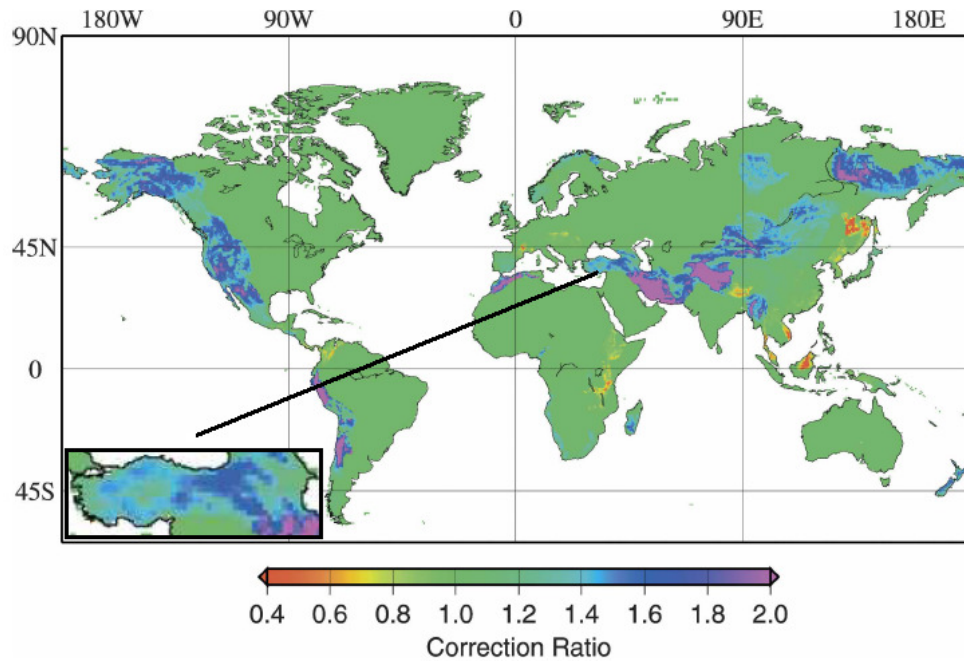


Figure 9.11 : Correction ratio for the mountainous river basins worldwide (Adam et. al., 2006).

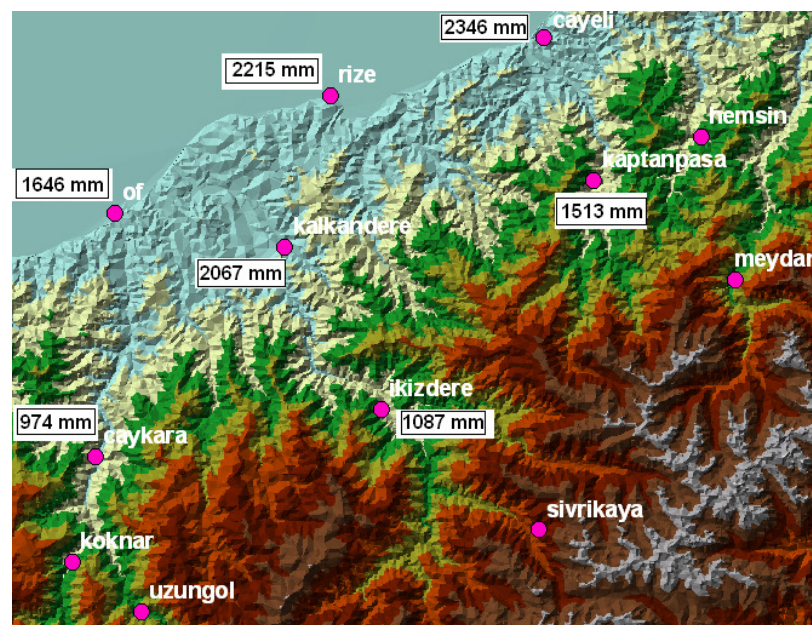


Figure 9.12 : Location of the Kalkandere gauge and it surrounding rain gauges with precipitation values.

10. CONCLUSIONS

In this study, spatial distribution of precipitation on poorly gauged coastal part of the Eastern Black Sea Region was determined. For this purpose, a number of hydrometeorological variables and concepts are used together. Since interrelated topics exist, conclusions are presented separately.

(1) First of all, the effects of coastline configuration and other geographical and topographical variables, such as longitude, latitude, elevation and distance from sea, on the mean annual precipitation of a coastal area were investigated. For this purpose, some graphical evaluations were presented. Following conclusions can be drawn from this part of the study:

- ✓ Mean annual precipitation increases with longitude and latitude. This condition may depend on location and height of the mountains and prevailing wind directions of the region.
- ✓ Mean annual precipitation seems to decrease with distance from sea.
- ✓ From the precipitation-longitude variation, coastline configuration has been found to affect precipitation.
- ✓ Although the study region is mountainous and assumed to have orographic characteristics, precipitation data obtained from the rain gauges were not proved this effect. Because rain gauges are mostly located on the valley floors, no outcome can be extracted for the slopes. Mean annual precipitation decreases with elevation for a given range in the valleys.

(2) The relationships between mean annual precipitation and geographical/topographical variables and coastline configuration were represented by regression equations. Isohyetal maps were then generated from regression equations and conventional methods such as Inverse Distance Weighted, Radial Basis Function and Kriging. These maps were compared and validated by means of annual runoff coefficients. Followings are conclusions born from these analyses:

- ✓ For the regression analysis, a new variable, the coastline angle, was introduced to represent the coastline configuration. However coastline configuration has been found to be a weighty variable that affects precipitation characteristics not only of the coastal but also the inland gauges. This effect has also been found to be valid even when the coastal and inland gauges were considered together.
- ✓ Although isohyetal maps generated by MLR equations and conventional methods were quite similar, the accuracy of maps was also validated using long-term runoff coefficients. This validation showed that the precipitation was underestimated for the region.
- ✓ Direct usage of rain gauge data in isohyetal mapping underestimated precipitation and/or streamflow. Therefore the accuracy of the precipitation map should absolutely be checked, when point scale precipitation is interpolated over a region.

(3) To avoid underestimation of precipitation, water balance approach was applied. Thus, flow depth and evapotranspiration maps were delineated and combined to create a new precipitation map. Previously developed regression equations with a better capability in representing precipitation distribution on coastline and valleys were embedded into foregoing new precipitation map called as adjusted isohyetal map. Following achievements were obtained.

- ✓ Regional flow depth map obtained by using a geostatistical method for the study area is the first application of this kind of approach for Turkey. The flow depth map can be a useful tool for flow estimation on ungauged locations in the Eastern Black Sea Region. Promising results of calibration and validation encourage one to suggest this method could be performed other regions over Turkey for different hydrologic applications.
- ✓ Inland part of the Eastern Black Sea Region is not accepted as an agricultural area because of its rough topography, consequently evapotranspiration studies for inland are limited. Although most of pan evaporation data obtained from the inland meteorological gauges was missing, evapotranspiration was extensively investigated for the study region. During the study, it was noticed that the number of studies on evapotranspiration is

limited not only for Eastern Black Sea Region but also for other regions in Turkey. This problem can be solved by establishment of new meteorological gauges and thus by increase in the evapotranspiration studies which may include satellite-based data and/or distributed hydrological models.

- ✓ Another unique contribution of this study is the combination of water balance approach with regression equations for the determination of precipitation distribution. It was seen that for an accurate spatial distribution of precipitation, the topographical characteristics of the regions should be considered, if necessary, different methods/approaches alternating each other should be used. Because conventional methods do not always give the most accurate results on precipitation distribution.

If quantitatively accurate precipitation analyses are to be performed for mountainous coastal regions, different methods are needed for further improvements. Improvements may be achieved by increased number of gauges to better represent distribution of precipitation in the basin. More advanced treatments for the problem of the spatial estimation of precipitation can be developed to include physical and/or dynamic methods incorporating detailed information (including model derived and remotely sensed data) on topographic structure, atmospheric motion, and atmospheric thermodynamics.

REFERENCES

- Adam, J. C., Clark, E. A., and Lettenmaier, D. P.**, 2006. Correction of Global Precipitation Products for Orographic Effects, *Journal of Climate*, **19**: 15-38.
- Agiralioglu, N., Cigizoglu, H.K., Yilmaz, L., Coskun, H.G., Aksoy, H., Toprak, Z.F., Eris, E., Alganci, U., Andic, G., Usta, G., Besiktas, M., Ulken, I.**, 2009. Akım ölçümleri olmayan akarsu havzalarında teknik hidroelektrik potansiyelin belirlenmesi (in Turkish), *The Scientific and Technological Research Council of Turkey (TUBITAK), Project No 106M043*, 188pp.
- Agnew, M., and Palutikof, J. P.**, 2000. GIS-based construction of baseline climatologies for the Mediterranean using terrain variables, *Climate Research*, **14** 115–127.
- Akdogar, M.**, 2006. Enerji Kaynakları ve Dogu Karadeniz'in Hidroelektrik Potansiyel Dengesi Etüdü (in Turkish), *Msc Thesis*, H. Onsoy, Karadeniz Technical University, Trabzon.
- Ang, H.-S., and Tang, W. H.**, 2006. *Probability Concepts in Engineering: Emphasis on Applications to Civil and Environmental Engineering* (v. 1), Wiley, NY, 406p.
- Armstrong, M.**, 1998. *Basic Linear Geostatistics*, Springer-Verlag Berlin, Heidelberg, Germany, 153p.
- Arnell, N. W.**, 1995. Grid mapping of river discharge, *Journal of Hydrology*, **167**: 39-56.
- Atkinson, P. M., and Lloyd, C. D.**, 1998. Mapping precipitation in Switzerland with ordinary and indicator kriging, *Journal of Geographic Information and Decision Analysis*, **2** (2): 65-76.
- Baker, D. R., Lynn, B.H., Boone, A., Tao, W.K., and Simpson, J.**, 2001. The influence of soil moisture, coastline curvature, and land-breeze circulations on sea-breeze-initiated precipitation, *Journal of Hydrometeorology*, **2** (2): 193–211.
- Bargaoui, Z. K., and Chebbi, A.**, 2009. Comparison of Two Kriging Interpolation Methods Applied to Spatiotemporal Rainfall, *Journal of Hydrology*, **365** 56-73.
- Basist, A., Bell, G.D., and Meentemeyer, V.**, 1994. Statistical relationship between topography and precipitation patterns, *Journal of Climate*, **7**: 1305–1315.
- Basistha, A., Arya, D. S., Goel, N. K.**, 2008. Spatial distribution of rainfall in Indian Himalayas-A case study of Uttarakhand region, *Water Resources Management*, **22** (10): 1325-1346.
- Bayazit, M.**, 2001. *Hydrology*, Birsen Pub., Istanbul, 229p.

- Bishop, G. D., and Church, M.R.**, 1992. Automated approaches for regional runoff mapping in the northeastern United States, *Journal of Hydrology*, **138** 361-383.
- Blume, T., Zehe, E., and Bronstert, A.**, 2007. Rainfall–runoff response, event-based runoff coefficients and hydrograph separation, *Hydrological Sciences Journal*, **52** (5): 843-862.
- Boer, E. P. J., De Beurs, K. M., and Hartkamp, A. D.**, 2001. Kriging and thin plate splines for mapping climate variables, *International Journal of Applied Earth Observation and Geoinformation*, **3** (2): 146-154.
- Boronina, A., Golubev, S., and Balderer, W.**, 2005. Estimation of actual evapotranspiration from an alluvial aquifer of the Kouris catchment (Cyprus) using continuous streamflow records, *Hydrological Processes*, **19**: 4055-4068.
- Bostan, P. A., and Akyurek, Z.**, 2007a. İkincil Veriler Kullanılarak Türkiye Ortalama Yıllık Yağış Değerlerinin Mekansal Dağılımının Modellenmesi, *TMMOB Harita ve Kadastro Mühendisleri Odası Ulusal Coğrafi Bilgi Sistemleri Kongresi*, KTU, Trabzon.
- Bostan, P. A., and Akyurek, Z.**, 2007b. Exploring the mean annual precipitation and temperature values over Turkey by using environmental variables., *ISPRS Joint Workshop: Visualization and Exploration of Geospatial Data*, Germany.
- Brooks, K. N., Follitt, P. E., Gregersen, H. M., and Thames, J. L.**, 1991. *Hydrology and the management of Watersheds*, Iowa States University Press, 392p.
- Buhmann, M. D.**, 2003. Radial Basis Functions on Grids and Beyond, *International Workshop on MeshFree Methods*, Portugal.
- Burak, S., Duranyildiz, I., and Yetis, U.**, 1997. National Environmental Action Plan: Water Resources Management, *State Planning Organization of Turkey*, Ankara, 116p.
- Burrough, P. A., and McDonnell, R. A.**, 1998. *Principles of geographical information systems*, Oxford University Press, Oxford, 333p.
- Cetin, M., and Tulucu, K.**, 1998. Doğu Karadeniz Bölgesinde Aylık Yağışların Yersel Değişimlerinin Jeostatistik Yöntemle İncelenmesi, *Turkish Journal of Engineering and Environmental Science*, **22**: 279-288.
- Chang, H.**, 2007. Comparative streamflow characteristics in urbanizing basins in the Portland Metropolitan Area, Oregon, USA, *Hydrological Processes*, **21**: 211-222.
- Childs, C.**, 2004. Interpolating Surfaces in ArcGIS Spatial Analyst, *ArcUser*, **July-September** 32-35.
- Chinayakanahalli, K., Kroeber, C., Hill, R., Tarboton, D. G., Olson, J., and Hawkins, C.**, 2006. *The Multi-Watershed Delineation Tool: GIS Software in Support of Regional Watershed Analyses*, Utah State University, Boston, USA.

- Cigizoglu, H. K., Bayazit, M., and Onoz, B.**, 2004. Trends in the Maximum, Mean and Low Flows of Turkish Rivers, *Journal of Hydrometeorology*, **6**: 280-290.
- Clarke, K. C.**, 1990. *Analytical and computer cartography*, Prentice-Hall, Englewood, New Jersey, 290p.
- Conceicao, M. A. F.**, 2002. Reference Evapotranspiration Based On Class A Pan Evaporation, *Scientia Agricola*, **59** (3): 417-420.
- Cuenca, R. H.**, 1989. *Irrigation system design. An engineering approach*, Prentice-Hall, Englewood Cliffs, N.J., 133p.
- Dalezios, N. R., Loukas, A., and Bampzelis, D.**, 2002. Spatial variability of reference evapotranspiration in Greece, *Physics and Chemistry of Earth*, **27** 1031-1038.
- Daly, C.**, 2006. Guidelines for assessing the suitability of spatial climate data sets, *International Journal of Climatology*, **26**: 707-721.
- Daly, C., Neilson, R. P., Phillips, D. L.**, 1994. A statistical-topographic model for mapping climatological precipitation over mountainous terrain, *Journal of Applied Meteorology*, **33** (2): 140-158.
- Dikbas, F., Firat, M., Koc, A. C., and Gungor, M.**, 2010. Homogeneity Test for Turkish Temperature Series, *BALWOIS 2010*, Ohrid-Republic of Macedonia, 25-29 May.
- Dingman, L. S.**, 2008. *Physical Hydrology*, Waveland Press Inc., Long Grove, IL, 656p.
- Diodato, N.**, 2005. The influence of topographic co-variables on the spatial variability of precipitation over small regions of complex terrain, *International Journal of Climatology*, **25** (3): 351-363.
- Dirks, K. N., Hay, J.E., Stow, C.D., and Harris, D.**, 1998. High-resolution studies of rainfall on Norfolk Island, Part II:interpolation of rainfall data, *Journal of Hydrology*, **208** (3-4): 187-193.
- Doorenbos, J., and Pruitt, W. O.**, 1977. *Crop water requirements: FAO Irrigation and Drainage Paper 24*, United Nations—Food and Agriculture Organization, Rome.
- DSI**, 2005. Su Kaynakları Potansiyeli (in Turkish), *State Hydraulics Works*, Trabzon.
- Durbin, J., and Watson, G. S.**, 1950. Testing for Serial Correlation in Least Squares Regression, I, *Biometrika*, **37** 409-428.
- Durbin, J., and Watson, G. S.**, 1951. Testing for Serial Correlation in Least Squares Regression, II, *Biometrika*, **38** 159–179.
- Eris, E., and Ağırlioğlu, N.**, 2009. Effect of coastline configuration on precipitation distribution in coastal zones, *Hydrological Processes*, **23** (25): 3610-3618.
- Fekete, B. M., Vörösmarty, C. J., and Grabs, W.**, 2000. Global composite runoff fields based on observed river discharge and simulated water balances, *Documentation for UNH-GRDC Composite Runoff Fields, v.1.0*, G. R. D. Center, Koblenz, Germany.

- Fernandez, C. J., Bravo, J. I.**, 2007. Evaluation of Diverse Geometric and Geostatistical Estimation Methods Applied to Annual Precipitation in Asturias (NW Spain), *Natural Resources Research*, **16** (3): 209-218.
- Forkuo, E. K.**, 2008. Digital Terrain Modeling in A GIS Environment, *The International Archives of the Photogrammetry, Remote Sensing and Spatial Information Sciences*, Vol. XXXVII, Part 2, Beijing, 1023-1029.
- Gokdemir, O., and Arikan, A.**, 2003. Determination of Regional Scale Evapotranspiration from NOAA-AVHRR Images: Application to The Afyon-Akarca Basin, Turkey, *Proceedings of Geoscience and Remote Sensing Symposium, IGARSS '03*, France.
- Gokturk, O. M., Bozkurt, D., Sen, O.L., and Karaca, M.**, 2008. Quality control and homogeneity of Turkish precipitation data, *Hydrological Processes*, **22**: 3210-3218.
- Goovaerts, P.**, 1997. *Geostatistics for Natural Resources Evaluation*, Oxford University Press, NY, 483p.
- Goovaerts, P.**, 2000. Geostatistical approaches for incorporating elevation into the spatial interpolation of rainfall, *Journal of Hydrology*, **228**: 113–129.
- Granger, R. J.**, 2000. Satellite-derived estimates of evapotranspiration in the Gediz basin, *Journal of Hydrology*, **229**: 70-76.
- Grismer, M. E., Orang, M., Snyder, R., and Maytaç, R.**, 2002. Pan evaporation to reference evapotranspiration conversion methods, *Journal of Irrigation and Drainage Engineering*, **128** (3): 180-184.
- Gundekar, H. G., Khodke, U. M., Sarkar, S., and Rai, R. K.**, 2008. Evaluation of pan coefficient for reference crop evapotranspiration for semi-arid region, *Irrigation Science*, **26** (2): 169-175.
- Haan, C. T.**, 2002. *Statistical Methods in Hydrology*, Iowa State Press, 482p.
- Haque, A.**, 2003. Estimating actual areal evapotranspiration from potential evapotranspiration using physical models based on complementary relationships and meteorological data, *Bulletin of Engineering Geology and the Environment*, **62** (1): 57-63.
- Hardy, R. L.**, 1990. Theory and applications of the multiquadric-biharmonic method, *Computers and Mathematics with Applications*, **19**: 163-208.
- Hastenrath, S. L.**, 1967. Rainfall distribution and regime in Central America, *Theoretical and Applied Climatology*, **15** (3): 201–241.
- Helsel, D. R., and Hirsch R M.**, 2002. *Statistical Methods in Water Resources, Techniques of Water Resources Investigations*, Book 4, Chapter A3, U.S. Geological Survey, 522p.
- Hevesi, J. A., Istok, J.D., and Flint, A.I.**, 1992a. Precipitation estimation in mountainous terrain using multivariate geostatistics. Part I: structural analysis, *Journal of Applied Meteorology*, **31**: 661-676.
- Hevesi, J. A., Istok, J.D., and Flint, A.I.**, 1992b. Precipitation estimation in mountainous terrain using multivariate geostatistics. Part II: isohyetal maps, *Journal of Applied Meteorology*, **31**: 677-688.

- Holdaway, M. R.**, 1996. Spatial modeling and interpolation of monthly temperature using kriging, *Climate Research*, **6**: 215-225.
- Huang, W. C., and Yang, F.T.**, 1998. Streamflow estimation using Kriging, *Water Resources Research*, **34** (6): 1599-1608.
- Irmak, A., Sing, R., Irmak, S., and Martin, D.L.**, 2007. Satellite remote sensing based estimation of land surface evapotranspiration in Great Plains, *2007 ASABE Annual International Meetings*, Minnesota, MI, June 14-17.
- Isaaks, E. H., and Srivastava, R. M.**, 1989. *Applied Geostatistics*, Oxford University Press, NY, 561p.
- JICA (Japan International Cooperation Agency)**, 2000. Eastern Black Sea Region Development Plan (in Turkish), Final Report, Volume 2, State Planning Organization of Turkey, 175p.
- Johansson, B., and Chen, D.**, 2003. The influence of wind and topography on precipitation distribution in Sweden: statistical analysis and modelling, *International Journal of Climatology*, **23**: 1523–1535.
- Johnson, L. E.**, 2009. *Geographic Information Systems in Water Resources Engineering*, CRC Press, NW.
- Johnston, K., Ver-Hoef, J. M., Krivoruchko, K., and Lucas, N.**, 2003. *Using ArcGIS Geostatistical Analyst*, ESRI, Redlands, 300p.
- Journel, A. G. and Huijbregts., Ch. J.**, 2003. *Mining Geostatistics*, The Blackburn Press, NJ, 600p.
- Kadioglu, M., and Sen, Z.**, 2001. Monthly precipitation-runoff polygons and mean runoff coefficients, *Hydrological Sciences Journal*, **46** (1): 3-11.
- Kahya, E., and Kalayci, S.**, 2004. Trend Analysis of Streamflow in Turkey, *Journal of Hydrology*, **289**: 128-144.
- Karatas, B. S., Akkuzu, E., and Avcı, M.**, 2006. Determination of Evapotranspiration Using Remote Sensing (in Turkish), *4th GIS Days in Türkiye*, Fatih University, Istanbul, September, 13-16.
- Karnieli, A.**, 1990. Application of Kriging Technique to Areal Precipitation Mapping in Arizona, *GeoJournal*, **22** (4): 391-398.
- Kennedy, H.**, 2009. *Introduction to 3D Data: Modeling with ArcGIS 3D Analyst and Google Earth*, Wiley, 360p.
- Keskiner, A. D.**, 2008. Determination Of Appropriate Method For Mapping Rainfall And Temperature With Different Probability Levels In GIS Environment And Producing M. Turc Runoff Map: A Case Study In The Seyhan Basin, *Msc Thesis*, M. Çetin, University Of Cukurova, Adana.
- Khan, S. I., Hong, Y., Vieux, B., and Liu, W.**, 2010. Development and evaluation of an actual evapotranspiration estimation algorithm using satellite remote sensing and meteorological observational network in Oklahoma, *International Journal of Remote Sensing*, **31** (14): 3799- 3819.
- Kholghi, M., and Hosseini, S. M.**, 2009. Comparison of groundwater level estimation using neuro-fuzzy and ordinary kriging, *Enviromental Model Assessment*, **14**: 729-737.

- Kite, G., Granger, R., and Jayansinghe, G.,** 2001. Evapotranspiration at the basin scale estimated from satellite data and by a hydrological model, *Remote Sensing and Hydrology 2000*, Santa Fe, New Mexico, USA, April 2000, IAHS Publ. No. 267.
- Kite, G. W., and Pietroniro, A.,** 1996. Remote sensing applications in hydrological modeling, *Hydrological Sciences Journal*, **41**: 563–592.
- Kolka, R. K., and Wolf, A. T.,** 1998. Estimating Actual Evapotranspiration for Forested Sites: Modifications to the Thornthwaite Model, *Research Note SRS-6, USDA Forest Service*, 7pp.
- Krige, D. G.,** 1951. A statistical approach to some mine valuations and allied problems at the Witwatersrand, *Msc thesis*, University of Witwatersrand, Johannesburg.
- Krug, W. R., Gebert, W.A., Graczyk, D.J., Stevens, D.L., Rochelle, B.P., and Church, M.R.,** 1990. Map of mean annual runoff for the northeastern, southeastern, and mid-Atlantic United States Water Years 1951- 80, *U.S. Geological Survey Water Resources Investigations Report*, Madison, WI.
- Leong, W. C., and Abustan, I.,** 2006. Development of Urban Runoff Characteristics of Sg. Kayu Ara Catchment and to Validate Rainfall-Runoff Charts in The Malaysian Urban Stormwater Management Manual (DID, 2000), *National Conference – Water for Sustainable Development Towards a Developed Nation by 2020*, Guoman Resort Port Dickson, 13-14 July.
- Li, S., Tarboton, D., and McKee, M.,** 2003. GIS-based temperature interpolation for distributed modeling of reference evapotranspiration, *23rd AGU Hydrology Days*, Fort Collins, Colorado, March 31 - April 2.
- Lloyd, C. D.,** 2005. Assessing the effect of integrating elevation data into the estimation of monthly precipitation in Great Britain, *Journal of Hydrology*, **308** (1-4): 128-150.
- Lloyd, C. D.,** 2010. *Spatial Data Analysis: an Introduction for GIS Users*, Oxford, USA, 218p.
- Lu, J., Sun, G., McNulty, S. G., and Amatya, D. M.,** 2005. A Comparison of Six Potential Evapotranspiration Methods For Regional Use in the Southeastern United States, *JAWRA*, **41** (3): 621-633.
- Maidment, D. R.,** 2002. *Arc Hydro: GIS for Water Resources*, Esri Press, California.
- Marquardt, D. W.,** 1970. Generalized inverses, ridge regression, biased linear estimation, and nonlinear estimation, *Technometrics*, **12**: 591-612.
- Marquinez, J., Lastra, J., and Garcia, P.,** 2003. Estimation models for precipitation in mountainous regions: the use of GIS and multivariate analysis, *Journal of Hydrology*, **270**: 1-11.
- Matheron, G.,** 1962. Traite De Geostatistique Appliquée, Tome II Le krigeage, *Memoires du Bureau de Recherches Geologiques et Minieres, No. 24, Editions B.R.G.M., Paris*.

- McNamara, J. P., Kane, D. L., and Hinzman, L. D.**, 1998. An analysis of streamflow hydrology in the Kuparuk River basin, Arctic Alaska: A nested watershed approach, *Journal of Hydrology*, **206** (1-2): 39–57.
- Menzel, L., and Lang, H.**, 1998. Spatial variation in évapotranspiration in Swiss Alpine regions, *Proceedings of the HeadWater'98 Conference*, Italy, April 1998, IAHS Publ. No. 248.
- Merz, R., and Blöschl, G.**, 2005. Flood frequency regionalisation—spatial proximity vs. catchment attributes, *Journal of Hydrology*, **302**: 283-306.
- Milly, P. C. D., and Dunne, K.A.**, 2002. Macroscale water fluxes: 1. Quantifying errors in the estimation of basin mean precipitation, *Water Resources Research*, **38** (10): 1205.
- Mimikou, M., and Ramachandira Rao, A.**, 1983. Regional monthly rainfall-runoff model, *Journal of Water Resources Planning and Management*, **109** (1): 75-93.
- Montgomery, D. C., Peck, E.A., and Vining, G.G.**, 2006. *Introduction to Linear Regression Analysis*, Wiley, 640p.
- Moran, P. A. P.**, 1950. Notes on continuous stochastic phenomena, *Biometrika*, **37**: 17-23.
- Mu, Q., Heinsch, F.A., Zhao, M., and Running, S.W.**, 2007. Development of a global évapotranspiration algorithm based on MODIS and global meteorology data, *Remote Sensing of Environment*, **111**: 519–536.
- Naoum, S., and Tsanis, I. K.**, 2004. Orographic precipitation modeling with multiple linear regression, *Journal of Hydrologic Engineering*, **9** (2): 73-102.
- Onsoy, H.**, 2010. Personal communication.
- Osborn, H. B.**, 1984. Estimating precipitation in mountainous regions, *Journal of Hydraulic Engineering*, **110**: 1859–1863.
- Parajka, J., and Szolgay, J.**, 1998. Grid-based mapping of long-term mean annual potential and actual évapotranspiration in Slovakia, *Hydrology, Water Resources and Ecology in Headwaters, Proceedings of the HeadWater'98*, Meran/Merano, Italy, April, IAHS Publ. No. 248.
- Pardo-Iguzquiza, E.**, 1998. Comparison of geostatistical methods for estimating the areal average climatological rainfall mean using data on precipitation and topography, *International Journal of Climatology*, **18**: 1031-1047.
- Park, J. I., and Singh, V.P.**, 1996. Temporal and spatial characteristics of rainfall in the Nam River dam basin of Korea, *Hydrological Processes*, **10**: 1155-1171.
- Partal, T., and Kahya, E.**, 2006. Trend analysis in Turkish precipitation data, *Hydrological Processes*, **20**: 2011-2026.
- Penman, H. L.**, 1956. Evaporation: An introductory survey, *Netherlands Journal of Agricultural Science*, **4**: 7-29.
- Pike, J. G.**, 1964. Estimation of annual run-off from meteorological data in tropical climate, *Journal of Hydrology*, **2** (2): 116-123.

- Prudhomme, C., and Reed, D. W.**, 1999. Mapping extreme rainfall in a mountainous region using geostatistical techniques: a case study in Scotland, *International Journal of Climatology*, **19** (12): 1337-1356.
- Puvaneswaran, K. M., and Smithson, P. A.**, 1991. Precipitation-elevation relationship over Sri Lanka, *Theoretical and Applied Climatology*, **43**: 113-122.
- Raghuwanshi, N. S., and Wallender, W. W.**, 1998. Converting From Pan Evaporation to Evapotranspiration, *Journal of Irrigation and Drainage Engineering*, **124** (5): 275-277.
- Ranhao, S., Baiping,Z., and Jing, T.**, 2008. A multivariate regression model for predicting precipitation in the Daqing mountains, *Mountain Research and Development*, **28** (3-4): 318–325.
- Richard, Y., Mihailescu, I.F., and Planchon, O.**, 2000. Spatial distribution of the precipitation in Dobruja, *International Journal of Climatology*, **20**: 1275–1284.
- Rochelle, B. P., Stevens, D.L. Jr., and Church, M. R.**, 1989. Uncertainty analysis of runoff estimates from a runoff contour map, *Water Resources Bulletin*, **25**: 491-498.
- Saghafian, B., and Bondarabadi, S.R.**, 2008. Validity of regional rainfall spatial distribution methods in mountainous areas, *Journal of Hydrologic Engineering*, **13** (7): 531–540.
- Sahin, S., and Cigizoglu, H. K.**, 2010. Homogeneity analysis of Turkish meteorological data set, *Hydrological Processes*, **24** (8): 981-992.
- Sahin, U., Angin, I., and Anapali, O.**, 2004. Evaluation of Reference Evapotranspiration Calculation Methods Applied to the Climatic Conditions of Turkey, *Journal of Hydrology and Hydromechanics*, **52** (2): 125-133.
- Sarangi, A., Cox, C.A., and Madramootoo, C. A.**, 2005. Geostatistical methods for prediction of spatial variability of rainfall in a mountainous region, *Transactions of the American Society of Agricultural Engineers*, **48** (3): 943-954.
- Sauquet, E.**, 2006. Mapping mean annual river discharges: Geostatistical developments for incorporating river network dependencies, *Journal of Hydrology*, **331**: 300-314.
- Sauquet, E., Gottschalk, L., and Leblois, E.**, 2000. Mapping average annual runoff: a hierarchical approach applying a stochastic interpolation scheme, *Hydrological Sciences Journal*, **45**: 799– 816.
- Savenije, H. H. G.**, 1996. The runoff coefficient as the key to moisture recycling, *Journal of Hydrology*, (176): 219–225.
- Sevruk, B.**, 1997. Regional dependency of precipitation-altitude relationship in the Swiss Alps, *Climatic Change*, **36**: 355–369.
- Shekhar, S., and Xiong, H. (Eds.)**, 2008. *Encyclopedia of GIS*, Springer, USA, 1370p.

- Shi, Y., Li, L., and Zhang, L.**, 2007. Application and comparing of IDW and kriging interpolation in spatial rainfall information, *Geoinformatics 2007: Geospatial Information Science*, Eds J. Chen, and Pu, Y. **Vol. 6753**: 675311, 67512p.
- SHODB (Turkish Navy Office of Navigation Hydrography and Oceanography)** 1991. Black Sea Meteorological Atlas, Istanbul, 39.
- Skøien, J. O., Merz, R., and Blöschl, G.**, 2006. Top-kriging – geostatistics on stream networks, *Hydrology and Earth System Sciences*, **10**: 277-287.
- Snyder, R. L.**, 1992. Equation for Evaporation Pan to Evapotranspiration Conversions, *Journal of Irrigation and Drainage Engineering*, **118** (6): 977-980.
- Sobrino, J. A., Gomez, M., Jimenez-Munoz, J.C., and Oliso, A.**, 2007. Application of a simple algorithm to estimate the daily evapotranspiration from NOAA-AVHRR images for the Iberian Peninsula, *Remote Sensing of Environment*, **110**: 139–148.
- Stewart, J. B., Watts, C.J., Rodriguez, J.C., De Bruin, H.A.R., Van Den Berg, A.R., and Garatuz-Payan, J.**, 1999. Use of satellite data to estimate radiation and evaporation for northwest Mexico, *Agricultural Water Management*, **38**: 181–193.
- Summer, D. M., and Jacobs, J. M.**, 2005. Utility of Penman–Monteith, Priestley–Taylor, reference evapotranspiration, and pan evaporation methods to estimate pasture evapotranspiration, *Journal of Hydrology*, **308**: 81-104.
- Tabios III, G. Q., and Salas, J.D.**, 1985. A comparative analysis of techniques for spatial interpolation of precipitation, *Water Resources Bulletin*, **21** (3): 265–380.
- Tayanc, M., Dalfes, H. N., Karaca, M., and Yenigun, O.**, 1998. A comparative assessment of different methods for detecting inhomogeneities in Turkish temperature data set, *International Journal of Climatology*, **18** (5): 561-578.
- Tezcan, L., and Arıkan, A.**, 1993. Spatial Distribution of Precipitation in the Western Taurids, *Hydrogeological in Karst Terranes, Proceedings of the Antalya Symposium and Field Seminar*, Antalya, 1990, IAHS Publication.
- Thornthwaite, C. W.**, 1948. An approach toward a rational classification of climate, *Geographical Review*, **38**: 55-94.
- Tomczak, M.**, 1998. Spatial interpolation and its uncertainty using automated anisotropic Inverse Distance Weighting (IDW)-Cross-Validation/Jack knife Approach, *Journal of Geographic Information and Decision Analysis*, **2** (2): 18-30.
- Topaloglu, F.**, 2006. Trend detection of streamflow variables in Turkey, *Fresenius Environmental Bulletin*, **15** (7): 644-653.
- Turc, L.**, 1954. Le Bilan D'eau des sols. Relation entre les precipitation, l'évaporation et l'écoulement (in French), *Annales Agronomique*, **5**: 491-595.
- Turkes, M., Sumer, U. M., and Demir, I.**, 2002. Re-evaluation of Trends and Changes in Mean, Maximum and Minimum Temperatures of Turkey for the Period 1929-1999, *International Journal of Climatology*, **22** (8): 947-977.

Url-1 <<http://en.wikipedia.org/wiki/>> accessed at 22.06.2010

Url-2 <<http://proceedings.esri.com/library>> accessed at 23.08.2010

Url-3 <<http://www.spatialanalysisonline.com>> accessed at 12.10.2010

Vicente-Serrano, S. M., Saz-Sanchez, M. A., and Cuadrat, J. M., 2003. Comparative analysis of interpolation methods in the Middle Ebro Valley (Spain): application to annual precipitation and temperature, *Climate Research*, **24**: 161-180.

Vieux, B. E., 2004. *Distributed Hydrologic Modeling Using GIS*, Water Science and Technology Library, Kluwer, Netherlands, 289p.

Wang, K., Wang, P., Li, Z., Sparrow, M., and Cribb, M., 2007. A simple method to estimate evapotranspiration from a combination of net radiation, vegetation indices and temperatures, *Journal of Geophysical Research*, **112** D15107.

Weib, M., and Menzel, L., 2008. A global comparison of four potential evapotranspiration equations and their relevance to stream flow modelling in semi-arid environments, *Advances in Geosciences*, **18**: 15-23.

Wilks, D. S., 2006. *Statistical Methods in the Atmospheric Sciences*, Elsevier, USA, 648p.

Willmott, C. J., 1982. Some comments on the evaluation of model performance, *Bulletin of the American Meteorological Society*, **63**: 1309–1313.

Xia, Y., 2008. Adjustment of global precipitation data for orographic effects using observed annual streamflow and the LaD model, *Journal of Geophysical Research*, **113**: D04106.

Xing, Z., Chow, L., Meng, F., Rees, H.W., Monteith, J., and Lionel, S., 2008. Testing Reference Evapotranspiration Estimation Methods Using Evaporation Pan and Modeling in Maritime Region of Canada, *Journal of Irrigation and Drainage Engineering*, **134** (4): 417–424.

Yates, D. N., 1997. Climate change impacts on the hydrologic resources of South America: an annual continental scale assessment, *Climate Research*, **9**: 147-155.

Yue, W., Xu, J., Liao, H., and Xu, L., 2003. Applications of Spatial Interpolation for Climate Variables Based on Geostatistics: A Case Study in Gansu Province, China, *Annals of GIS*, **9** (1): 71-77.

Zhang, Y., Liu, C., Tang, Y., and Yang, Y., 2007. Trends in pan evaporation and reference and actual evapotranspiration across the Tibetan Plateau, *Journal of Geophysical Research*, **112**: D12110.

APPENDIX

Appendix A : Availability of precipitation and streamflow data

CURRICULUM VITAE

Candidate's full name: Ebru Eriş

Place and date of birth: Izmir, 1979

Permanent Address: Ege University, Faculty of Engineering, Department of Civil Engineering, Bornova, Izmir, Turkey

Universities and Colleges attended: Ege University

Publications:

Papers

- Aksoy, H., Kurt, I., **Eris, E.**, 2009. Filtered Smoothed Minima Baseflow Separation Method, *Journal of Hydrology*, 372 (1-4): 94-101.
- Toprak, Z. F., **Eris, E.**, Agiralioglu, N., Cigizoglu, H. K., Yilmaz, L., Aksoy, H., Coskun, G. H., Andic, G., Alganci, U., 2009, Modeling Monthly Mean Flow in a Poorly Gauged Basin by Fuzzy Logic, *Clean*, 37(7): 555-564, doi: 10.1002/clen.200800152.
- **Eris, E.**, Agiralioglu, N., 2009, Effect of Coastline Configuration on Precipitation Distribution in Coastal Zones, *Hydrological Processes*, 23 (25): 3610-3618.
- Coskun, H. G., Alganci, U., **Eris, E.**, Agiralioglu, N., Cigizoglu, H. K., Yilmaz, L. and Toprak, Z. F., 2010, Remote Sensing and GIS Innovation with Hydrologic Modelling for Hydroelectric Power Plant (HPP) in Poorly Gauged Basins, *Water Resources Management*, 24 (14): 3757-3772.

International Proceedings

- Kaya, B., Daneshfaraz, R., Alkan, A., **Eris, E.**, 2004. Channel Capacity Analysis of Laka Stream for Floods, *EWRA Symposium on Water Resources Management: Risks And Challenges For The 21st Century Proceedings Book, 2: 687-692, 2-4 September, Izmir.*
- **Eris, E.**, Ercan, E., 2006. Akarsu Yatağı Bozulan Fetrek Demiryolu Köprüsünün Mecra Düzenlemesi ve Koruma Yapısı Uygulaması, *7th International Congress on Advances in Civil Engineering, CD (Abstract book, 493), 11-13 October, Istanbul.*
- Şeşeoğulları, B., **Eris, E.**, Kahya, E., 2007. Trend Analysis of Sea Levels Along Turkish Coasts, *AGU Hydrology Days, 19-21 March, Colorado, Poster.*

- **Eris, E.**, Ünal, N. E., Aksoy, H., Alkan, A., 2007. Station-Based Frequency Analysis of Annual Maximum Flows in Gediz Basin, Western Turkey, Proceedings of the AMHY-FRIEND International Workshop on Hydrological Extremes, Variability in space and time of extreme rainfalls, floods and droughts, 163-170, 6-8 June, Cosenza (Italy).
- Alganci, U., Coskun, H.G., Agiralioglu, N., Usta, G., Cigizoglu, H. K., Aksoy, H., Yilmaz, L., **Eris, E.**, and Dagci, M., 2008. Hydrological Modeling of Ungauged Basins Using Remote Sensing and GIS: A Case Study of Solaklı Watershed In Turkey, 28th EARSeL Symposium and Workshops, Remote Sensing for a Changing Europe, Abstract Book, 2-7 June, Istanbul.
- **Eris, E.**, Aksoy, H. 2008. Persistency in Wet And Dry Periods in Goztepe Meteorological Station In Istanbul, Turkey, Proceedings of the AMHY-FRIEND International Workshop on Hydrological Extremes, Analyses and images of hydrological extremes in Mediterranean environments, 93-99, 10-12 July, Cosenza (Italy).
- Coskun, H.G., Karayusufoglu, S., **Eris, E.**, Alganci, U., 2010. Estimation of Hydraulic Modeling Parameters of Poorly Gauged Basins Using Remote Sensing and GIS, Proceedings of the 5th IASME / WSEAS International Conference on Water Resources, Hydraulics & Hydrology (WHH'10), 154-159, 23-25 February, University of Cambridge, UK.
- **Eris, E.**, Agiralioglu, N., 2010. Determination of Relationship between Precipitation and Geographical/Topographical Variables, The 4th International Student Conference on Advanced Science and Technology (ICAST2010) Book, 305-306, 25-26 May, Ege University, Izmir, Poster.

National Proceedings

- Altun, S., Göktepe, B., **Eriş, E.**, 2004. Önyüzü Beton Kaplamalı Kaya Dolgu Barajlar ve Dinamik Etkiler Altındaki Davranışları, I. Ulusal Barajlar ve Hidroelektrik Santraller Sempozyumu ve Fuarı Bildiriler Kitabı, 511-519, 01-03 Haziran, Ankara.
- **Eriş, E.**, Daneshfaraz, R., Kaya, B., Alkan, A., 2005. Laka Deresi Taşkın Pik Debileri ve Kesit Kapasiteleri, II. Ulusal Su Mühendisliği Sempozyumu Bildiriler Kitabı, 495-502, 21-24 Eylül, İzmir.
- **Eriş, E.**, Alkan, A., Kaya, B., 2006. Belirli Süreli ve Tekerrürlü Ötelenmiş ve Ötelenmemiş Taşkın Akımlarının Bornova Deresi Örneğinde İncelenmesi, I.Ulusal Taşkın Sempozyumu Bildiriler Kitabı, 371-376, 10-12 Mayıs, Ankara.
- Pektaş, S. B., Alkan, A., **Eriş, E.**, 2006. Gediz Havzası Zirve Akışları için Uygun Olasılık Dağılımları, I.Ulusal Taşkın Sempozyumu Bildiriler Kitabı, 377-388, 10-12 Mayıs, Ankara.
- Mesci, S. B., Ağırlioğlu, N., **Eriş, E.**, 2007. Dolgu Barajlarda Sızma Hattının Belirlenmesi ve Kullanılan Metotların Karşılaştırılması, 1.Ulusal Baraj Güvenliği Sempozyumu ve Sergisi Bildiriler Kitabı, 171-182, 28-30 Mayıs, Ankara.
- Algancı, U., Coşkun, G., Ağırlioğlu, N., Aksoy, H., Yılmaz, L., Cığızoğlu K. H., Toprak, Z. F., **Eriş, E.**, Andiç, G., Kaya, D., Usta, G., 2007. Solaklı Havzasının Uzaktan Algılama ve Coğrafi Bilgi Sistemi ile Hidrolojik Amaçlı İrdelenmesi, III. Ulusal Su Mühendisliği Sempozyumu Bildiriler Kitabı, 433-443, 10-14 Eylül, Gümüşhanev.

- Şahin, M., Cıgızoğlu, K. H., Ağırlioğlu, N., Aksoy, H., Yılmaz, L., Coşkun, G., Toprak, Z. F., **Eriş, E.**, Andiç, G., Algancı, U., Kaya, D., 2007. Doğu Karadeniz Havzasında Yağış-Akış İlişkisinin Yapay Sinir Ağları ile Belirlenmesi, III. Ulusal Su Mühendisliği Sempozyumu Bildiriler Kitabı, 533-544, 10-14 Eylül, Gümüldür.
- Andiç, G., Ağırlioğlu, N., Yılmaz, L., Aksoy, H., Cıgızoğlu, K. H., Coşkun, G., Toprak, Z. F., **Eriş, E.**, Şahin, M., Algancı, U., Kaya, D., 2007. Akım Ölçümleri Yetersiz Havzalarda Aylık Akımların ve Hidroelektrik Potansiyelin Belirlenmesi”, III. Ulusal Su Mühendisliği Sempozyumu Bildiriler Kitabı, 587-598, 10-14 Eylül, Gümüldür.
- Ağırlioğlu, N., **Eriş, E.**, Algancı, U., Toprak, Z. F., Yılmaz, L., Cıgızoğlu, K. H., Coşkun, G. H., Andiç, G., 2008. Akım Ölçümü Az Olan Havzalarda Hidroelektrik Potansiyelin Belirlenmesi: Doğu Karadeniz Bölgesi, 5. Dünya Su Forumu Bölgesel Hazırlık Süreci, Türkiye Bölgesel Su Toplantısı, Su ve Enerji Konferansı, Bildiriler Kitabı II: 1-32 (Çağrılı Bildiri), 25-26 Eylül, Artvin.
- Algancı, U., Coşkun, H. G., **Eriş, E.**, Ağırlioğlu, N., Cıgızoğlu, K., Yılmaz, L., Toprak, Z. F., 2009. Akım Ölçümleri Olmayan Akarsu Havzalarında Hidroelektrik Potansiyelin Belirlenmesine Yönelik Uzaktan Algılama ve CBS ile Hidrolojik Modelleme, 12. Türkiye Bilimsel Harita ve Teknik Kurultayı Özet Kitabı, 144-145, 11-15 Mayıs, Ankara.
- Ağırlioğlu, N., **Eriş, E.**, 2009. Akarsu Düzenlemesinde Gelişmeler, Su Yapıları Sempozyumu Bildiriler Kitabı, 1-19, 29-30 Mayıs, Samsun.
- **Eriş, E.**, Ağırlioğlu, N., 2010. Kıyı Alanlarında Kıyı Şeklinin Yağış Dağılımına Etkisi, VI. Ulusal Hidroloji Kongresi Bildiriler Kitabı, 428-438, 22-24 Eylül, Denizli.

Other

- Ağırlioğlu, N., **Eriş, E.**, 2009. Akarsu Düzenlemesinde Disiplinler Arası Planlama, Yapı Dünyası, Eylül 162, 11-14.
- Ağırlioğlu, N., **Eriş, E.**, 2010. Akarsu Düzenlemesinde Gelişmeler, TMMOB İnşaat Mühendisleri Odası İstanbul Şubesi, İstanbul Bülten, Sayı 106 (Şubat), 19-25.
- Algancı, U., Coşkun, H. G., **Eriş, E.**, Ağırlioğlu, N., Cıgızoğlu, K., Yılmaz, L., Toprak, Z. F., 2010, Akım Ölçümleri Olmayan Akarsu Havzalarında Hidroelektrik Potansiyelin Belirlenmesine Yönelik Uzaktan Algılama ve CBS ile Hidrolojik Modelleme, TBMMOB Harita ve Kadastro Mühendisleri Odası, Jeodezi, Jeoinformasyon ve Arazi Yönetimi Dergisi, Sayı 101-12. THBTK Özel Sayı, 5-11.
- Karayusufoglu, S., **Eris, E.**, Coskun, H. G., 2010. Estimation of Basin Parameters and Precipitation Distribution of Solakli Basin, Turkey, WSEAS Transactions on Environment and Development, 6 (5): 385-394.

